Université de Sherbrooke

Radiolysis of water induced by the recoil ions of the $^{10}B(n,\alpha)^{7}Li$ nuclear reaction: Calculation of the yields of primary species up to 350 °C and *in situ* generation of ultrafast transient "acid spikes" along the radiation tracks

Par

Muhammad Mainul ISLAM
Département de médecine nucléaire et radiobiologie

Mémoire présenté à la Faculté de médecine et des sciences de la santé en vue de l'obtention du diplôme de maître ès sciences (M.Sc.) en "sciences des radiations et imagerie biomédicale"
Sherbrooke, Québec, Canada

April 2018

Jury

Pr Éric Rousseau	Examinateur, Département d'obstétrique-gynécologie, Faculté de médecine et des sciences de la santé
Pr Johannes Van Lier	Examinateur, Département de médecine nucléaire et radiobiologie, Faculté de médecine et des sciences de la santé
Pr Jean-Paul Jay-Gerin	Directeur de recherche, Département de médecine nucléaire et radiobiologie, Faculté de médecine et des sciences de la santé

RÉSUMÉ

Radiolyse de l'eau induite par les ions de recul de la réaction nucléaire $^{10}B(n,\alpha)^{7}Li$: calcul des rendements des espèces primaires jusqu'à 350 °C et génération *in situ* de pics d'acidité ultra-rapides transitoires le long des trajectoires de rayonnement

Muhammad Mainul ISLAM

Département de médecine nucléaire et radiobiologie

Mémoire présenté à la Faculté de médecine et des sciences de la santé en vue de l'obtention du diplôme de maître ès sciences (M.Sc.) en "sciences des radiations et imagerie biomédicale", Faculté de médecine et des sciences de la santé, Université de Sherbrooke, Sherbrooke, Québec, Canada J1H 5N4

La réaction nucléaire $^{10}B(n,\alpha)^{7}Li$ de capture de neutrons par le bore est très importante pour l'industrie nucléaire ainsi que pour la radiobiologie, car la thérapie par capture neutronique par le bore est utilisée dans des radiothérapies biochimiques ciblées pour plusieurs traitements anticancéreux. L'acide borique enrichi en ^{10}B est utilisé dans les réacteurs nucléaires pour contrôler le flux de neutrons et la réactivité dans le cœur. Cependant, les noyaux de recul (particules α de 1,47 MeV et ions $^{7}Li^{3+}$ de 0,84 MeV) résultant de la réaction $^{10}B(n,\alpha)^{7}Li$ agissent comme sources de rayonnement à transfert d'énergie linéaire élevé (TEL) compliquant ainsi le processus radiolytique à l'intérieur du réacteur. La simulation Monte-Carlo est utilisée dans ce travail pour prédire les rendements (valeurs *G*) des radicaux et des produits moléculaires dus à la radiolyse de l'eau par la réaction $^{10}B(n,\alpha)^{7}Li$ en fonction de la température de 25 à 350 °C. Nos calculs montrent des rendements plus bas en radicaux libres et plus élevés en produits moléculaires en comparaison avec un rayonnement de faible TEL (*e.g.*, rayons γ de ^{60}Co). Les résultats de nos simulations concordent bien avec les estimations expérimentales existantes à 20 et 289 °C. Cependant, l'inflexion prédite par certains auteurs dans les rendements moléculaires H_2 et H_2O_2 au-dessus de ~150 °C ne peut être confirmée dans la mesure où l'on adopte la constante de vitesse de la réaction (e^-_{aq} + e^-_{aq}) en solution neutre ou légèrement acide. De plus, dans cette étude, nous avons également calculé la concentration de H_3O^+ formé *in situ* le long des trajectoires du rayonnement en considérant un « modèle de trajectoire cylindrique » pour un rayonnement à fort TEL. Pour ces ions, le pH le long des trajectoires est proche de 0 jusqu'à ~100 ps, puis revient progressivement à un pH neutre (7) à ~0,1 ms. Cependant, dans l'eau cellulaire, le "pic d'acidité" demeure plus longtemps à cause de la faible mobilité du proton dans ce milieu, ce qui soulève plusieurs questions en relation avec la boroneutrothérapie et, plus généralement, l'hadronthérapie.

Mots-clés: Radiolyse de l'eau, réaction de capture de neutrons par le bore, ions hélium et lithium de recul, transfert d'énergie linéaire (TEL), température, simulations Monte-Carlo, rendements radicalaires et moléculaires, pH, effet de pic acide dans les trajectoires en fonction du temps, réacteurs nucléaires, boroneutrothérapie, hadronthérapie.

ABSTRACT

Radiolysis of water induced by the recoil ions of the $^{10}B(n,\alpha)^{7}Li$ nuclear reaction: Calculation of the yields of primary species up to 350 °C and *in situ* generation of ultrafast transient "acid spikes" along the radiation tracks

Muhammad Mainul ISLAM

Département de médecine nucléaire et radiobiologie

Thesis presented at the Faculty of Medicine and Health Sciences in order to obtain the Master of Sciences (M.Sc.) degree in "Radiation Sciences and Biomedical Imaging", Faculty of Medicine and Health Sciences, Université de Sherbrooke, Sherbrooke, Québec, Canada J1H 5N4

The $^{10}B(n,\alpha)^{7}Li$ nuclear reaction is very important for the nuclear industry as well as in radiobiology, as boron neutron capture therapy (BNCT) is used in biochemically targeted radiotherapies for several malignant cancer treatments. Boric acid enriched with ^{10}B is used in nuclear reactors to control the neutron flux and the reactivity in the core. However, recoil nuclei (1.47 MeV α-particles and 0.84 MeV $^{7}Li^{3+}$ ions) resulting from this reaction act as sources of high linear energy transfer (LET) radiation, thereby complicating the radiolytic processes inside the reactor. Monte Carlo simulations are used to predict the yields (*G*-values) of the radicals and molecular products due to the radiolysis of water by the $^{10}B(n,\alpha)^{7}Li$ recoil ions as a function of temperature from 25 to 350 °C. Our computed yields show lower yields of free radicals and higher yields of molecular products in comparison with low-LET radiation (^{60}Co γ-rays). Our simulation results agree well with existing experimental estimates at 20 and 289 °C. However, the non-monotonic downward inflection of the yields of molecular H_2 and H_2O_2 above ~150 °C can be confirmed if we could get the rate constant of the (e^{-}_{aq} + e^{-}_{aq}) reaction measured under neutral or slightly acidic conditions. Moreover, in this study, we also calculated the *in situ* concentrations of H_3O^{+} and the corresponding pH values along the radiation tracks using a "cylindrical track model" characteristic of high-LET radiation. For both considered recoil ions, the pH along the tracks is near zero up to ~100 ps, after which it progressively returns to neutrality at ~0.1 ms. However, in cellular water, this "acid spike" retains for a longer period of time due to the slower diffusion of free protons in this medium, a result that may have several implications in BNCT and, more generally, in the overall field of hadrontherapy.

Keywords: Water radiolysis, boron neutron capture reaction, He and Li recoil ions, linear energy transfer (LET), temperature, Monte Carlo simulations, radical and molecular yields, pH, "acid spike" effect along the radiation tracks as a function of time, nuclear reactors, BNCT, hadrontherapy.

TABLE OF CONTENTS

LIST OF FIGURES

Chapter 1: Introduction

LIST OF TABLES

LIST OF ABBREVIATION

$^{10}B(n,\alpha)^{7}Li$	Boron Neutron Capture Nuclear (BNCT) reaction
D	Diffusion coefficient
DEA	Dissociative electron attachment
DNA	Deoxyribonucleic acid
e^{-}_{aq}	Hydrated electron
eV	Electron-volt
G_X or $g(X)$	Primary yield of the radiolytic species X
$G(X)$	Experimental yield of the final product X
Gy/s	Gray/second (dose rate)
IRT	Independent reaction times
k	Reaction rate constant
keV	Kilo-electron-Volts
LET	Linear energy transfer
MC	Monte Carlo
MeV	Mega-electron-Volts
µm	Micrometer
µs	Microsecond
ps	Picosecond
SOD	Superoxide dismutase
ΔG	Yields variation

1. INTRODUCTION

Radiation chemistry is a comprehensive field of study including many areas of research. The absorption of ionizing radiation in matter causes chemical changes in the matter, which is known as radiation chemistry. Radiation chemistry has been originated with the discovery of X-ray in 1895. In the following year, Becquerel discovered the radioactivity of uranium. Pierre Curie and Marie Curie conducted their research on different mineral salts to investigate the 'radioactivity' of the materials. However, the term 'radioactivity' had been used by them first. They discovered polonium and radium, which are also highly radioactive materials (see, for example: FERRADINI and BENSASSON, 1989; SPINKS and WOODS, 1990; ZIMBRICK, 2002). In 1901, Curie and Debierne observed the evolution of hydrogen and oxygen from water and from the solution of radium salts (CURIE and DEBIERNE, 1901; DEBIERNE, 1914). This study was the first trigger on the radiolysis of water by ionizing radiation. Sir William Ramsay and Frederick Soddy did a quantitative study of some simple radon-induced reactions (RAMSAY and SODDY, 1903). BRAGG (1907) analyzed the data obtained from Ramsay and Soddy and reported that the number of the water molecules decomposed was nearly equal to the number of ions produced in air by the radon employed. In 1912, Samuel Lind modeled several studies to determine the relation between the number of ion-pair formed by α-rays in a gas and the number of chemicals subjected to chemical changes (LIND, 1912, 1921).

By the 1930's, the advent of powerful X-ray equipment for medical and industrial purposes instigated the research in this field. X-ray is more penetrating and better suited to the irradiation of bulk liquid and solid samples. The development of X-ray equipment and use of radiation in the medical field also increased the interest of research in the effect of X-rays and other types of radiation on aqueous solution including biological materials. Hugo Fricke, another true pioneer in the field of radiation chemistry, published several systematic studies on the effect of radiation on aqueous solutions. A solution of ferrous ions in 0.4 M sulfuric acid at this time has now become a routine chemical means to measure the energy absorption in irradiated systems, constituting the so-called "Fricke dosimeter" (SPINKS and WOODS, 1990; FRICKE and HART, 1966).

A great impetus on research in radiochemistry occurred in 1942 with the advent of nuclear energy. The research asserts on the two important practical problems, namely, the study and prevention of undesired radiation effects or radiation damage, and the utilization of the tremendous amounts of radiation energy for beneficial purposes. The former includes the study of the damage of materials due to the radiation used in reactor construction and in the processing of radioactive fuels as well as the development of radiation resistant materials. Another extremely important area of research is the effect of radiation on living systems and utilization of radiation for medical treatment. To use the radiation energy for humans, it is very important to understand physical and chemical processes of the ionizing radiation in a material. Though the fundamental ionization processes are similar in all system, the properties of the medium such as phase, polarity, and composition can greatly affect the chemistry. In all systems, it is very important to understand what chemical species are formed, what the internal energies are, how they are dispersed spatially, and what reactions can occur (JONAH, 1995). The understanding of the simpler chemical systems is necessary for unraveling the complexity of events incurred by irradiation of living systems.

A large fraction of the radiation chemistry studies has been concerned with the studies of water and aqueous solutions because of the unique importance of water in biological systems. Moreover, it also has a large number of practical applications, for instance, radiotherapy and diagnostic radiology, environmental management of radioactive waste materials, nuclear power generation and radiation effect in space (LAVERNE, 2004; MEESUNGNOEN and JAY-GERIN, 2011).

All biological systems are very sensitive to ionizing radiation. Since living cells and tissue consist mainly of water (~70-80% by weight), the knowledge of the radiation chemistry of aqueous solutions is very critical to our understanding of the early stages in the complicated chain of radiobiological events that follows the passage of radiation. Therefore, we have to understand and clearly model the interaction of ionizing radiation with water and aqueous solutions and analyze the subsequent effect of the species produced due to ionizing radiation. Not only for biological aspect analysis but also to understand the

corrosion of materials and safety of the nuclear power reactors, such kind of studies are very relevant.

The absorption of ionizing radiation by living cells can cause damage of different molecular structures of biological relevance, can disrupt the biochemical processes in the cell and can produce new reactive chemical species that may damage nucleic acids, proteins and lipids. The biological cell damage by ionizing radiation can be done by 'direct' or 'indirect' effect. In case of the direct effect, the biological species absorb the energy from the ionizing radiation directly, which disrupts their initial constituents and functions. In the indirect effect, however, the water molecules in the cell absorb the ionizing radiation and produce several radiolytic products such e^-_{aq}, $H^\bullet$, $^\bullet OH$, $HO_2^\bullet/O_2^{\bullet-}$, H_2, H_2O_2, O_2, etc., which subsequently might act as triggers of signalling or other damaging effects (AZZAM et al., 2012; MUROYA et al., 2006; NATHAN, 2003; FORMAN et al., 2004; VEAL et al., 2007).

Deoxyribonucleic acid (DNA) is a large molecule with a double helix structure which carries the genetic instructions and biological information of the living cells. DNA is a highly charged poly-anion that is hydrated with water molecules. Exposure to ionizing radiation causes a plethora of DNA damage, which is responsible for genomic instability, potential tumorigenesis, mutagenicity and finally, cell death. Different types of DNA damages and repair mechanisms have been reported and studied over the years. The main types of DNA damages are base damage, apyrimidinic/apurinic (AP) site, single-strand break (SSB), double-strand break (DSB), tandem lesions and various clustered lesions (von SONNTAG, 2006). It is considered that the complex lesions or multiply damaged sites (MDS) composed of more than one lesion (base damage, base loss or strand break) within one or two helical turns of DNA, have significant biological effects, including mutation and cytotoxicity (CHAPMAN, 1980; NIKJOO et al., 1997; GOODHEAD, 1994; WARD, 1994). The complexity and nature of DNA damages induced by ionizing radiation largely depend on the cellular phenotype, type of ionizing radiation, radiation quality or "linear energy transfer" (LET) (*i.e.*, stopping power, -dE/dx), dose, and dose rate. For example, exposure to high-LET radiations (*e.g.*, α-particles, highly charged and high energy particles), the yield of locally multiply damaged (LMDS) sites in DNA is greatly increased

(KRYSTON, 2011; WARD, 1985; GEORGAKILAS, 2011). Moreover, radiation-induced generation of reactive oxygen (ROS) and nitrogen species (RNS) may spread from targeted cells to non-targeted bystander cells through intercellular communication mechanism. More importantly, mitochondria are the richest source of ROS. The premature leakage of electrons reduces O_2 to produce superoxide radicals ($O_2^{\bullet -}$). Radiation-induced ROS/RNS production by mitochondria plays multiple roles in signaling cascades, mediates apoptosis, mutation of mitochondrial DNA, autophagy and propagation of non-targeted responses (PETKAU, 1987; HEI et al., 2011, PRISE, 2009; WERNER and WERB, 2002; MALAKHOVA et al., 2005; AZZAM et al., 2012). The research in radiobiology is very important to improve treatment and imaging procedures. The research in this domain also opens a new horizon to early detect cancer cells and specifically treat them.

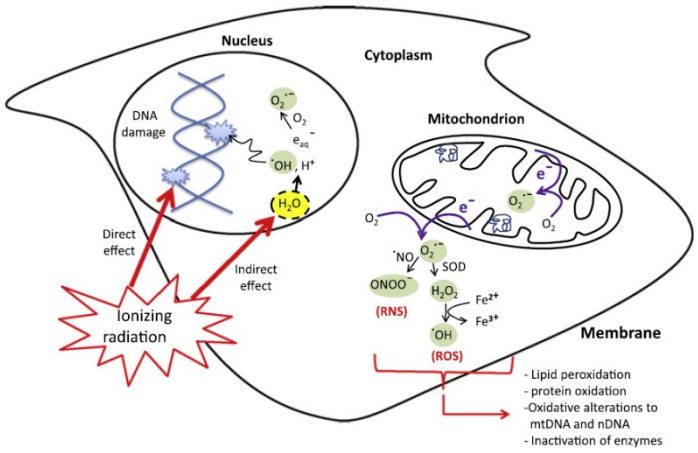

Fig. 1.1: Simplest representation of the mode of action (direct and indirect) of radiation on a cell. Absorption of ionizing radiation may damage the cell directly attacking the DNA or producing the radiolysis products of water or perturbing the function of the mitochondria. From AZZAM et al. (2012).

Boron-10 is one of the stable isotopes of boron with a natural abundance of ~20%. It is known to exhibit a high propensity to absorb thermal neutrons with a neutron-capture cross-section of 3835 barns (1 barn = 10^{-28} m^2), which is about six times greater than that of uranium-235 and three orders of magnitude greater than that of the nuclei of living tissues. When boron-10 (^{10}B) captures slow neutrons, a fission reaction takes place which produces α-particles (He) and excited lithium ions (Li) with energy of 1.47 MeV and 0.84

MeV, respectively. The excited lithium ion returns to the ground stage with the emission of a low energy gamma (γ)-ray. Though α-particles and excited lithium ions produce high-LET tracks, the path length of those ions is limited (*e.g.*, 5-8 μm) (ISLAM et al., 2017). A schematic boron neutron capture nuclear reaction is shown in Fig. 1.2.

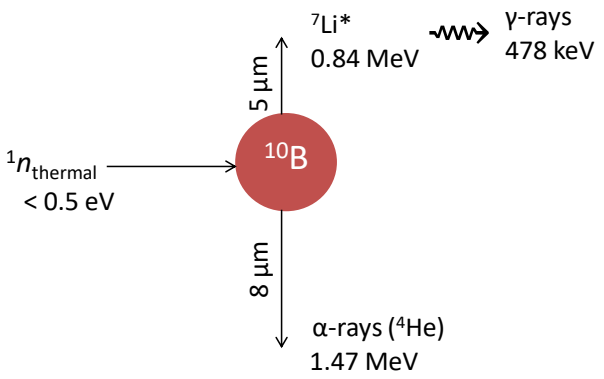

Fig. 1.2: Scheme of the nuclear reaction resulting from the low-energy (< 0.5 eV) thermal neutron capture by a ^{10}B atom. After absorption, 94% of the reactions leave the ^{7}Li ion in its first excited state (^{7}Li*) which rapidly de-excites to the ground state by releasing a 478-keV γ-ray. For the remaining 6% of the reactions, the ^{7}Li ion is left directly in its ground state resulting in the emission of a 1.78 MeV α-particle and a 1.02 MeV ^{7}Li ion. Note that the ^{4}He and ^{7}Li recoil ions are in opposite directions (i.e., at a 180° angle), away from the site of the compound nucleus, and hence they form one straight track.

The Boron Neutron Capture nuclear reaction $^{10}B(n,\alpha)^{7}Li$ has been used in clinical studies of biochemically targeted radiotherapies for cancer treatment known as "boron neutron capture therapy" (BNCT) (SAUERWEIN, 2012; HOSMANE, 2012). The $^{10}B(n,\alpha)^{7}Li$ nuclear reaction is also a very important reaction in the nuclear industry. In the nuclear industry, boron carbide (B_4C) rods are used to control the reaction by absorbing neutrons inside the reactor in the Boiling Water Reactor (BWR). Moreover, boric acid (H_3BO_3) is generally added as a water-soluble neutron poison in the primary coolant of pressurized water reactors (PWRs) to control the neutron flux and the reactivity in the core (PUCHEAULT, 1952; KOIKE et al., 1969; COHEN, 1980). The $^{10}B(n,\alpha)^{7}Li$ nuclear reaction inside the nuclear reactor produces several oxidizing species that contribute to the corrosion of the reactor and piping materials. Understanding the radiation chemistry inside

the reactor is very important to maintain the proper chemical environment and minimize the corrosion of the materials.

Monte Carlo computer simulations are now a standard tool in scientific fields such as condensed matter physics, including surface-physics and applied physics problems, chemical physics, including studies of solutions, chemical reactions, polymer statistics. Monte Carlo simulations, as well as other simulation methods, are used to investigate and answer subtle theoretical questions that arise in a complex system. Monte Carlo simulation methods are well suited to take into account the stochastic nature of the complex sequence of events that are generated in aqueous systems following the absorption of ionizing radiation. Simulations allow the reconstruction of the intricate action of radiation. The relationship between initial radiation track structure, the ensuing chemical processes, and the stable products formed in the radiolysis of both pure water and different solutions have been studied using this simulation tool. Stochastic simulation codes employing Monte Carlo procedures have been used with success by a number of investigators to model the entire water radiolysis process as a function of time, LET of the radiation, pH, presence or absence of oxygen, temperature, *etc.* (for reviews, see, for example: BALLARINI et al., 2000; UEHARA and NIKJOO, 2006; KREIPL et al., 2009; MEESUNGNOEN and JAY-GERIN, 2011). Those theoretical modeling and calculations for water radiolysis process provide a realistic description of the early physical aspect of the radiation track structure and spatio-temporal development of the track. It also depicts the diffusion of different water radiolysis products and the reactions with one another or the milieu (MUROYA et al., 2006; MEESUNGNOEN and JAY-GERIN, 2011).

In such perspective, we used the Monte Carlo track chemistry simulations to predict the yields (*G*-values) of all primary radical and molecular species produced in the radiolysis of pure, neutral water and 0.4 M sulfuric acid aqueous solutions by the recoil ions of the $^{10}B(n,\alpha)^{7}Li$ nuclear reaction as a function of temperature from 25 to 350 °C. The calculations were performed individually for 1.47- MeV α-particles and 0.84 MeV lithium nuclei with “dose-average” linear energy transfer (LET) values of ~196 and 225 eV/nm at 25 °C, respectively (ISLAM et al., 2017). We also analyzed the change of pH along the track structure region produced due to the passage of ionizing radiation through pure, de-

aerated water during and shortly after the irradiation. The concentrations of hydronium ions (H_3O^+) generated *in situ* in water induced by the recoil ions (α-particles and lithium nuclei) released from the $^{10}B(n,\alpha)^7Li$ nuclear reaction were obtained from our calculated yields (or *G*-values) of H_3O^+ as a function of time (in the interval of ~1 ps to 1 μs). We observed that for these two high linear energy transfer (LET) irradiating ions, the pH remains near 0 on a time scale of ~100 ps after which the system gradually returns to neutral pH at ~1 ms. In bulk cell water, these initial conditions of high acidity persist over a much longer period of time due to the much lower value of the intracellular diffusion coefficient of the free proton. Apparently, this ultrafast transient "acid spike" effect has never been explored in water or in a cellular environment exposed to high-LET (densely ionizing) radiations. In this regard, the present work raises the question as to the implications of this effect in "Boron Neutron Capture Therapy" (BNCT), a therapeutic modality that is used for treating locally malignant tumors, or other high-LET radiations therapeutic modality such as 'Carbon therapy'. Moreover, this present study also prompts a number of important questions about the effect of the change of acidity due to radiation inside the nuclear reactor in terms of the material corrosion and damage.

1.1 Energy deposition events and interaction of ionizing radiation

Ionizing radiations are defined as those types of energetic particles and electromagnetic radiations that, either directly or indirectly, cause ionization of a medium, *i.e.*, the removal of a bound orbital electron from an atom or a molecule and thereby, the production of a residual positive ion radical. Some molecules, instead of being ionized, may also be excited to upper electronic states (*e.g.*, see: EVANS, 1955; ANDERSON, 1984; IAEA, 1995; MOZUMDER, 1999; TOBUREN, 2004). Directly ionizing radiations are fast moving charged particles (*e.g.*, electrons, protons, α-particles, stripped nuclei, or fission fragments) that produce ionizations through direct Coulomb interactions. In this case, note that particle-particle contact is not necessary since the Coulomb force between the incoming particle and the molecular electrons acts at a distance. Indirectly ionizing radiations are energetic electromagnetic radiations (like X- or γ-ray photons) or neutrons that can also liberate bound orbital electrons, but secondarily to a preliminary interaction. For photons, this interaction is predominantly via production of Compton electrons and

photoelectrons (and, if the incident photon energy is greater than 1.02 MeV, then there is the production of electron-positron pairs). The final common result in all modes of absorption of ionizing radiation depends on the formation of tracks of physical energy-loss events in the form of ionization and excitation processes and in a geometrical pattern that depends on the type of radiation involved.

Generally, the electrons ejected in the ionization events may themselves have sufficient energy to ionize one or more other molecules of the medium. In this way, the primary high-energy electron can produce a large number ($\sim 4 \times 10^4$ for a 1 MeV particle) of secondary or higher-order generation electrons (it is customary to refer to all electrons that are not primary as "secondary") along its track as it gradually slows down (ICRU REPORT 31, 1979). From atomic physics, it is known that most energy-loss events by fast electrons involve small transfers of energy. In fact, the probability of a given energy transfer, Q, varies inversely with the square of that energy loss (EVANS, 1955). "Distant" or "soft" collisions, in which the energy loss is small, are therefore strongly favored over "close" or "hard" collisions, in which the energy loss is large (MOZUMDER, 1999). The vast majority of these secondary electrons have low initial kinetic energies with a distribution that lies essentially below 100 eV and a most probable energy below 10 eV (LAVERNE and PIMBLOTT, 1995; SANCHE, 2002; AUTSAVAPROMPORN, 2006). In most cases, they lose all their excess energy by multiple quasi-elastic (*i.e.*, elastic plus vibrational excitations) and inelastic interactions with their environment, including ionizations and/or excitations of electronic, intramolecular vibrational or rotational modes of the target molecules (MICHAUD et al., 2003) and quickly reach thermal equilibrium (*i.e.*, they are "thermalized"). Determining exactly which of these competing interaction types will take place is a complex function of the target medium and the energy range of the incident electron. By definition, a measure of the probability that any particular one of these interactions will occur is called the "cross section" (expressed in units of area) for that particular interaction type (see, for example, JOACHAIN, 1975). The total interaction cross section σ, summed over all considered individual processes i, is used to determine the distance to the next interaction, and the relative contributions σ_i to σ are used to determine the type of interaction. Actually, the mean distance between two consecutive interactions or "mean free path" λ is defined by

$$\lambda = {}^{1}/_{N\sigma} \tag{1.1}$$

where N is the number of atoms or molecules per unit volume, and

$$\sigma = \sum_i \sigma_i \tag{1.2}$$

In a dilute aqueous environment, thermalized electrons undergo trapping and hydration in quick succession (within ~10 ps) as a result of the water electric dipoles rotating under the influence of the negative charge (BERNAS et al., 1996). Some electrons that have kinetic energies lower than the first electronic excitation threshold of the medium, the so-called "subexcitation" electrons (PLATZMAN, 1955), may also undergo, prior to thermalization, prompt geminate ion recombination (FREEMAN, 1987) or induce the production of energetic (~1-5 eV) anion fragments via formation of dissociative negative ion states (resonances) (*i.e.*, dissociative electron attachment, or DEA) (CHRISTOPHOROU et al., 1984; BASS and SANCHE, 2003). As a consequence of the energy gained by the medium, a sequence of very fast reactions and molecular rearrangements lead to the formation of new, highly non-homogeneously distributed 5 chemical species in the system, such as charged and/or neutral molecular fragments, reactive free radicals, and other excited chemical intermediates. The trail of the initial physical events, along with the chemical species, is generally referred to as the track of a charged particle and its overall detailed spatial distribution, including contributions from secondary electrons, is commonly known as "track structure" (see, for example PARETZKE, 1987; MAGEE and CHATTERJEE, 1987; KRAFT and KRÄMER, 1993; PARETZKE et al., 1995; MOZUMDER, 1999; LAVERNE, 2000, 2004).

1.1.1 Linear energy transfer (LET) and interaction cross sections for heavy charged particles

Different experiments have been done to determine the radiation-chemical effects in liquid water, where we observed that the yields of different radiolytic products depended on the types of the radiation. The total energy deposition and the spatial distribution of this energy are the determining elements for the quantitative yields of the species. The "Linear Energy Transfer", or LET, is the measure of the energy deposition along and within the

track of a penetrating charged particle. This value is also termed as "stopping power" in radiation physics. The quantity of the energy deposition or LET value of a particular type of radiation is very important to evaluate the overall chemical effect. It is defined as

$$LET = -\frac{dE}{dx} \tag{1.3}$$

where dE is the average energy locally (*i.e.*, in the vicinity of the particle track) imparted to the medium by the particle in traversing a distance d*x* (ICRU REPORT 16, 1970). Usually, LET values are in the units of keV per micron (keV/μm) (the conversion into SI unit is: 1 keV/μm ≈ 1.602×10^{19} J/nm).

The Bethe theory of stopping power describes the average energy loss due to the electromagnetic interactions between fast charged particles and the electrons in absorber atoms (see, for example: FANO, 1963). For kinetic energies of ions that are small compared to their rest-mass energy, the non-relativistic stopping power formula of Bethe (BETHE, 1930; BETHE and ASKIN, 1953) is given by (in SI units):

$$-\frac{dE}{dx} = \left(\frac{1}{4\mu\varepsilon}\right)^2 \frac{4\pi Z^2 e^4}{m_0 V^2} N \ln\left(\frac{2m_0 V^2}{I}\right) \tag{1.4}$$

where Ze is the charge of on the incident ion, V is the ion velocity, m_o is the mass of electron, N is the number of electron per cubic meter of the absorbing medium, and I is the mean of all the ionization and excitation potentials of the bound electrons in the absorber. For liquid water, $I = 79.7 \pm 0.5$ eV (BICHSEL and HIRAOKA, 1992).

We can observe that the LET value of an incident particle depends on the velocity of the particle. The velocity term in the numerator of the logarithm term and in the dominator of the pre-logarithmic term gives rise to the familiar Bragg peak, *i.e.*, with decreasing velocity of the incident particle the LET increases to a maximum and then decreases to lower velocities (LAVERNE, 2000, 2004) (Fig. 1.3).

We also can see from the equation (1) that the LET value is also proportional to the square of the projectile charge number Z^2. This Z^2 is very important for providing the cross section for the intrinsic scattering by fully ionized or stripped (in another word "bare") ion projectiles. On average the net positive (or effective) charge on an incident ion decreases

when the speed decreases (IAEA, 1995; ICRU REPORT 55, 1996; LAVERNE, 2004; MEESUNGNOEN, 2007).

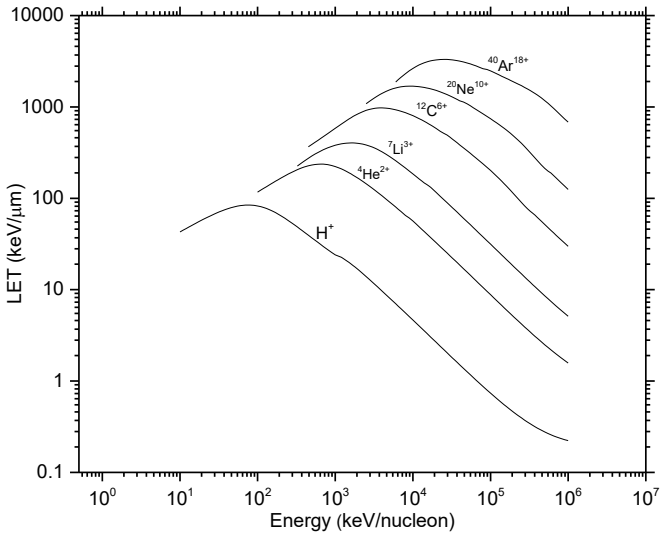

Fig. 1.3: LET of some heavy ions as a function of energy in liquid water using SRIM program (WATT, 1996).

1.2 Radiolysis of water

The term *radiolysis* refers to any chemical changes induced by ionizing radiation, and includes synthesis as well as degradation. Water radiolysis of water is defined as the chemical decomposition of the water molecules due to the action of the ionizing radiation. A large fraction of radiation chemistry studies has been concerned with the studies of water and aqueous solutions because of the unique importance of the water in biological system and in different industrial purpose. Moreover, water or aqueous solutions are used in different industries where radiation is involved, for instance, nuclear power industry uses water to cool down the reactor and control the reactions in the reactor and the environmental management of the radioactive materials or waste. Since a large portion of living cells and tissue is water (~70-85% by weight), the knowledge of water radiolysis is very important in case of radiotherapy and diagnostic radiology (LAVERNE, 2004; GARRETT et al., 2005; MEDIN, 2006). The radiolysis of water depends on the absorbed dose and the quality of the radiation. Due to the influence of ionizing radiation, radiolysis

of water takes place and produces different radicals such as e^-_{aq}, $H^\bullet$, $^\bullet OH$, and $HO_2^\bullet/O_2^{\bullet-}$, and also the molecular products such as H_2, H_2O_2, and O_2.

1.2.1 Track structure in radiation chemistry of water

The distribution of the track structure is mainly defined by the distribution of the physical energy deposition events and their geometrical dispositions. Interestingly, the track structure is known as "LET effects" as most of the early studies used this parameter to characterize the different radiation chemical yields for various radiation-induced ions in liquid water. Furthermore, the radiation track structure is an important concept in identifying the precise spatial location of the radiolytic species and free-radical intermediates generated in the tracks, and their subsequent radiobiological action at the molecular and cellular levels. However, the tracks are not static. As a function of time, the tracks are constantly expanding due to the diffusion of different reactive species. It can be noted that the diffusion co-efficient of different species in the liquid water medium is different (FRONGILLO et al., 1998). Overall, the scientific community agrees that different qualities of radiation must be analyzed in terms of track structure (CHATTERJEE and HOLLEY, 1993; MUROYA et al., 2006).

1.2.1.1 Low-LET radiation and track structure

In case of low-LET radiation, the deposition of energy along the track is comparatively lower. The energy loss of a fast-moving charged particle in a medium takes place due to the electromagnetic interactions and collisions between the fast-moving charged particles and the absorber atom. The LET value for high energy ionizing radiation such as fast electrons generated from X- or γ-ray beams is very low. For example, the average LET of a 1-MeV Compton electron in water is ~0.3 keV/μm. The track-averaged mean energy loss per collision event by such an electron is in the region ~47-57 eV (COBUT, 1993; LAVERNE and PIMBLOTT, 1995; COBUT et al., 1998; AUTSAVAPROMPORN, 2006; KOHAN et al., 2013). This means that the energy-loss events are, on the average, separated by distances of ~200 nm. This non-homogeneous distribution of energy deposition events in space gives rise to the "spur" theory for low-LET track structure (ALLEN, 1948; MAGEE, 1953; MOZUMDER and MAGEE,

1966*a*,*b*), according to which the entire track is to be viewed as a random succession of (more or less spherical) spurs, or spatially localized energy-loss events. The few tens of electron-volts deposited in a spur cause a secondary electron to be ejected from a molecule. As the ejected electron moves away, it undergoes collisions with surrounding water molecules, loses its excess energy, and becomes thermalized (~0.025 eV at 25 °C) within ~8-12 nm of its geminate positive ion (GOULET et al., 1990, 1996; PIMBLOTT and MOZUMDER, 2004; MEESUNGNOEN and JAY-GERIN, 2005*a*; UEHARA and NIKJOO, 2006). This average "electron thermalization distance" or "penetration range" (r_{th}) can be viewed as an estimate of the spur's initial radius, prior to spur expansion. Thus, the individual spurs produced by low-LET radiation are so far apart along the track that they are not initially overlapping (but they will overlap somewhat later as they develop in time).

To model the radiation-chemical consequences of different energy-loss processes, MOZUMDER and MAGEE (1966*a*,*b*) considered, somewhat arbitrarily, a low-LET track as composed of a random sequence of three types of essentially non-overlapping entities: "spurs, blobs, and short tracks" (Fig. 1.4). The spur category contains all track entities created by the energy losses between the lowest excitation energy of water and 100 eV; in most cases, there are one to three ion pairs in such isolated spatial areas and about the same number of excited molecules (PIMBLOTT and MOZUMDER, 1991). Blobs were defined as track entities with energy transfers between 100-500 eV, and short tracks as those with energy transfers between 500 eV and 5 keV. Secondary electrons produced in energy transfers above 5 keV were considered as "branch tracks". Short and branch tracks are, collectively, described as δ-rays. This old concept of track entities proved to be very helpful in greatly facilitating the visualization of track processes and in modeling radiation-chemical kinetics. It is still a useful approach for the classification of track structures, since it takes into account the spatial arrangements of initial species, which affect their subsequent reactions.

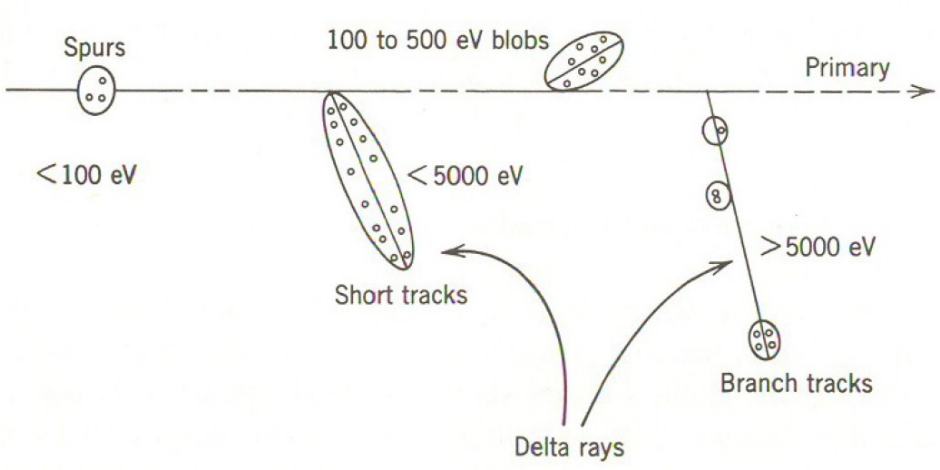

Fig. 1.4: Track structure entities classified as spurs (spherical entities, up to 100 eV), blobs (spherical or ellipsoidal, 100-500 eV) and short tracks (cylindrical, 500 eV-5 keV) for a primary high energy electron (not to scale) (BURTON, 1969).

The partition between the three entities strongly depends on the incident particle energy (PIMBLOTT et al., 1990). In case of low LET radiation, the tracks are formed initially by well-separated "spurs" (spherical in shape). With the increase of LET, the distance between the spurs decreases and the isolated spur structure changes to a situation in which the spurs overlap and form a dense continuous column. For instance, when α-particles ($^{4}He^{2+}$) with 0.84 MeV energy passes through liquid water, it produces a cylindrical track with high concentration of water radiolytic products (ISLAM et al., 2017). However, we observe several distinct "spur" in water when it is irradiated by 300 MeV protons (LET ~ 0.3 keV/μm) (KANIKE et al., 2015*a*).

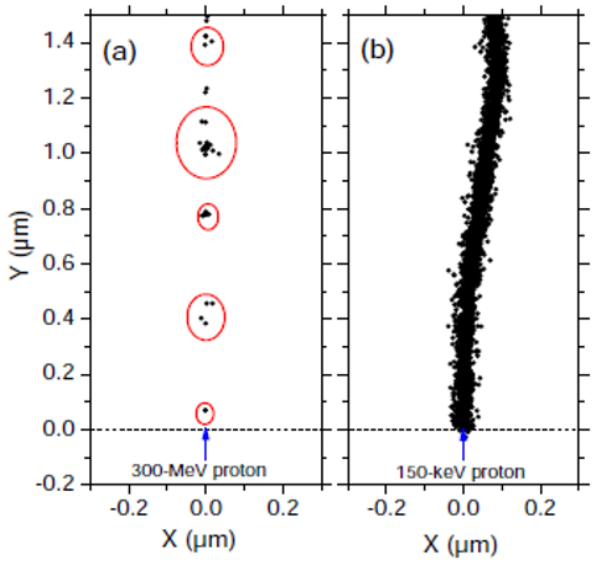

Fig. 1.5: Monte Carlo track simulation of 300 MeV protons (a) and 150 keV protons (b) (LET~ 0.3 and 70 keV/μm) incident on liquid water at 25 °C (KANIKA, 2015*a*).

1.2.1.2 High-LET radiation and track structure

High-LET tracks produced by the heavy particles consist initially of a cylindrical "core" and a surrounding region traversed by the emergent, comparatively low-LET secondary electrons, called the "penumbra" (MOZUMDER et al., 1968; CHATTERJEE and SCHAEFER, 1976; FERRADINI, 1979; MAGEE and CHATTERJEE, 1980, 1987; MOZUMDER, 1999; LAVERNE, 2000, 2004).

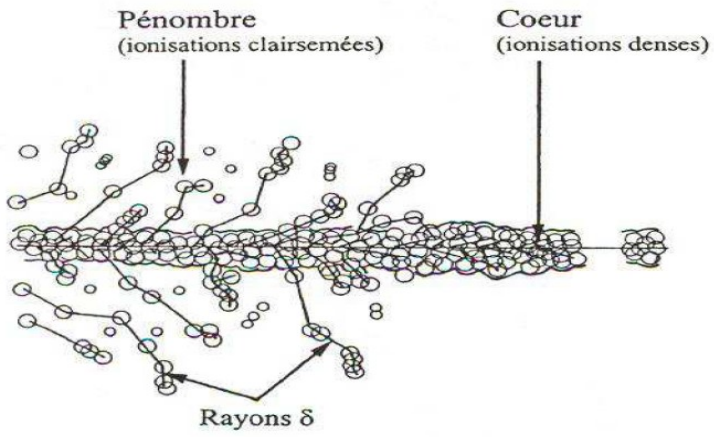

Fig. 1.6: Primary energy-loss events in high-LET radiation tracks (FERRADINI, 1979).

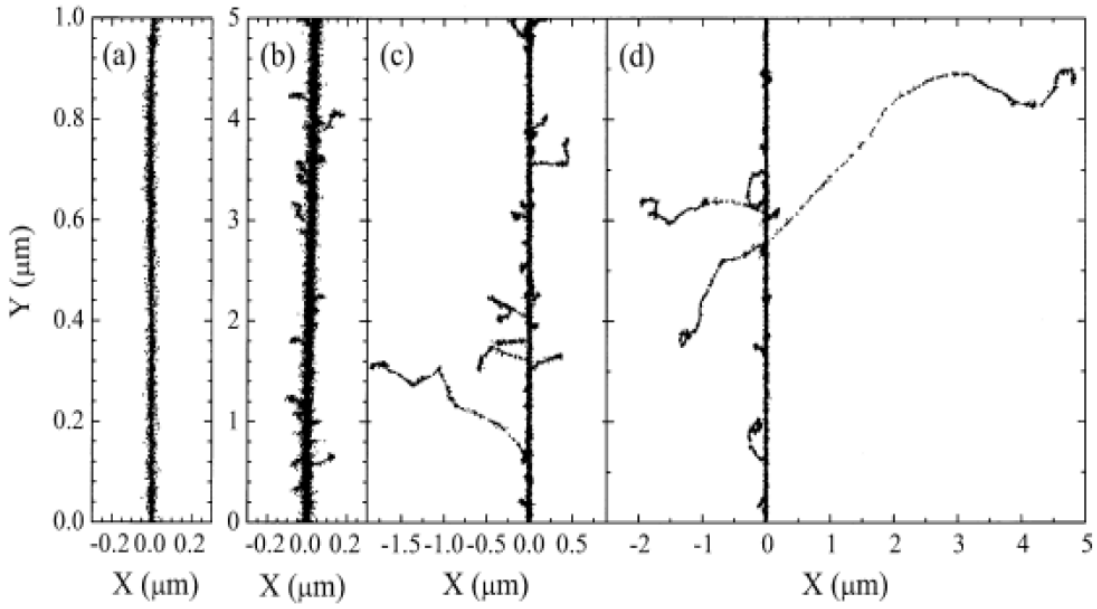

Fig. 1.7: Projections over the *XY*-plane of track segments calculated (at ~10-13 s) for (a) H^+ (0.15 MeV), (b) $^4He^{2+}$ (1.75 MeV/nucleon), (c) $^{12}C^{6+}$ (25.5 MeV/nucleon), and (d) $^{20}Ne^{10+}$ (97.5 MeV/nucleon) impacting ions. Ions are generated at the origin and along the *Y* axis in liquid water under identical LET conditions (~70 keV/μm). Dots represent the energy deposited at points where an interaction occurred. From MUROYA et al. (2006), with permission.

Figure 1.7 illustrates typical two-dimensional representations of short (1-5 μm) track segments of H^+, $^4He^{2+}$, $^{12}C^{6+}$, and $^{20}Ne^{10+}$ ions. The Monte Carlo simulation code IONLYS developed in our laboratory was used to calculate the track segment under the same LET conditions (~70 keV/μm). We can observe that these tracks can be considered as straight lines with the ejected high-energy secondary electrons traveling to a greater average distance away from the track core as the velocity of the incident ion increases, from protons to neon ions. In other words, even though all those particles are depositing the same amount of energy per unit path length, that energy is lost in a volume that increases in the order $H^+ < {}^4He^{2+} < {}^{12}C^{6+} < {}^{20}Ne^{10+}$, indicating that the higher-Z particle (where Z is the ion charge number) has the lower mean density of reactive species (MUROYA et al., 2006; MEESUNGNOEN and JAY-GERIN, 2011). The fact that tracks of different ions with the same LET have different radial distributions of energy deposited by δ-rays is in accord with Bethe's theory of stopping power (BETHE, 1930; BETHE and ASHKIN, 1953) and

indicates that LET is not a unique descriptor of the radiation chemical effects within heavy-charged particle tracks (SCHULER and ALLEN, 1957; SAUER et al., 1977; LAVERNE and SCHULER, 1987; KAPLAN and MITEREV, 1987; FERRADINI, 1990; FERRADINI and JAY-GERIN, 1999; LAVERNE, 2000, 2004).

1.2.2 Time scale of events and formation of primary products (free radicals and molecules) in neutral water radiolysis

The bombardment of the water molecule with high-energy radiation commences the overall chemical change of the water. Depending on the quality of the radiation, the radiation may cause direct ionization or indirect ionization of water. Electromagnetic radiations (X- and γ- rays) and neutral particles (neutrons) are indirectly ionizing; on the other hand, heavy charged particles such α-rays or $^{7}Li^{3+}$ or $^{12}C^{6+}$ cause direct ionization of the water. Indirectly ionizing radiations are always more penetrating than directly ionizing particulate radiations. The overall chemical change of water terminates with re-establishing the chemical equilibrium.

The complex events that accompany the absorption of high energy photons or the passage of fast charged particles in liquid water can be divided in three consecutive, temporal stages: physical, physico-chemical, chemical stages (PLATZMAN, 1958; KUPPERMANN, 1959). These stages correspond with the initial dissipation of energy in the system, the establishment of thermal equilibrium, and the establishment of chemical equilibrium, respectively (Fig. 1.8) (MEESUNGNOEN and JAY-GERIN, 2011). However, in a physiologic system, there follows a biological stage in which the products produced in the physical, physico-chemical, chemical stages interact with the bio-molecules present in the cells (AZZAM et al., 2012).

(i) The physical stage
(ii) The physico-chemical stage
(iii) The chemical stage
(iv) The biological stage

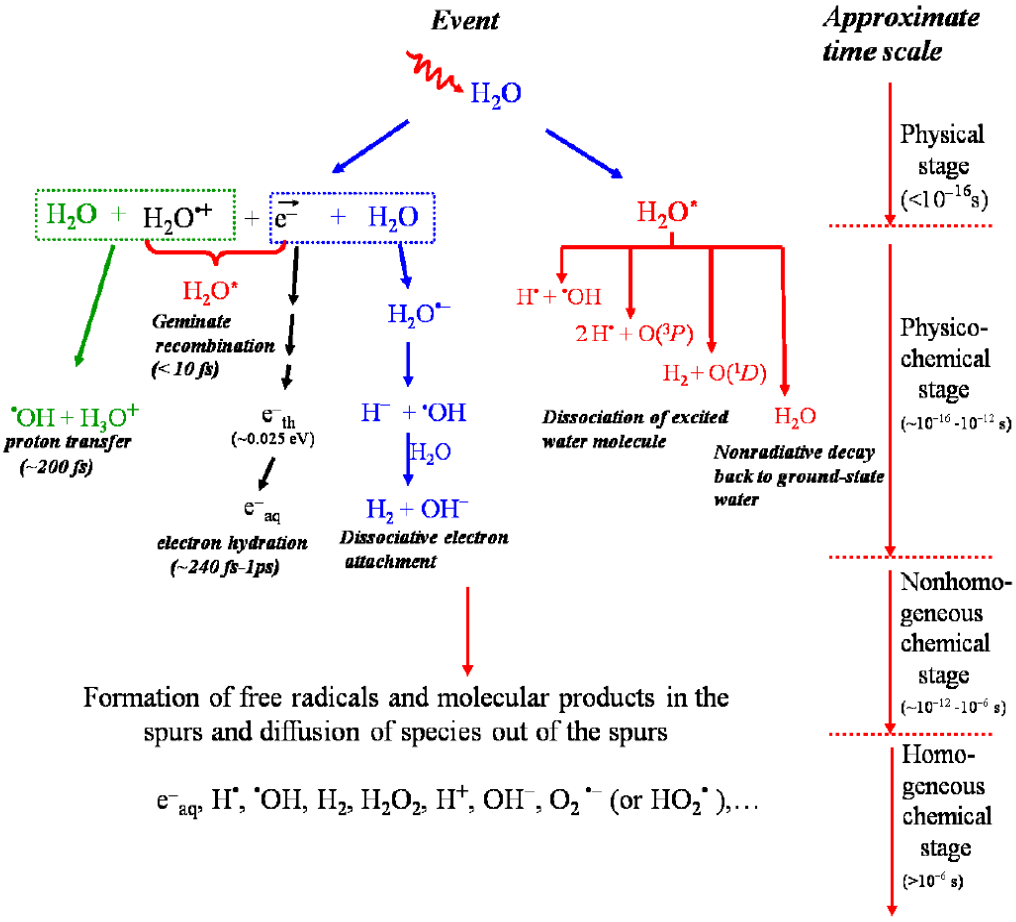

Fig. 1.8: Time scale of events that occur in the low-LET radiolysis of neutral, deaerated water (MEESUNGNOEN, 2007; MEESUNGNOEN and JAY-GERIN, 2010). As a guide to the eyes, we use different colors in the figure in order to contrast the individual processes occurring during the radiolysis of water.

(i) The "physical" stage

The duration of the physical stage is approximately 10^{-16} s, when the transfer of the energy from the incident high-energy radiation to the water takes place. Such absorption of the energy by the water molecules, along with the path of the radiation, produces a large amount of ionized and electronically excited water molecules, which are denoted as $H_2O^{\bullet+}$ and $H_2O^*_{elec}$, respectively.

$$H_2O \rightsquigarrow H_2O^{\bullet+} + e^- \text{ (ionization)} \quad (1.5)$$

$$H_2O \rightsquigarrow H_2O^*_{elec} \text{ (excitation)} \quad (1.6)$$

Note that $H_2O^*_{elec}$ represents here many excited states, including the so-called "superexcited" states (PLATZMAN, 1962*a*) and the excitations of collective electronic oscillations of the "plasmon" type (HELLER et al., 1974; KAPLAN and MITEREV, 1987; LAVERNE and MOZUMDER, 1993; WILSON et al., 2001).

Generally, the electron ejected (which is called a "secondary" electron) in the ionization event has sufficient energy either to ionize or excite one or more other water molecules in the vicinity, and this leads to the formation of "spurs" or "cylindrical track" that contain the products of the events.

(ii) The "physicochemical" stage

The physicochemical stage consists of the processes which lead to the establishment of the thermal equilibrium in the system. The duration of this stage is about 10^{-12} s. During this stage, the ions and excited water dissipate their excess energy by bond rupture, luminescence, energy transfer to neighboring molecules, *etc.*

The secondary ("dry") electron produced from ionized water molecules undergoes scattering as it moves away from its parent ion. The secondary electrons transfer energy due to collision with other water molecules and eventually, it reaches at thermal equilibrium with the water. However, PLATZMAN (1955) stated that the secondary electrons form subexcitation electrons (e^-_{sub}) before it thermalized (e^-_{th}). Once it is thermalized (e^-_{th}) (after ~10-40 fs at 25 °C; see (GOULET et al., 1990, 1996; MEESUNGNOEN et al., 2002*a*), it can get localized or "trapped" (e^-_{tr}) in a pre-existing potential energy well of appropriate depth in the liquid (then forming the so-called "wet" electron whose exact physicochemical nature is still the subject of investigation) before reaching a fully relaxed, hydrated state (e^-_{aq}) as the dipoles of the surrounding molecules orient in response to the negative charge of the electron. In liquid water at room temperature, thermalization, trapping, and hydration can then follow in quick succession (on the time scale of ~240 fs-1 ps, as revealed from time-resolved femtosecond laser

spectroscopic studies) (MOZUMDER, 1999; JAY-GERIN et al., 2008; MEESUNGNOEN and JAY-GERIN, 2011):

$$e^- \rightarrow e^-_{th} \rightarrow e^-_{tr} \rightarrow e^-_{aq} \qquad (1.7)$$

The ejected electron that escapes process (1.7), after reaching the final stage of the energy degradation, can also be temporarily captured by a water molecule to produce a transient water molecule anion. This anion is unstable and undergoes dissociation mainly into H^- and $^{\bullet}OH$:

$$e^- + H_2O \rightarrow H_2O^{\bullet -} \rightarrow H^- + {}^{\bullet}OH \qquad (1.8)$$

The hydride ion produced in this reaction reacts with another water molecule through a fast proton transfer:

$$H^- + H_2O \rightarrow H_2 + OH^- \qquad (1.9)$$

Reactions (1.7)-(1.9) correspond to the so-called "dissociative electron attachment" or DEA process, which has been observed in amorphous solid water at ~20 K for electron energies between about 5 and 12 eV (ROWNTREE et al., 1991). It has been suggested that DEA to water was responsible, at least in part, for the yield of "nonscavengeable" molecular hydrogen observed experimentally in the radiolysis of liquid water at early times (PLATZMAN, 1962*b*; FARAGGI and DÉSALOS, 1969; GOULET and JAY-GERIN, 1989; KIMMEL et al., 1994; COBUT et al., 1996; MEESUNGNOEN et al., 2015). Experimental works have sustained this proposed mechanism, by showing that the previously accepted "nonscavengeable" yield of H_2 is due to precursors of e^-_{aq} and it can be lowered with appropriate dry electron scavengers at high concentrations (PASTINA et al., 1999).

In the course of their thermalization, "dry" electrons can be recaptured by their parent ions due to the Coulomb attraction of the latter which tends to draw them back together to undergo electron-cation "geminate" recombination:

$$H_2O^{\bullet +} + e^- \rightarrow H_2O^*_{vib} \qquad (1.10)$$

As the electron is recaptured, the parent ion is transformed into a (vibrationally) excited neutral molecule.

The positive ion $H_2O^{\bullet+}$, produced in the physical stage of radiation, decomposes to form an $^{\bullet}OH$ radical by transferring a proton to a neighbouring water molecule:

$$H_2O^{\bullet+} + H_2O \rightarrow H_3O^+ + {}^{\bullet}OH \qquad (1.11)$$

where H_3O^+ (or equivalently, H^+_{aq}) represents the hydrated proton. However, OGURA and HAMILL (1973) pointed out that H_3O^+ may randomly migrate during its very short life time (<10 fs) by means of a sequence of resonant electron transfers from neighboring water molecules to the $H_2O^{\bullet+}$ hole (or electron-loss center). The ranges of a migrating hole are a few molecular diameters (COBUT et al., 1998).

Excited water molecules may be produced directly in an initial act [(reaction (1.6)] or by neutralization of an ion [reaction (1.10)]. Very little is known about the decay channels for an excited water molecule in the liquid phase and the branching ratios associated with each of them. Fortunately, the contribution of the water excited states to the primary radical and molecular products in water radiolysis is of relatively minor importance in comparison with that of the ionization processes, so that the lack of information about their decomposition has only limited consequences. Hence, the competing de-excitation mechanisms of H_2O^* are generally assumed to be essentially the same as those reported for an isolated water molecule namely (for example, see: SWIATLA-WOJCIK and BUXTON, 1995; COBUT et al., 1998; MEESUNGNOEN and JAY-GERIN, 2005*a*; SANGUANMITH et al., 2011*a*; KANIKE et al., 2015*b*)

$$H_2O^* \rightarrow H^{\bullet} + {}^{\bullet}OH \qquad (1.12)$$

$$H_2O^* \rightarrow H_2 + O(^1D) \qquad (1.13)$$

$$H_2O^* \rightarrow 2H^{\bullet} + {}^{\bullet}O^{\bullet}(^3P) \qquad (1.14)$$

$$H_2O^* \rightarrow H_2O + \text{release of thermal energy} \qquad (1.15)$$

where $O(^1D)$ and $^{\bullet}O^{\bullet}(^3P)$ represent the oxygen atom in its singlet ^1D first excited state and triplet ^3P ground state, respectively (Fig. 1.7). Note that the dissociation of the excited water molecules via reaction (1.12) is the main source of the initial yield of hydrogen atoms. As for the values of the branching ratios (or decay probabilities) used for the different decay channels (1.12)-(1.15), they are chosen in order to consistently match the

observed picosecond *G*-values of the various spur species (MUROYA et al., 2002; MEESUNGNOEN and JAY-GERIN, 2005*a*). The $O(^1D)$ atoms produced in reaction (13) react very efficiently with water to form H_2O_2 or possibility also $2^{\bullet}OH$ (TAUBE, 1957; BIEDENKAPP et al., 1970). In contrast, ground-state oxygen atoms $^{\bullet}O^{\bullet}(^3P)$ in aqueous solution are rather inert to water but react with most additives (AMICHAI and TREININ, 1969).

By ~1 ps following the passage of the radiation, the various initial radiolysis products are e^-_{aq}, $H^{\bullet}$, H_2, $^{\bullet}OH$, H_2O_2, H^+ (or H_3O^+), OH^-, $O_2^{\bullet-}$ (or $HO_2^{\bullet}$, depending on the pH), $^{\bullet}O^{\bullet}(^3P)$, *etc*. At this time, these species begin to diffuse away from the position where they were originally produced. The result is that a fraction of them react together within the spurs/tracks as they develop in time while the remainders escape into the bulk solution in the chemical stage.

(iii) The "chemical" stage

The third or chemical stage consists of diffusion and reactions of the reactive species present at the end of the physicochemical stage and initially distributed nonhomogeneously with high concentrations in the center of spurs or along the axis of tracks. These species diffuse according to the microscopic diffusion law. This stage is usually divided into two parts. The first part corresponds to the stage of "nonhomogeneous chemistry", which consists of the period after ~10^{-12} s, during which spurs or tracks develop in time. A number of radicals will combine to form the molecular products H_2 and H_2O_2 and to re-form H_2O, while the remainder will diffuse out into the bulk solution. At 25 °C, the spur/track expansion is essentially complete by ~10^{-7}-10^{-6} s (for example, see: BUXTON et al., 1987; SANGUANMITH et al., 2012). At this time, the species that have escaped from spur or track reactions become homogeneously distributed throughout the bulk solution (*i.e.*, the system at large) (PLANTE et al., 2005; MUROYA et al., 2006). Beyond a few microseconds, the reactions which occur in the bulk solution can usually be described with conventional homogeneous chemistry methods. This is the second part of the chemical stage, the so-called stage of "homogeneous chemistry". The radical and molecular products which emerge from the spurs/tracks are then available for reaction with

homogeneously distributed solutes (if any) present (in low or moderate concentrations) at the time of irradiation.

(iv) The "biological" stage

When the irradiation of the water in a biological system takes place, in that case, the biological stage is the final stage in a physiologic system. In this stage, the biomolecules interact with radiolytic products, produced due to radiolysis of the water molecules. The cells responding to the damage resulting from the products formed in the preceding stages. During this stage (~10^{-3} s or longer, depending very much upon the medium), the biological responses affecting the long-term consequences of radiation exposure are induced. In a biological system (cells), there are several macromolecules such as proteins, lipids, carbohydrates as well as ions, for instance, Na^+, K^+, Ca^{2+}, and Cl^-. The diffusions (or mobilities) of the radiolytic products are different than in pure water (NEGENDANK and EDELMANN, 1988; SWIETACH and VAUGHAN-JONES, 2005). In biological systems, ionizing radiation can also stimulate inducible nitric oxide synthase (iNOS) activity in hit cells (MIKKELSEN and WARDMAN, 2003), thereby generating large amounts of nitric oxide $^{\bullet}NO$ (officially called nitrogen monoxide). Although $^{\bullet}NO$ is chemically inert toward most cellular constituents (except for heme), it reacts quickly with $O_2^{\bullet-}$ to form the peroxynitrite anion ($ONOO^-$) with a rate constant (1.9×10^{10} M^{-1} s^{-1}) that is larger than that for the copper/zinc-superoxide dismutase (SOD)-catalyzed disproportionation of $O_2^{\bullet-}$ (4×10^9 M^{-1} s^{-1}) (KOPPENOL, 1998; JAY-GERIN and FERRADINI, 2000). Like $^{\bullet}OH$ radicals, $ONOO^-$ and its conjugate acid, peroxynitrous acid ONOOH (pK_a = 6.8 at 37 °C) (PRYOR and SQUADRITO, 1995), are powerful oxidizing agents. They are capable of attacking a wide range of cellular targets, including lipids, thiols, proteins, and DNA bases (for example, see: HALLIWELL and GUTTERIDGE, 2015).

1.3 Boron neutron capture nuclear reaction

Boron-10 is a non-radioactive material. It has high propensity to capture thermal neutron with the neutron capture cross section of 3835 barns (1 barn = 10^{-28} m^2), which is 6 times higher than uranium-235 and three orders of magnitude higher than nuclei of living tissue (SAUERWEIN, 2012). Boron-10 becomes a boron-11 nuclide upon absorbing a thermal neutron and undergoes the fission reaction, which produces an α-particle ($^4He^{2+}$) and a lithium ion ($^7Li^{3+}$). These low energy recoil heavy ions have very short penetration lengths (~5-9 μm) in water and high-LET characteristics (BARTH, 2003). Because of the unique properties of boron-10, it has been extensively used in the field of nuclear industry. Moreover, the $^{10}B(n,\alpha)^7Li$ nuclear reaction has been used in clinical studies of biochemically targeted radiotherapies for cancer treatment known as "boron neutron capture therapy" or BNCT (HOSMANE et al., 2012).

1.3.1 Boron neutron capture nuclear reaction in nuclear industry

Water is used as a coolant and a neutron moderator in light water reactors (LWRs), which is one of the abundant commercial type nuclear reactors at present. LWRs are categorized into two types: boiling water reactors (BWRs) and pressurized water reactor (PWRs), based on the coolant flow structure, phase of water, and operating condition.

Water is inevitably exposed to the extreme conditions of high temperature, high pressure (~285 °C, 7.2 MPa), as well as intense flux of ionizing radiation (mostly fast neutrons and γ-rays) when it passes through the core of the nuclear reactors for BWRs (BUXTON, 2003). Boron carbide (B_4C), enriched in ^{10}B, is used as a control-rod material (neutron absorber) in BWRs. In addition, boron as boric acid (H_3BO_3) is generally added as a water-soluble neutron poison in the primary coolant of PWRs to control the neutron flux and the reactivity in the core (PUCHEAULT, 1961; KOIKE et al., 1969; COHEN, 1980). Therefore, the recoil ions arising from $^{10}B(n,\alpha)^7Li$ reaction act as a source of high-LET radiation in the primary coolant of the PWRs, thereby leading to the formation of different types of chemical species such as e^-_{aq}, $H^\bullet$, $^\bullet OH$, and $HO_2^\bullet/O_2^{\bullet-}$, H_2, H_2O_2, and O_2, *etc.*, due to the radiolysis of water. The presence of H_2O_2 and O_2 from water radiolysis is widely known to create an oxidizing environment in the water coolant (WADA et al., 2001;

SATOH et al., 2004). Understanding the radiation chemistry of the coolant water in reactors is important for maintaining the proper chemical environment that will minimize the degradation of materials. Unfortunately, there is not enough experimental data available on the formation of the primary species and their yields (*G*-values) for $^{10}B(n,\alpha)^{7}Li$ recoil irradiation of neutral water or water at nuclear reactor conditions (COHEN, 1980; CHRISTENSEN, 2006). The yields of the different species due to ionizing radiation in the nuclear reactor are very important to control the corrosion of the reactor and to maintain a proper chemical environment inside it.

1.3.2 Boron neutron capture nuclear reaction in cancer treatment

BNCT is another very important use of the $^{10}B(n,\alpha)^{7}Li$ nuclear reaction for cancer treatment. BNCT is a technique that selectively aims tumor cells while sparing healthy cells using boron compounds. In 1936, Gordon LOCHER proposed the principle of this method, where he hypothesized that boron compounds could be selectively accumulated in tumor cells. This is followed by irradiation with thermal or epithermal neutrons. A non-radioactive boron-10 atom absorbs a low energy neutron and subsequently produces two ionizing recoil ions, namely, a α-particle ($^{4}He^{2+}$) and a lithium ion ($^{7}Li^{3+}$) with high-LET characteristics; the LET values are ~196 and 210 keV/µm, respectively. However, the ranges of these ionizing radiations are very short (~5-9 µm), which is approximately the same as the diameter of biological cells. Hence, their energy deposition is almost limited to the diameter of a single cell (LOCHER, 1936; ISLAM et al., 2017).

Figure 1.9 represents the basic principle of BNCT.

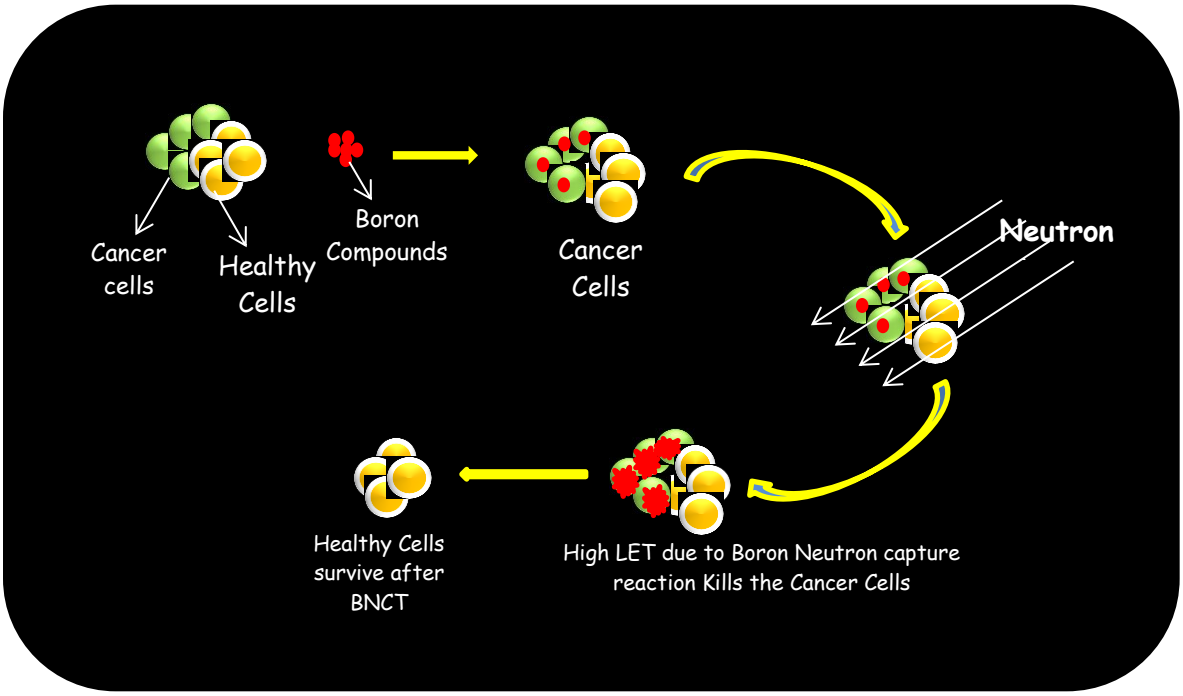

Fig. 1.9: Graphical representation of the Boron Neutron Capture Therapy.

1.4 Effect of temperature on water radiolysis due to the $^{10}B(n,\alpha)^{7}Li$ nuclear reaction

The effect of temperature on water radiolysis is practically applicable in nuclear reactor, since it is operated at high temperature ~275-375 °C. The cooling water is subjected to an intense mixed radiation field such as low-LET γ-radiation and also fast neutrons. Boron carbide (B_4C) rods and boric acid (H_3BO_3) are used as neutron poisons in the primary coolant of BWRs and PWRs, respectively, to control the neutron flux and the reactivity in the core (PUCHEAULT, 1952; KOIKE et al., 1969; COHEN, 1980). Upon capturing a thermal neutron, the boron neutron capture nuclear fission reaction takes place inside the reactor producing short-range, high-LET radiations, which interact with water molecules to produce several unwanted radiolytic oxidizing species, such as $^{\bullet}OH$, H_2O_2, O_2, and $O_2^{\bullet-}$ (or $HO_2^{\bullet}$, depending on the pH). These oxidizing species are highly reactive with most metal alloys and can significantly increase the corrosion and degradation of reactor components. It is necessary to select optimum conditions in the reactor in order to suppress formation of oxidizing species, which can furthermore cause deleterious corrosion, hydriding, and cracking processes both in the core and in the associated piping

components (BURNS and MOORE, 1976; COHEN, 1980; HICKEL, 1991; ELLIOT, 1994; ELLIOT et al., 1996*a*; McCRACKEN et al., 1998; BUXTON, 2001; STUART et al., 2002; KATSUMURA, 2004; CHRISTENSEN, 2006; EDWARDS et al., 2007). This can be achieved most efficiently when the radiation chemistry of water under reactor operation conditions is understood. However, direct measurement of the chemistry in and around reactor cores is extremely difficult, due to the conditions of high temperature, pressure, and mixed neutron/gamma radiation fields. For these reasons, theoretical calculations and chemical models using computer simulation methods are very powerful tools to predict the detailed radiation chemistry in the core of nuclear reactor and the consequences for materials.

To predict the effect of radiation at elevated temperatures in particular or in reactor conditions in general, it is necessary to know the temperature dependence of the chemical yields of oxidizing ($^{\bullet}OH$ and H_2O_2) and reducing (e^-_{aq}, $H^{\bullet}$, and H_2) radiolytic species for the $^{10}B(n,\alpha)^7Li$ recoil ions as well as the temperature dependence of the rate constants for the various reactions taking place in spurs and tracks that result in these primary yields. In this study, we computed the yields of these primary species as a function of temperature. We observed that the computed values for yields of free radicals are lower than the yields of the molecular products. This general trend is a reflection of the high-LET character of the $^{10}B(n,\alpha)^7Li$ recoils. Overall, the simulation results agreed very well with existing estimates at 20 and 289 °C from COHEN (1980) and CHRISTENSEN (2006), respectively. For deaerated 0.4 M H_2SO_4 solutions, reasonable agreement between experiment and simulation was also found at room temperature. Nevertheless, more experimental data for both neutral and acidic solutions would be needed to better describe the dependence of radiolytic yields on temperature and to test our modeling calculations more thoroughly. We also observed the non-monotonic inflection in the yields of H_2 and H_2O_2 around 150 °C. The bimolecular self-reaction of the hydrated electrons is known to play a very important role in the formation of molecular hydrogen:

$$e^-_{aq} + e^-_{aq} \rightarrow H_2 + 2OH^- \qquad (1.16)$$

However, the reaction is believed to be two-step reaction (MARIN et al., 2007) with formation of the dielectron:

$$e^-_{aq} + e^-_{aq} \rightarrow e_2^{2-}{}_{aq} \quad (1.17)$$

$$e_2^{2-}{}_{aq} \rightarrow H_2 + 2OH^- \quad (1.18)$$

Moreover, the experimental values of the rate constant of the bimolecular self-reaction of the hydrated electron in neutral or slightly acidic water are required to accurately determine the yields of H_2 and H_2O_2 above ~150 °C.

1.5 Formation of H_3O^+ in spurs or tracks

In the physical stage, the water molecules along the radiation path absorb energy from the ionizing radiation which causes the ionization of the water molecule ($H_2O^{\bullet+}$) by ejecting an electron. The formation of H_3O^+ takes place via a proton transfer reaction, therefore rendering the spur or track more acidic than the surroundings (SPINKS and WOODS, 1990). Hydrolysis of the aqueous solution of 1,1-diethoxyethane [$CH_3CH(OC_2H_5)_2$] buffered at pH 7 was observed when irradiated with 40 kV_p X-rays. In neutral condition, the hydrolysis of 1,1-diethoxyethane does not occur. The pH of the spur would need to be ~1.4 to account for the observed hydrolysis (SMITH and STEVENS, 1963). Another experiment indicative of an acid spur was the observation of a transient absorption attributed to $Cl_2^{\bullet-}$ in the pulse radiolysis of neutral aqueous sodium chloride solutions at Cl^- concentrations of 0.1 M or greater (ANBAR and THOMAS, 1964). An acidic medium is the pre-requisite for the production of $Cl_2^{\bullet-}$. Radiation-induced $^\bullet OH$ radicals react with chloride ions to produce chloride radicals ($Cl^\bullet$) according to reaction (1.19). However, this reaction is pH-dependent, which represents the importance of the acidity in the irradiated solution (MATSUYAMA and NAMIKI, 1965):

$$Cl^- + {}^\bullet OH + H_3O^+ \rightarrow Cl^\bullet + 2H_2O \quad (1.19)$$

$$Cl^\bullet + Cl^- \rightarrow Cl_2^{\bullet-} \quad (1.20)$$

Apart from these experiments, there are virtually no other demonstrations of this transient acidic pH effect in irradiated water although its potential biological impact has already been discussed by some authors (BYAKOV and STEPANOV, 2006). Using Monte Carlo simulations, KANIKA et al. (2016) estimated that the pH inside a spur, produced by low-LET radiation such as cobalt-60, fast electrons or 300-MeV protons (LET ~ 0.3 keV/μm),

is about 3.3 up to nanoseconds (10^{-9} s). In case of $^{10}B(n,\alpha)^{7}Li$ fission reaction in aqueous or other media, it produces high-LET α-rays and $^{7}Li^{3+}$ recoil ions which produce tracks in opposite directions. In this study, we have calculated the concentration of H^+ and subsequently the pH value along the tracks produced in water by the $^{10}B(n,\alpha)^{7}Li$ reaction. The concentration of H^+ is calculated using equation (1.21) and the pH is calculated using equation (1.22):

$$C = \rho\, \mathcal{D}\, G \tag{1.21}$$

where C is the concentration of the considered species, ρ is the density of the solution (1 g/cm^3 for liquid water at 25 °C), $\mathcal{D}$ is the radiation dose, and G is the chemical yield (for example, see: HUMMEL, 1995). Note that with C in mol/dm^3, $\mathcal{D}$ in J/kg (or Gy), and G in mol/J, the density is to be expressed in kg/dm^3 in order to have a consistent set of units. Acidity of a system is described by its pH, defined as the negative logarithm (base 10) of the concentration of H_3O^+ ions:

$$\mathrm{pH}(t) = -\log\{[H_3O^+](t)\} \tag{1.22}$$

For high-LET radiation, we consider the track as being an axially homogeneous cylinder, of length L = 1 μm and initial radius r_c equal to the radius of the physical track "core" (which corresponds to the tiny radial region within the first few nanometers around the impacting ion trajectory). In this region, the density of energy deposition is very high (CHATTERJEE and HOLLEY, 1993; MEESUNGNOEN and JAY-GERIN, 2011; MOZUMDER, 1999; MAGEE and CHATTERJEE, 1980, 1987). We first used our Monte Carlo simulation code to calculate $G(H_3O^+)$ and then the concentration of H^+ along the radiation track is obtained using equation (23):

$$[H_3O^+] = G(H_3O^+)(t) \times \left(\frac{LET}{\pi\, r(t)^2}\right) \tag{1.23}$$

where

$$r(t)^2 = r_c^2 + 4\, D\, t\,. \tag{1.24}$$

$r(t)$ represents the change with time of r_c due to the three-dimensional diffusive expansion of the track. Here, r_c was estimated directly from our simulations (ISLAM et al., 2017). The diffusion (mobility) of the proton in intracellular water in ~100-1000 times lower than in free water (NEGENDANK and EDELMANN, 1988; SWIETACH and VAUGHAN-JONES, 2005). It is thus considered that the slow diffusion of the proton in the cellular water may cause an intense, much longer acidity effect on the cell (ISLAM et al., 2017).

1.7 Research objective

The goal of this research is to better understand the radiation chemistry and the mechanisms involved in the radiolysis of water by the $^{10}B(n,\alpha)^{7}Li$ nuclear reaction recoils as a function of temperature in the range of 25-350 °C. In this research work, we have reported the yields of the various radiolytic products as a function of temperature and our simulation results agree well with the existing experimental results. Our calculated yields of H_2 and H_2O_2 above ~150 °C show a non-monotonic behavior. However, to confirm this result, more experimental data of the (e^-_{aq} + e^-_{aq}) reaction rate constant in near-neutral water or slightly acidic solution are needed.

We use here Monte Carlo track chemistry simulations to calculate, at 25 °C, the time evolution of the yields of H_3O^+ produced in the radiolysis of pure, deaerated water from ~1 ps to 1 μs due to the $^{10}B(n,\alpha)^{7}Li$ nuclear reaction. The concentrations of H_3O^+ and the corresponding pH values for each recoil ion considered are then obtained from our calculated yields of H_3O^+ along the ionizing radiation track. Such estimation of the acidic pH might play an important role for the corrosion safety assessment of the reactor in nuclear power plants. Moreover, the primary biological response of living organisms to the passage of the ionizing radiation is traditionally considered to be dominated by the chemical reactions of the radiolytic products of the radiolysis of the cellular water ($^{\bullet}OH$, $H^{\bullet}$, e^-_{aq}, $O_2^{\bullet-}$, H_2, H_2O_2, *etc*.). However, in bulk cell water, the initial conditions of high acidity persist over a much longer period of time (about 2-3 orders of magnitude) due to the much lower value of the intracellular diffusion coefficient of the free proton. This research work indicates that hydronium ions or protonated water molecules might play a very significant role in the biological action of ionizing radiations as it is well known that biological systems are very sensitive to variations in acidity.

2. MONTE CARLO SIMULATIONS

The complex sequence of events that are generated in liquid water and dilute aqueous solutions after the absorption of ionizing radiation can be modelled using Monte-Carlo simulation techniques. Such a procedure is well adapted to account for the *stochastic* nature of the phenomena, provided the realistic probabilities and the cross sections for all possible events. The simulation then allows one to reconstruct the complicated action of the radiation. It also offers a powerful tool for estimating the validity of different assumptions, for making a critical examination of proposed reaction mechanisms, and for estimating some unknown parameters. The accuracy of these calculations is best determined by comparing their predictions with experimental data on well-characterized chemical systems that have been examined with a wide variety of incident radiation particles and energies.

TURNER and his coworkers (1981,1983,1988*b*) at the Oak Ridge National Laboratory (Oak Ridge, Tennessee, U.S.A.) jointly with MAGEE and CHATTERJEE at Lawrence Berkeley Laboratory (Berkeley, California, U.S.A.) were the first to use Monte-Carlo calculations to derive computer-plot representations of the chemical evolution of a few keV electron tracks in liquid water at times between ~10^{-12} and 10^{-7} s. ZAIDER and BRENNER (1984) also described such an approach, and their calculated time-dependent yields of e^-_{aq} and $^{\bullet}OH$ radicals were somewhat similar to values measured or derived in pulse-radiolysis studies of pure water. Following these pioneering works, stochastic simulation codes employing Monte Carlo procedures were used with success by a number of researchers to study the relationship between the track structure and the following chemical processes that occur in the radiolysis of both pure water and water containing solutes (for a comprehensive list and reviews, see, for example: BALLARINI et al., 2000; UEHARA and NIKJOO, 2006). Two main approaches have been widely used: (1) the "step-by-step" (or random flights Monte Carlo simulation) method, in which the trajectories of the diffusing species of the system are modeled by time-discretized random flights and in which reaction occurs when reactants undergo pair wise encounters, and (2) the "independent reaction times" (IRT) method (CLIFFORD et al., 1986; PIMBLOTT et al., 1991; PIMBLOTT and GREEN, 1995), which allows the calculation of reaction times

without having to follow the trajectories of the diffusing species. Among the stochastic approaches, the most reliable is certainly the full random flights simulation, which is generally considered as a measure of reality. However, this method can be exceedingly consuming in computer time when large systems (such as complete radiation tracks or track segments) are studied. The IRT method, a computer efficient stochastic simulation technique, has been devised to achieve much faster realisation than are possible with the full Monte-Carlo model. In essence, it relies on the approximation that the distances between pairs of reactants evolve independently of each other, and therefore the reaction times of the various potentially reactive pairs are independent of the presence of other reactants in the system.

In a program begun in the early 1990's, our group has also developed and progressively refined with very high levels of detail several Fortran-based Monte Carlo codes that simulate the track structure of ionizing particles in water, the production of the various ionized and excited species, and the subsequent reactions of these species in time with one another or with available solutes (COBUT et al., 1994, 1998; FRONGILLO et al., 1996, 1998; HERVÉ DU PENHOAT et al., 2000; MEESUNGNOEN et al., 2001, 2003, 2013, 2015; MEESUNGNOEN and JAY-GERIN, 2005*a*,*b*; MUROYA et al., 2002, 2006). A most recent version of the codes, called IONLYS-IRT (MEESUNGNOEN and JAY-GERIN, 2005*a*,*b*), has been used in the present work. Briefly, the IONLYS step-by-step simulation program models all events of the physical and physicochemical stages in the track development. The third and final nonhomogeneous chemical stage is covered by the program IRT, which employs the IRT method (CLIFFORD et al., 1986; GREEN et al., 1990; PIMBLOTT et al., 1991) to model the chemical development that occurs during this stage and to simulate the formation of measurable yields of chemical products. The detailed description and implementation of the IONLYS-IRT has already been given (MEESUNGNOEN and JAY-GERIN, 2005*a*,*b*, and references therein), and will not be reproduced here, only a brief overview of the most essential features of the simulation methodology and reaction scheme, pertinent to the current calculations, is given below.

2.1 The IONLYS code

The IONLYS simulation code is used to cover the early "physical" and "physicochemical" stages of radiation action up to ~10^{-12} s. It is actually composed of two codes, one (named TRACPRO) for transporting the investigated incident charged particle (proton or any other heavy ion projectile) and another one (named TRACELE) for transporting all of the energetic electrons (collectively named "secondary electrons") that result from the passage of ionizing particle in liquid water. The code models, event by event, *all* the basic physical interactions (energy deposition) and the subsequent establishment of thermal equilibrium in the system (conversion of the physical products created locally after completion of the physical stage into the various "initial" chemical species of the radiolysis).

In particular, IONLYS provides the detailed distribution of coordinates of *all* physical events, including ionization, electronic and vibrational excitation of single water molecules, and excitation of plasmon-type collective modes, that occur locally during the slowing-down of the irradiating charged particle and of all the secondary electrons that it has generated. The particle will interact with water based on the probability per unit distance of each particle's energy or cross section. The code begins by selecting a particular distance to the first interaction site for the incident particle. The calculation continues with the random choice of the type of interaction (ionization, excitation of electronic, vibrational and rotational levels of single water molecules, excitation of plasmon-type collective modes, and elastic scattering) that occurs. This cross section entered as input data in the code, based on direct measurement or on theoretical estimations. These collisions cross sections are needed to follow the history of the charged particle. If an inelastic collision is ionization, the particle's energy is reduced by the energy loss selected. The secondary electron produced is given a kinetic energy equal to this energy loss minus the binding energy (or ionization energy) of the target electron. The energy-dependent cross sections for the elastic and inelastic processes occurred, angular distributions, are entered as input data as well. Delta rays are produced at sites of high energy loss. Each time a secondary electron is produced, the code proceeds by transporting it until its energy falls below the threshold for electronic excitations, equal to ~7.3 eV for

liquid water (MICHAUD et al., 1991) (these electrons are denoted as "subexcitation" electrons). If a collision is elastic, an angle of scattering is selected and the flight distance for the next collision site is chosen. The probabilities or cross sections for all of the individual molecular processes and their alternatives are entered as input data in Monte-Carlo code, based on direct measurements (where available, cross section data in the case of liquid water are scarce) or on the theoretical estimations (COBUT et al., 1998; MEESUNGNOEN and JAY-GERIN, 2005*a*). These collision cross sections are needed to follow the history of an energetic charged particle and its products, covering all ranges of energy transferred in individual collisions. Most importantly, they provide the mean free path used to determine the distance to the next interaction, the type of interaction at each event, energy loss, and the angle of emission of the scattered particle (for example, see: DINGFELDER and FRIEDLAND, 2001; NIKJOO et al., 2006; DINGFELDER et al., 2008). The computer simulation thus provides complete information on the spatial distribution of ionized and excited water, $H_2O^{\bullet+}$ and H_2O^*, and subexcitation electrons, e^-_{sub} (energy < 7.3 eV), produced along the incident charged particle trajectory during the physical stage of the radiation action. This stage is concluded in ~10^{-15} s. Full details of the *cross-section database* used in the IONLYS code can be found in the references cited (COBUT, 1993; COBUT et al., 1998; MEESUNGNOEN and JAY-GERIN, 2005*a*). It is worth mentioning that this code, which uses protons or heavy ions as the primary particles, is particularly well adapted to the study of the fast-neutron radiolysis of water, since the ionizing particles involved in this case are proton and oxygen ion recoils. Interestingly, the choice of proton impact in the Sherbrooke code was originally adopted owing to the fact that protons represent, by far, the most comprehensive database of cross sections for bare ion collisions (not only on water but also on a number of different target atoms or molecules; *e.g.*, see RUDD, 1990; RUDD et al., 1992; IAEA-TECDOC-799, 1995; DINGFELDER et al., 2000), and also because they constitute a valuable tool for studying LET effects on radiolytic yields (COBUT et al., 1998). Another great advantage of the code is that, while it was devised for protons, it can also be used for heavier ion projectiles by assuming that the interaction cross sections scale as Z^2, where Z is the projectile charge number. In this scaling procedure, based on the lowest-order (or first Born) approximation of perturbation theories, the cross sections for bare ion impact are approximately Z^2 times

the cross sections for proton impact *at the same velocity*. This simple Z^2 scaling rule, which holds at sufficiently high impact energies (say above ~1 MeV/nucleon) where the interactions are not too strong, is particularly useful for providing cross sections for ionization and excitation by ion projectiles, especially as there are only limited experimental data available involving ions heavier than proton or helium in collision with water molecules (MEESUNGNOEN and JAY-GERIN, 2005; MEESUNGNOEN, 2007; MEESUNGNOEN and JAY-GERIN, 2010; INOKUTI, 1971). In practice, the stochastic selection of the scattering events is done with various sampling techniques (direct inversion, *etc.*; *e.g.*, see KNUTH, 1998; DEGROOT and SCHERVISH, 2002) in accordance to the appropriate scattering cross sections for each process induced by the considered charged particle. All these techniques use pseudo-random numbers uniformly distributed on the interval between 0 and 1.

The simulations performed with IONLYS consist in the generation of short high-energy proton (ion) *track segments* in water. The primary particle is simulated until it has penetrated the chosen length of the track segment into the medium. Note that, due to its large mass, the proton (or the impacting heavy ion) is almost not deflected by collisions with the target electrons. In the present simulations, these deflections are simply neglected. The use of small path segments is particularly useful as the instantaneous LET of the incident particle is nearly constant over such segments and can be varied simply by changing its energy. All of the produced energetic (dry) secondary electrons are explicitly transported spatially from their initial energies until they reach the subexcitation energy region below ~7.3 eV, the threshold assumed for electronic excitation in liquid.[1] The location, type of collision, specific quantum transition, and energy transferred are determined by the IONLYS code, event by event. All physical details about the various elastic and energy-loss processes involved and the corresponding scattering cross sections employed by IONLYS for the simulation can be found in COBUT (1993), COBUT et al. (1998), and MEESUNGNOEN and JAY-GERIN (2005*a*).

[1] Recall here that most energy-loss events by the fast primary charged particle involve small transfers of energy. In fact, Monte-Carlo simulations have shown that the most probable energy loss for liquid water is 15-20 eV, while the track-averaged mean energy loss is around 50-60 eV, depending on the authors (LAVERNE and PIMBLOTT, 1995; COBUT et al., 1998; AUTSAVAPROMPORN, 2006). COBUT et al. (1998) also calculated that, if we sum all the electrons ejected directly by the primary particle and by the successive generations of secondary electrons, 88% of them have kinetic energies less than 20 eV.

The time that a secondary electron takes to reach a subexcitation energy is $<10^{-15}$ s. The thermalization of subexcitation electrons is treated by IONLYS using the distribution of thermalization distances obtained from Monte Carlo track-structure calculations (GOULET and JAY-GERIN, 1989; GOULET et al., 1990, 1996; MEESUNGNOEN et al., 2002*b*) based on experimental scattering cross sections of slow (~1-100 eV) electrons in amorphous ice films at 14 K (MICHAUD et al., 2003) with corrections to account for the liquid phase. Given the initial position of the subexcitation electron, its position is simply displaced in a randomly selected, isotropic direction by the corresponding, energy-dependent mean penetration distance.

At this new position, the electron is regarded as thermalized and subsequently trapped and hydrated. However, an approximation likely to be valid in a highly polar medium such as liquid water in which very low energy (*e.g.*, "sub-vibrational") electrons have a strong tendency – due to the presence of a large density of possible electron trapping sites – to get instantly trapped prior to thermalization (MOZUMDER, 1999). As mentioned before, the time scale of thermalization, trapping, and hydration of a subexcitation electron in liquid water at 25 °C is less than $\sim 10^{-12}$ s. Finally, it is worth recalling here that a certain proportion of subexcitation electrons actually never get thermalized, but instead undergo prompt recombination[2] with their positive parent ion $H_2O^{\bullet +}$ or dissociative attachment (DEA) onto a surrounding H_2O molecule (see Figure 1.2). All details about the various parameters intervening in the IONLYS code to describe this competition between thermalization, geminate recombination, and dissociative attachment, as well as the values of the branching ratios used in the code for the different dissociative decay channels of the electronically and vibrationally excited H_2O molecules, can be found in SANGUANMITH et al. (2011*a*).

[2]About 25.5% of the subexcitation electrons are found to initially recombine with $H_2O^{\bullet +}$ (MEESUNGNOEN and JAY-GERIN, 2005*a*), with an average recombination time as short as a few femtoseconds (GOULET et al., 1990). This average recombination time shows that the recombination process mainly occurs on the water cation and *not* on H_3O^+, that is, before the proton transfer reaction $H_2O^{\bullet +} + H_2O \rightarrow H_3O^+ + {}^{\bullet}OH$ takes place (~10 fs) (which would change the nature of the cation and therefore affect the values of the recombination cross section). In other words, the subexcitation electron recombines quickly (in the first steps of its random walk) on $H_2O^{\bullet +}$. If it does not recombine quickly, it will never recombine, and will thus become thermalized (unless, of course, it makes a dissociative attachment on a water molecule) (~56 fs), trapped (~50-300 fs), and hydrated (~240 fs-1 ps) (MEESUNGNOEN and JAY-GERIN, 2005a; JAY-GERIN et al., 2008 and references therein).

2.2 The IRT code

The complex spatial distribution of reactants at the end of the physicochemical stage (~1 ps; we assume that this time also marks the beginning of diffusion), which is provided as an output of the IONLYS program, is then used directly as the starting point for the subsequent nonhomogeneous chemical stage. This third and final stage, during which the individual reactive species diffuse randomly at rates determined by their diffusion coefficients and react with one another (or with any added solutes present at the time of irradiation) until all spur or track processes are complete, is covered by the IRT program (CLIFFORD et al., 1986; GREEN et al., 1990; PIMBLOTT et al., 1991). IRT is a computer efficient stochastic simulation technique that is used to simulate reaction times without following the trajectories of the diffusing species. This method is based on the approximation that the distances between pairs of reactants evolve independently of each other, and therefore the reaction times of the various potentially reactive pairs are independent of the presence of other reactants in the system. In essence, the simulation begins by considering the initial, or "zero-time", spatial distribution of the reactants (given by the IONLYS program). The separations between all the pairs of reactants are first calculated. Overlapping pairs (*i.e.*, pairs formed in a reactive configuration) are assumed to combine immediately. For each remaining pair, a reaction time is stochastically sampled according to the reaction time probability distribution function (GREEN et al., 1990; GOULET and JAY-GERIN, 1992; FRONGILLO et al., 1998) that is appropriate for the type of reaction considered. This function depends upon the initial distance separating the species, their diffusion coefficients, their Coulomb interaction (for reactions between ionic species), their encounter distance (derived from the Smoluchowski equation), and the probability of reaction during one of their encounters. The competition between the various reactions is taken into account by realizing them in the ascending order of sampled reaction times.

When a reaction occurs, the reactants become unavailable for the competing reactions that are sampled to occur at longer times but one must then consider the possible reactions of the newly formed products with the species that have survived up to that point.

The minimum of the new ensemble of reaction times is the next reaction time. The simulation proceeds in this manner until a pre-defined cut-off time is reached or all the potentially reactive pairs have reacted. Since the IRT method is solely based on a comparison of reaction times, it does not follow the trajectories of the diffusing species.

Therefore, a special procedure must be devised to sample the positions of the reaction products and of the species with which newly formed species can, in turn, react (CLIFFORD et al., 1986). The inclusion of a scavenger in the system does not affect the general simulation technique. In fact, the IRT program allows one to incorporate in a simple way pseudo first-order reactions of the radiolytic products with various scavengers that are homogeneously distributed in the solution, such as H^+, OH^-, and H_2O itself, or more generally any solute for which the relevant reaction rates are known. Similarly, the truly first-order fragmentations of the species are easily simulated. Finally, the IRT method is very well suited for the description of reactions that are only partially diffusion-controlled (most reactions that occur in irradiated water are not diffusion-controlled even at room temperature), an adequate description of the activation processes that are involved in those reactions is a prerequisite for the modeling of the effects of high temperature on water radiolysis), in which the species do not react instantaneously on encounter but experience, on the average, many encounters and separations before they actually react with each other. The ability of the IRT method to give accurate time-dependent chemical yields under different irradiation conditions has been well validated by comparison with full random flights (or "step-by-step") Monte-Carlo simulations, which do follow the particle trajectories in detail (PIMBLOTT et al., 1991; GOULET et al., 1998; PLANTE, 2009).

An approximate dependence of the diffusion coefficient on temperature in liquids can often be found using the Stokes–Einstein equation, which predicts that (ELLIOT, 1994)

$$D\eta / T = \text{constant} = 6.657 \times 10^{-15} \text{ kg m s}^{-2} \text{ K}^{-1} , \qquad (2.1)$$

where D is the diffusion coefficient of the species (m^2/s), η is the dynamic viscosity of the solvent (kg m^{-1} s^{-1}), and T is the absolute temperature (K). Compared to the original version of our IRT program some diffusion coefficients of reactive species and the temperature

dependence of reaction rate constants have been updated. Figure 2.1 shows the diffusion coefficients of various species as a function of temperature that are used in our Monte-Carlo simulations. The list of the main track chemical reactions and the values of reaction rate constants considered in our simulations of the radiolysis of pure liquid water as a function of temperature is taken, for a large part, from the recent report compiled by ELLIOT and BARTELS (2009). For reference, this list is given, at 25 °C, in Table 1.

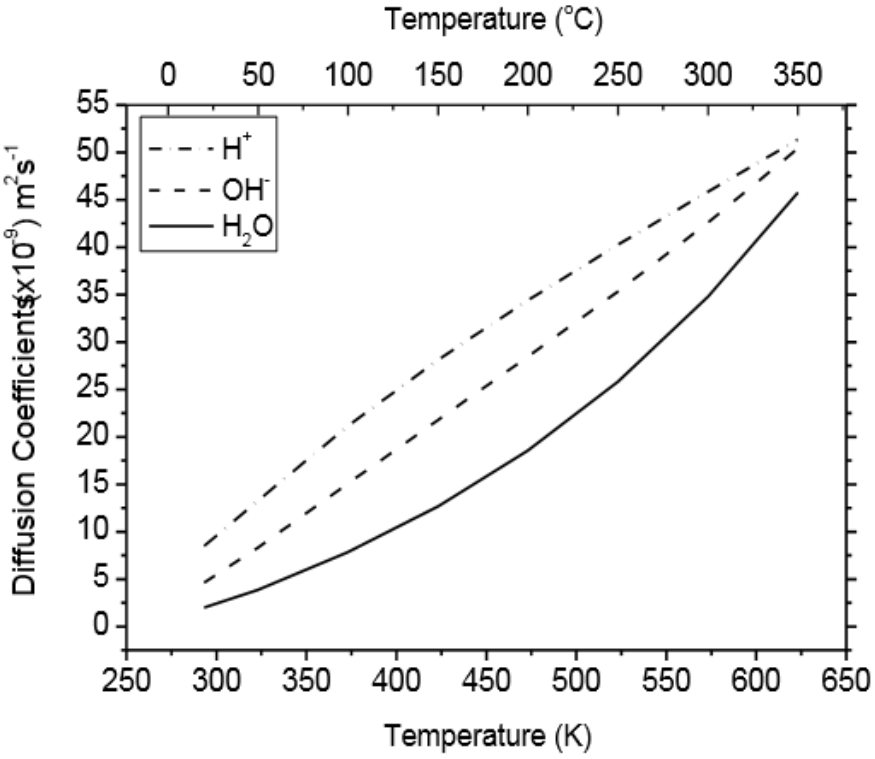

Fig. 2.1: Diffusion coefficients (*D*) for various track species involved in our simulations (ELLIOT and BARTELS, 2009).

Finally, in the present study, all our calculations were performed by simulating short (typically, ~1-5 μm) track segments of the two He and Li ions emitted from the $^{10}B(n,\alpha)^{7}Li$ nuclear reaction, over which the energy and LET of each ion are well defined and remain nearly constant. Such model calculations thus gave "track segment" yields (LAVERNE, 2004) at a well-defined LET. The number of individual ion "histories" (usually ~2-10) was chosen so as to ensure only small statistical fluctuations in the computed averages of chemical yields, while keeping acceptable computer time limits.

Table 1: Main track reaction scheme and rate constants (k) for the radiolysis of pure liquid water at 25 °C (MEESUNGNOEN, 2007). Some values of k have been updated by using the most recently available data of ELLIOT and BARTELS (2009). For first-order reactions, the value of k is given in s^{-1}.

Reaction	k ($M^{-1}s^{-1}$)	Reaction	k ($M^{-1}s^{-1}$)
$H^{\bullet} + H^{\bullet} \rightarrow H_2$	5.2×10^{9}	$e^{-}_{aq} + e^{-}_{aq} \rightarrow H_2 + 2\,OH^{-}$	7.3×10^{9}
$H^{\bullet} + {}^{\bullet}OH \rightarrow H_2O$	1.6×10^{10}	$e^{-}_{aq} + H^{+} \rightarrow H^{\bullet}$	2.1×10^{10}
$H^{\bullet} + H_2O_2 \rightarrow H_2O + {}^{\bullet}OH$	3.6×10^{7}	$e^{-}_{aq} + O_2^{\bullet-} \rightarrow H_2O_2 + 2\,OH^{-}$	1.3×10^{10}
$H^{\bullet} + e^{-}_{aq} \rightarrow H_2 + OH^{-}$	2.8×10^{10}	$e^{-}_{aq} + HO_2^{-} \rightarrow O^{\bullet-} + OH^{-}$	3.51×10^{9}
$H^{\bullet} + OH^{-} \rightarrow H_2O + e^{-}_{aq}$	2.4×10^{7}	$e^{-}_{aq} + O^{\bullet-} \rightarrow 2\,OH^{-}$	2.31×10^{10}
$H^{\bullet} + O_2 \rightarrow HO_2^{\bullet}$	1.3×10^{10}	$e^{-}_{aq} + H_2O \rightarrow H^{\bullet} + OH^{-}$	15.8
$H^{\bullet} + HO_2^{\bullet} \rightarrow H_2O_2$	1.1×10^{10}	$e^{-}_{aq} + O_2 \rightarrow O_2^{\bullet-}$	2.3×10^{10}
$H^{\bullet} + O_2^{\bullet-} \rightarrow HO_2^{-}$	1.1×10^{10}	$e^{-}_{aq} + HO_2^{\bullet} \rightarrow HO_2^{-}$	1.3×10^{10}
$H^{\bullet} + HO_2^{-} \rightarrow {}^{\bullet}OH + OH^{-}$	1.5×10^{9}	$e^{-}_{aq} + O(^3P) \rightarrow O^{\bullet-}$	2.0×10^{10}
$H^{\bullet} + O(^3P) \rightarrow {}^{\bullet}OH$	2.0×10^{10}	$e^{-}_{aq} + O_3 \rightarrow O_3^{\bullet-}$	3.6×10^{10}
$H^{\bullet} + O^{\bullet-} \rightarrow OH^{-}$	2.0×10^{10}	$H^{+} + O^{\bullet-} \rightarrow {}^{\bullet}OH$	5.0×10^{10}
$H^{\bullet} + O_3 \rightarrow O_2 + {}^{\bullet}OH$	3.7×10^{10}	$H^{+} + O_2^{\bullet-} \rightarrow HO_2^{\bullet}$	5.0×10^{10}
$H^{\bullet} + O_3^{\bullet-} \rightarrow OH^{-} + O_2$	1.0×10^{10}	$H^{+} + OH^{-} \rightarrow H_2O$	1.2×10^{11}
${}^{\bullet}OH + {}^{\bullet}OH \rightarrow H_2O_2$	6.3×10^{9}	$H^{+} + O_3^{\bullet-} \rightarrow {}^{\bullet}OH + O_2$	9.0×10^{10}
${}^{\bullet}OH + H_2O_2 \rightarrow HO_2^{\bullet} + H_2O$	2.9×10^{7}	$H^{+} + HO_2^{-} \rightarrow H_2O_2$	5.0×10^{10}
${}^{\bullet}OH + H_2 \rightarrow H^{\bullet} + H_2O$	4.0×10^{7}	$OH^{-} + O(^3P) \rightarrow HO_2^{-}$	4.2×10^{8}
${}^{\bullet}OH + e^{-}_{aq} \rightarrow OH^{-}$	3.6×10^{10}	$OH^{-} + HO_2^{\bullet} \rightarrow O_2^{\bullet-} + H_2O$	1.3×10^{10}
${}^{\bullet}OH + OH^{-} \rightarrow O^{\bullet-} + H_2O$	1.3×10^{10}	$O_2 + O^{\bullet-} \rightarrow O_3^{\bullet-}$	3.7×10^{9}
${}^{\bullet}OH + HO_2^{\bullet} \rightarrow O_2 + H_2O$	9.0×10^{9}	$O_2 + O(^3P) \rightarrow O_3$	4.0×10^{9}
${}^{\bullet}OH + O_2^{\bullet-} \rightarrow O_2 + OH^{-}$	1.1×10^{10}	$HO_2^{\bullet} + O_2^{\bullet-} \rightarrow HO_2^{-} + O_2$	9.7×10^{7}
${}^{\bullet}OH + HO_2^{-} \rightarrow HO_2^{\bullet} + OH^{-}$	8.3×10^{9}	$HO_2^{\bullet} + HO_2^{\bullet} \rightarrow H_2O_2 + O_2$	1.94×10^{8}
${}^{\bullet}OH + O(^3P) \rightarrow HO_2^{\bullet}$	2.02×10^{10}	$HO_2^{\bullet} + O(^3P) \rightarrow O_2 + {}^{\bullet}OH$	2.02×10^{10}
${}^{\bullet}OH + O^{\bullet-} \rightarrow HO_2^{-}$	1.0×10^{9}	$HO_2^{\bullet} + H_2O \rightarrow H^{+} + O_2^{\bullet-}$	1.4×10^{4}
${}^{\bullet}OH + O_3^{\bullet-} \rightarrow O_2^{\bullet-} + HO_2^{\bullet}$	8.5×10^{9}	$O_2^{\bullet-} + O^{\bullet-} \rightarrow O_2 + 2\,OH^{-}$	6.0×10^{8}
${}^{\bullet}OH + O_3 \rightarrow O_2 + HO_2^{\bullet}$	1.11×10^{8}	$O_2^{\bullet-} + H_2O \rightarrow HO_2^{\bullet} + OH^{-}$	0.155
$H_2O_2 + e^{-}_{aq} \rightarrow OH^{-} + {}^{\bullet}OH$	1.1×10^{10}	$O_2^{\bullet-} + O_3 \rightarrow O_3^{\bullet-} + O_2$	1.5×10^{9}
$H_2O_2 + OH^{-} \rightarrow HO_2^{-} + H_2O$	1.33×10^{10}	$HO_2^{-} + H_2O \rightarrow H_2O_2 + OH^{-}$	1.27×10^{6}
$H_2O_2 + O(^3P) \rightarrow HO_2^{\bullet} + {}^{\bullet}OH$	1.6×10^{9}	$HO_2^{-} + O^{\bullet-} \rightarrow O_2^{\bullet-} + OH^{-}$	8.02×10^{8}
$H_2O_2 + O^{\bullet-} \rightarrow HO_2^{\bullet} + OH^{-}$	5.55×10^{8}	$HO_2^{-} + O(^3P) \rightarrow O_2^{\bullet-} + {}^{\bullet}OH$	5.3×10^{9}
$H_2 + O(^3P) \rightarrow H^{\bullet} + {}^{\bullet}OH$	4.77×10^{3}	$O^{\bullet-} + O^{\bullet-} \rightarrow H_2O_2 + 2\,OH^{-}$	1.0×10^{8}
$H_2 + O^{\bullet-} \rightarrow H^{\bullet} + OH^{-}$	1.3×10^{8}	$O^{\bullet-} + O_3^{\bullet-} \rightarrow 2\,O_2^{\bullet-}$	7.0×10^{8}
$O(^3P) + O(^3P) \rightarrow O_2$	2.2×10^{10}	$O^{\bullet-} + H_2O \rightarrow {}^{\bullet}OH + OH^{-}$	1.3×10^{6}
$O(^3P) + H_2O \rightarrow 2\,{}^{\bullet}OH$	1.9×10^{3}	$O_3^{\bullet-} + H_2O \rightarrow O^{\bullet-} + O_2$	46.5

3. STOPPING AND RANGE OF IONS IN MATTER (SRIM)

The "Stopping and Range of Ions in Matter" (SRIM) is a group of computer programs which calculate the interactions of energetic ions penetrating into matter; the core of SRIM originated as a DOS-based program named "Transport of Ions in Matter" (TRIM). The programs were developed by James F. Ziegler and Jochen P. Biersack around 1983 and are being continuously upgraded with the major changes occurring approximately every six years (ZIEGLER et al., 1985, 2008, 2010, 2015; BIERSACK and HAGGMARK, 1980). SRIM is based on a Monte Carlo simulation method, namely, the binary collision approximation with a random selection of the impact parameter of the next colliding ion.

Using SRIM, the energy loss, range and straggling distribution of ions in matter can be calculated. More elaborate calculations include targets with complex multi-layer configurations. Ion beams are used to modify samples by injecting atoms to change the chemical and electronic properties of the target. The ion beam also causes damage to solid targets by atom displacement.

The most recent version of SRIM uses the "Core and Bond" (CAB) approach to predict the stopping power of compounds. Previously, the stopping power of a compound was estimated only by Bragg's rule (BRAGG and KLEEMAN, 1905), that is, by considering the linear combination of the stopping powers of its individual elements. SRIM uses the CAB approach to generate corrections between Bragg's rule and compounds containing the common elements in compounds: H, C, N, O, F, S, and Cl. These light atoms have the largest bonding effect on stopping powers. SRIM correctly predicts the stopping of H and He ions in compounds with an accuracy of better than 2% at the peak of their stopping power curve (ZIEGLER et al., 2010, 2015). As for the stopping power of high-energy heavy ions ($Z > 3$), the charge state of the projectile ion is also an important parameter to consider. The Brandt-Kitagawa (BK) dielectric-response approximation (BRANDT and KITAGAWA, 1982) is a very useful tool to derive the effective charge of heavy ions. BK improved an earlier theory suggesting that an energetic heavy ion would lose any of its electrons whose classical velocity was slower than the ion's velocity. These authors showed that one should consider instead the loss of any electrons whose velocity

was slower than the relative velocity of the projectile ion to the target medium. This lowered the charge state of heavy ions since the relative velocity of the ion was always lower than its absolute velocity. BK then presented a simple method of calculating this relative velocity based on considering the target to be a perfect Fermi conductor. This significantly improved the calculation of stopping powers (ZIEGLER et al., 1985).

SRIM uses several different stopping theories to evaluate the accuracy of experimental stopping powers. Specifically, calculations are made for all ions in individual targets (which eliminates common difficulties with target dependent quantities such as shell corrections and mean ionization potentials). If the experimental values are within reasonable agreement with these theoretical calculations, then the experimental values are weighted with the theoretical values to obtain final values.

In the current study, we used SRIM program to observe the trajectories of the Li and He recoil ions through liquid water.

4. ARTICLE no. 1

Monte Carlo track chemistry simulations of the radiolysis of water induced by the recoil ions of the $^{10}B(n,\alpha)^{7}Li$ nuclear reaction. 1. Calculation of the yields of primary species up to 350 °C.

Authors: **Muhammad Mainul Islam,** Phantira Lertnaisat, Jintana Meesungnoen, Sunuchakan Sanguanmith, Jean-Paul Jay-Gerin, Yosuke Katsumura, Satoru Mukai, Ryuji Umehara, Yuichi Shimizu and Masashi Suzuki

Status: Published in *Royal Society of Chemistry Advances*, 2017, vol.: **7** (issue: 18), pages: 10782-10790 (DOI: 10.1039/c6ra28586d). Impact factor: 3.108.

Forward: This work focuses on the calculation of the yields of all primary species produced in the radiolysis of pure neutral liquid water and 0.4 M H_2SO_4 aqueous solutions by the α and Li recoils of the $^{10}B(n,\alpha)^{7}Li$ nuclear reaction from 25 to 350 °C, using Monte Carlo track chemistry simulations. The yields are obtained at 10^{-7} s and 10^{-6} s and agree well with existing estimates. Our simulations show downward inflections in the yields of both H_2 and H_2O_2 above 150 °C. Measurements of the (e^-_{aq} + e^-_{aq}) reaction rate constant in near-neutral water would help determine whether these predicted non-monotonic inflections are confirmed. This study is important for the nuclear industry where the radiolysis of water by high-LET radiation takes place under extreme operating conditions of high temperatures and pressures.

Résumé : Dans ce travail, nous calculons les rendements des espèces primaires de la radiolyse de l'eau pure et de solutions aqueuses H_2SO_4 0,4 M par les ions de recul de la réaction nucléaire $^{10}B(n,\alpha)^{7}Li$ en fonction de la température entre 25 et 350 °C, en utilisant des simulations Monte Carlo. Les rendements, obtenus à 10^{-7} et 10^{-6} s, sont en bon accord avec l'expérience. Nos résultats montrent des inflexions dans les courbes de $G(H_2)$ et de $G(H_2O_2)$ au-dessus de 150 °C. Des mesures de la constante de vitesse de la réaction bi-moléculaire des électrons hydratés (e^-_{aq} + e^-_{aq}) en solution neutre ou faiblement acide permettraient de déterminer si l'existence de ces inflexions est confirmée. Cette étude est importante pour l'industrie nucléaire où la radiolyse de l'eau se fait par des rayonnements de TEL élevé, dans des conditions extrêmes de haute température et pression.

Monte Carlo track chemistry simulations of the radiolysis of water induced by the recoil ions of the $^{10}B(n,\alpha)^{7}Li$ nuclear reaction. 1. Calculation of the yields of primary species up to 350 °C.

Muhammad Mainul Islam,[a] Phantira Lertnaisat,[b] Jintana Meesungnoen,[a] Sunuchakan Sanguanmith,[a] Jean-Paul Jay-Gerin,[*a] Yosuke Katsumura,[†*b] Satoru Mukai,[c] Ryuji Umehara,[d] Yuichi Shimizu[d] and Masashi Suzuki[c]

[a]Département de Médecine Nucléaire et de Radiobiologie, Faculté de Médecine et des Sciences de la Santé, Université de Sherbrooke, Sherbrooke, Québec, J1H 5N4, Canada.
E-mail: jean-paul.jay-gerin@USherbrooke.ca

[b]Department of Nuclear Engineering and Management, School of Engineering, University of Tokyo, 7-3-1 Hongo, Bunkyo-ku, Tokyo 113-8686, Japan.
E-mail: katsu@n.t.u-tokyo.ac.jp

[c]Nuclear Chemistry Engineering, Nuclear Environment R&D Department, Nuclear Development Corporation, 622-12 Funaishikawa, Tokai-mura, Ibaraki 319-111, Japan.

[d]Water Chemistry Technology Group, Nuclear Energy Systems Headquarters, Mitsubishi Heavy Industries Ltd., 1-1-1 Wadasaki-cho, Hyogo-ku, Kobe 652-8585, Japan.

†Present address: Japan Radioisotope Association, Honkomagome 2-28-45, Bunkyo-ku, Tokyo 113-8941, Japan.

*Corresponding author.

RSC Adv. **7**, 10782-10790 (2017).

ABSTRACT

Monte Carlo track chemistry simulations were carried out to predict the yields (*G*-values) of all primary radical and molecular species produced in the radiolysis of pure, neutral water and 0.4 M sulfuric acid aqueous solutions by the recoil ions of the $^{10}B(n,\alpha)^{7}Li$ nuclear reaction as a function of temperature from 25 to 350 °C. The calculations were performed individually for 1.47 MeV α-particles and 0.84 MeV lithium nuclei with "dose-average" linear energy transfer (LET) values of ~196 and ~225 eV nm^{-1} at 25 °C, respectively. The overall yields were calculated by summing the *G*-values for each recoil ion weighted by its fraction of the total energy absorbed. In the calculations, the actual effective charges carried by the two helium and lithium ions (due to charge exchange effects) were taken into account and the (small) contribution of the 0.478 MeV γ-ray, also released from the $^{10}B(n,\alpha)^{7}Li$ reaction, was neglected. Compared with data obtained for low-LET radiation (^{60}Co γ-rays or fast electrons), our computed yields for the $^{10}B(n,\alpha)^{7}Li$ radiolysis of neutral deaerated water showed essentially similar temperature dependence over the range of temperatures studied, but with lower values for yields of free radicals and higher values for molecular yields. This general trend is a reflection of the high-LET character of the $^{10}B(n,\alpha)^{7}Li$ recoil ions. Overall, the simulation results agreed well with existing estimates at 20 and 289 °C. For deaerated 0.4 M H_2SO_4 solutions, reasonable agreement between experiment and simulation was also found at room temperature. Nevertheless, more experimental data for both neutral and acidic solutions would be needed to better describe the dependence of radiolytic yields on temperature and to test our modeling calculations more thoroughly. Moreover, measurements of the (e^-_{aq} + e^-_{aq}) reaction rate constant in near-neutral water would help us determine whether the predicted non-monotonic inflections above ~150 °C in $G(H_2)$ and $G(H_2O_2)$ are confirmed.

1. Introduction

Boron-10 is one of the stable isotopes of boron with a natural abundance of ~20%. It is known to exhibit a high propensity to absorb thermal neutrons with a neutron-capture cross-section of 3835 barns (1 barn = 10^{-28} m^2), which is about six times greater than that of uranium-235 and three orders of magnitude greater than that of the nuclei of living tissues.[1] On absorption of a slow neutron, a fission reaction occurs with the release of two energetic heavy ions: an α-particle (1.47 MeV) and, in ~94% of all reactions, a $^{7}Li^{3+}$ nucleus in its first excited state (0.84 MeV) which quickly returns to its ground state (half-life of ~10^{-13} s) by releasing a low-energy γ-ray (478 keV).[2] These heavy charged particles have path lengths in the range of ~5-8 μm in water or biological tissues and exhibit high linear energy transfer (LET, or energy loss per unit path length $-dE/dx$, in units of eV nm^{-1}) characteristics, as shown in Fig. 1.[3,4] Because of this high energy deposition to the surrounding environment and the α and Li recoils' short travel distances, which are typically of the order of a cell diameter, the $^{10}B(n,\alpha)^{7}Li$ nuclear reaction has been used in clinical studies of biochemically targeted radiotherapies for cancer treatment known as "boron neutron capture therapy" (BNCT).[1,5]

BNCT is a potentially ideal radiotherapy modality for glioblastoma, which is a type of brain tumor that is rarely removed surgically. When a cancer cell is allowed to take up preferentially a sufficient concentration of ^{10}B, it can be selectively irradiated by the very densely ionizing ion recoils from the $^{10}B(n,\alpha)^{7}Li$ reaction without damaging the surrounding normal tissue. This basic idea was first proposed by Locher in 1936,[6] shortly after the discovery of the neutron by Chadwick.[7] Interest in BNCT was spurred by Kruger's study in 1940, who reported a low transplantation efficiency for tumors treated by BNCT *in vitro* and subsequently implanted in mice.[8,9] Although the full clinical application of BNCT presents several difficulties, including the inadequate selectivity and toxicity of ^{10}B delivery agents and the poor distribution of neutron flux, clinical trials of BNCT are still under way and new neutron irradiation facilities continue to be developed in Japan, the United States, Finland, and several other countries.[1,5,10–12]

Apart from BNCT, the unique properties of boron-10 have also been extensively applied in the field of nuclear industry. For example, boron carbide (B_4C), enriched in ^{10}B, is used as a control-rod material (neutron absorber) in boiling water reactors (BWRs). In

addition, boron as boric acid (H_3BO_3) is generally added as a water-soluble neutron poison in the primary coolant of pressurized water reactors (PWRs) to control the neutron flux and the reactivity in the core.[13–16] However, recoil ions arising from the $^{10}B(n,\alpha)^7Li$ reaction act as sources of high-LET radiation in the primary coolant of PWRs, thereby leading to the formation of oxidizing species, such as hydrogen peroxide and oxygen, due to the radiolysis of water.[17,18]

The radiolysis of water is closely linked to the corrosion of structural materials. Water, which is used as the neutron moderator and the reactor coolant, is unavoidably exposed to extreme conditions of high temperature (~275-325 °C), pressure (~7-15 MPa), and intense mixed neutron and β-γ radiation fields (which have characteristically different LET values). Under these conditions, the radiolysis of water results in the formation of free radical (e^-_{aq}, $^\bullet OH$, $^\bullet H$, and $HO_2^\bullet/O_2^{\bullet-}$) and molecular ($H_2$,$H_2O_2$, and O_2) species which alter the chemical environment of the coolant.[18–20] The presence of the oxidizing species H_2O_2 and O_2 can significantly increase the corrosion potential of coolant water in BWRs.[16,21,22] In PWRs, the presence of boron-10 results in high-LET recoil ions and complicates the radiolytic process. Although ^{10}B has been widely studied both in nuclear technology and clinical research, little attention has been devoted to ^{10}B-induced reactions. In particular, data on the formation of primary products and their yields (*G*-values) for $^{10}B(n,\alpha)^7Li$ recoil irradiation of neutral water are scarce and uncertain.[15,19] In fact, the only reported measurements at room temperature were made in acid (0.4 M H_2SO_4) solution.[23–25] Similarly, the *G*-values at reactor temperatures are not well known. To the best of our knowledge, there is only one report[19] that estimated a complete set of water decomposition yields induced by the $^{10}B(n,\alpha)^7Li$ reaction at 289 °C.

Understanding the radiation chemistry of the coolant water in reactors is important for maintaining the proper chemical environment that will minimize the degradation of materials. Recently, computer simulations have played a substantial role in evaluating the concentrations of oxidizing species produced from coolant-water radiolysis, which is difficult to observe directly because of the extreme operating conditions involved. In this current work, Monte Carlo track chemistry simulations were undertaken to predict the *G*-values for the various primary radical and molecular products formed from the radiolysis of pure, neutral water and 0.4 M H_2SO_4 aqueous solutions by the $^{10}B(n,\alpha)^7Li$ reaction as a

function of temperature from 25 to 350 °C. The paper is organized as follows. The main features of our simulation approach are given in the next section. Sections 3 and 4 present, respectively, the results of our simulations of the $^{10}B(n,\alpha)^{7}Li$ radiolysis of water at neutral pH and of 0.4 M H_2SO_4 aqueous solutions at 25 °C and as a function of temperature up to 350 °C, and their discussion. Conclusions are drawn in the final section.

A brief preliminary report of this work has been presented elsewhere.[26]

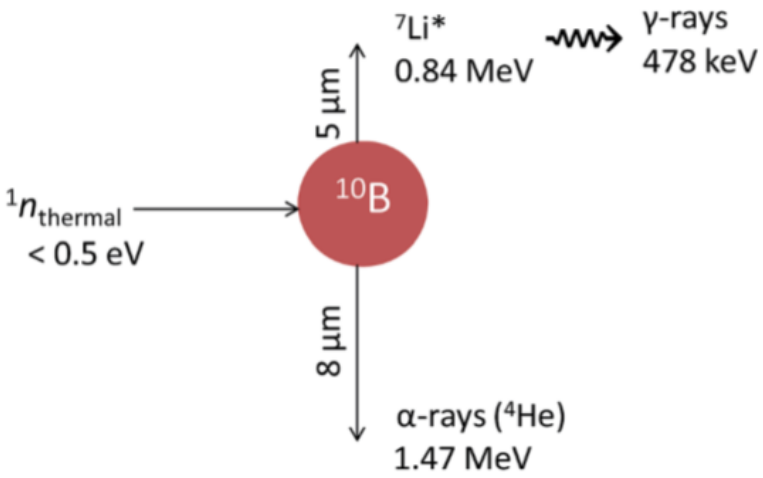

Fig. 1 Scheme of the nuclear reaction resulting from the low-energy (< 0.5 eV) thermal neutron capture by a ^{10}B atom. After absorption, 94% of the reactions leave the ^{7}Li ion in its first excited state ($^{7}Li^{*}$) which rapidly de-excites to the ground state by releasing a 478 keV γ-ray. For the remaining 6% of the reactions, the ^{7}Li ion is left directly in its ground state resulting in the emission of a 1.78 MeV α-particle and a 1.02 MeV ^{7}Li ion. Note that the ^{4}He and ^{7}Li recoil ions are in opposite directions (*i.e.*, at a 180° angle), away from the site of the compound nucleus, and hence they form one straight track.

2. Monte Carlo track chemistry simulations

The entire sequence of events generated in the radiolysis of liquid water by $^{10}B(n,\alpha)^{7}Li$ recoil ions was modeled using our Monte Carlo track chemistry simulation code called IONLYS-IRT. This computer program simulates, in a 3D geometrical environment, the highly nonhomogeneous distribution of reactive species initially produced by the absorption of incident radiation and all of the energetic secondary electrons, as well as the subsequent diffusion and chemical reactions of these species. A detailed description of the current version of the code at both ambient and elevated

temperatures and under low- and high-LET irradiation conditions has been reported previously.[27–30] In brief, the IONLYS step-by-step simulation program models all of the events of the early "physical" and "physicochemical" stages[31] of radiation action up to ~1 ps in the track development. The complex, highly nonhomogeneous spatial distribution of reactants formed at the end of the physicochemical stage [e^-_{aq}, H^+, OH^-, $H^\bullet$, $^\bullet OH$, H_2, H_2O_2, $HO_2^\bullet$/ $O_2^{\bullet-}$, $^\bullet O^\bullet$ (^3P), O(^1D), O_2,...], which is provided as an output of the IONLYS program, is then used directly as the starting point for the subsequent "nonhomogeneous chemical" stage[31] (typically, from ~1 ps to the μs time scale at 25 °C). This third stage, during which the different radiolytic species diffuse randomly at rates determined by their diffusion coefficients and react with one another (or with dissolved solutes, if any) until all track processes are complete, is covered by our IRT program. This program employs the "independent reaction times" (IRT) method,[32–34] a computationally efficient stochastic simulation technique that is used to simulate reaction times without having to follow the trajectories of the diffusing species. The IRT method relies on the approximation that the reaction time of each pair of reactants is independent of the presence of other reactants in the system. Its ability to give accurate time dependent chemical yields under different irradiation conditions has been well validated by comparison with full random flights (or step-by-step) Monte Carlo simulations, which do follow the reactant trajectories in detail.[35,36] This IRT program can also be used to efficiently describe the reactions that occur in the bulk solution during the "homogeneous chemical" stage,[31] *i.e.*, in the time domain beyond a few microseconds. The model assumptions and procedures employed to carry out the Monte Carlo simulations of the radiolysis of aqueous 0.4 M H_2SO_4 solutions (pH ~ 0.46) with IONLYS-IRT have already been given.[37,38] In the current version of IONLYS-IRT, we used the self consistent radiolysis database, including rate constants and diffusion coefficients, recently compiled by Elliot and Bartels.[20] This new database provides recommendations for the best values to use in high-temperature modeling of water radiolysis over the range of 20-350 °C.

Pre-simulations were performed using the SRIM simulation program[39] to calculate 1000 tracks of 1.47 MeV α-particles and 0.84 MeV lithium nuclei emitted from the $^{10}B(n,\alpha)^7Li$ reaction, and the energies and LET values of the 2 recoil ions as a function of penetration depth in water (Fig. 2). As shown, the initial LETs of helium and lithium ions

were ~193 and 304 eV nm^{-1}, respectively. The LET of 1.47 MeV $^4He^{2+}$ ions calculated using our Monte Carlo simulations agreed very well with the SRIM simulation results. Since the SRIM program incorporates the change of charge state of the moving ion as it goes into and through the target (due to the effects of electron capture and loss by the ion), this agreement indicates that the helium ion, when it travels with this energy, is fully stripped of its electrons. However, for 0.84 MeV $^7Li^{3+}$ ions, our calculations gave a LET which is more than twice the expected value. This difference was explained as being caused by a change in the charge state of the lithium ion, which always acts to reduce its LET relative to the LET of the bare nucleus. Our Monte Carlo simulations were used to calculate the "effective charge" (Z^*) of a 0.84 MeV lithium ion in water that was required to reproduce the SRIM LET value of 304 eV nm^{-1}. A value very close to +2 (instead of +3) was actually obtained, clearly indicating a partial neutralization of the lithium ion at this energy.

The above results confirm the importance of making charge state calculations for each recoil ion in this study. In this work, however, to avoid complexity arising from energy-dependent charge exchange processes, simulations were performed under the simplifying approximation that the energies of the two recoil ions remained constant when passing through the water medium. These constant average energy values $\bar{E}_{He}$ and $\bar{E}_{Li}$ were chosen according to the following procedure: (1) Watt's compilation of quantities for radiation dosimetry in liquid water[3] was first used to determine the "dose-average" LET values for both 1.47 MeV helium and 0.84 MeV lithium ions. The values thus obtained were ~196 and 225 eV nm^{-1}, respectively; (2) using Fig. 2(c), these two LET values were then related to the corresponding penetration depths of the two recoil ions in water, namely, ~5.5 and 1.5 μm, respectively; and (3) $\bar{E}_{He}$ and $\bar{E}_{Li}$ were finally deduced from Fig. 2(b) as being equal to the energies of the two ions at these penetration depths, namely, ~0.3 and 0.4 MeV, respectively. Once these two energies are known, the actual effective charges carried by the two helium and lithium ions having these energies were determined as described above by using our Monte Carlo simulations and by adjusting Z^* so as to reproduce the expected LET values. Z^*_{He} and Z^*_{Li} were found to be about +1.6 and +1.7, respectively.

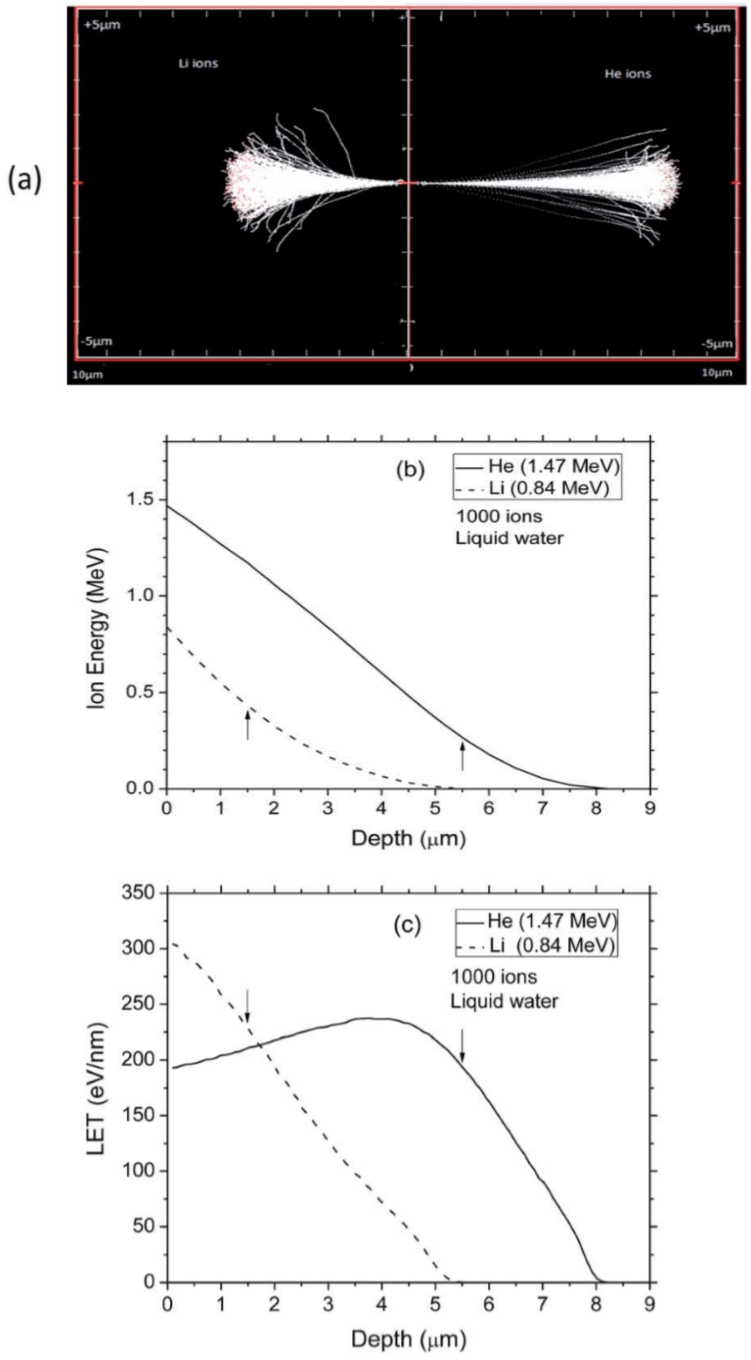

Fig. 2 SRIM simulation of the penetration of the recoil helium and lithium ions of the $^{10}B(n,\alpha)^{7}Li$ reaction into liquid water at room temperature: (a) simulated ion trajectories; (b) and (c) variations of the energy and LET of the two ions as a function of penetration depth, respectively (the points selected in this study are indicated by arrows). Total ions calculated: 1000.

All calculations were performed by simulating short (typically, ~1-5 μm) ion track segments, over which the energy and LET of the ion are well defined and remain nearly constant. Such model calculations thus gave "track segment" yields[40] at a well defined LET. The number of individual ion "histories" (usually ~2-100, depending on the irradiating ion and energy) was chosen to ensure only small statistical fluctuations in the computed averages of chemical yields while keeping acceptable computer time limits. Finally, the yields of primary free radical or molecular products of water radiolysis induced by the recoil ions of the nuclear reaction $^{10}B(n,\alpha)^{7}Li$ were calculated by summing the *G*-values for each recoil ion (obtained from our Monte Carlo simulations) weighted by its fraction of the total energy absorbed according to[38,41]

$$G(X_i) = \frac{G(X_i)_{He}\, E_{He} + G(X_i)_{Li}\, E_{Li}}{E_T}, \qquad (1)$$

where $G(X_i)_{He}$ and $G(X_i)_{Li}$ are the yields of species X_i associated with the recoil helium and lithium ions, respectively, and $E_T = E_{He} + E_{Li}$ is the sum of the initial energies of the ion products of the reaction (*i.e.*, 2.31 MeV).

Absorption of the accompanying 0.478 MeV γ-ray in the aqueous solution (see Fig. 1) is small in our area of interest. Indeed, the range of an electron of this energy is ~1 mm in liquid water at 25 °C;[42] this is more than 100 times larger than the penetration ranges of the He and Li ions, which are only 5–8 μm. Thus, its contribution to the overall chemical reaction was neglected in this study.

Throughout this paper, *G*-values are quoted in units of molecules formed or consumed per 100 eV of radiation energy absorbed. For conversion into SI units, 1 molecule/100 eV = 0.10364 μmol J^{-1}.

3. Results and discussion

The temperature dependences of our computed yields of e^-_{aq}, $H^\bullet$, $^\bullet OH$, H_2 and H_2O_2 in pure, deaerated liquid water irradiated by the $^{10}B(n,\alpha)^{7}Li$ recoil ions from ambient up to 350 °C are shown in Fig. 3 along with estimated *G*-values at 20 °C (ref. 15) and 289 °C.[19] For the sake of comparison, our *G*-values were calculated at two different times, namely 10^{-7} and 10^{-6} s after energy deposition at all temperatures (solid, blue and red lines shown

in Fig. 3, respectively). Compared with the data obtained for low-LET radiation (γ-rays from ^{60}Co or fast electrons), our computed yields for ^{10}B(n,α)^{7}Li recoil irradiation show essentially similar temperature dependences over the range of temperatures studied, but with much lower values for yields of free radicals and higher values for molecular yields. This is particularly true for the yields of e^-_{aq} and H$^\bullet$ atoms, which remain extremely small at the microsecond time scale even at high temperatures [Fig. 3(a) and (c)]. This general trend is a result of the high-LET character of the ^{10}B(n,α)^{7}Li recoil ions. Indeed, upon increasing the LET of the radiation, there is an increased intervention of radical–radical reactions as the local concentrations of radicals along the radiation tracks are high and many radical interactions occur before the products can escape into the bulk solution. This allows fewer radicals to escape combination and recombination reactions during the expansion of tracks and in turn leads to the formation of more molecular products.[28]

A striking feature of our simulated results is the marked downward inflection that is observed above ~150 °C in the yields of H_2 and H_2O_2. This is in contrast to the corresponding estimates of Christensen[19] at 289 °C, which seem to indicate a rather monotonic variation of $G(H_2)$ [Fig. 3(e)] and $G(H_2O_2)$ [Fig. 3(d)] with temperature. Similar non-monotonic behavior in the temperature dependence of the yields of primary products in low-[29,45,46] and high-[47,48] LET irradiated water has already been predicted, and is due to the fact that the rate constant for the bimolecular self-reaction of the hydrated electron (k_2):

$$e^-_{aq} + e^-_{aq}\ (+2H_2O) \rightarrow H_2 + 2OH^- \qquad (2)$$

drops sharply between ~150 and 200 °C.[20] This non-Arrhenius behavior of reaction (2) above ~150 °C readily explains the sharp decrease in H_2 yields in Fig. 3(e). Moreover, as a consequence of the drop in k_2, more and more e^-_{aq} are available as the temperature increases to either react in other intra-track reactions, such that[20]

$$e^-_{aq} + {}^\bullet OH \rightarrow OH^-\ (k_3 = 3.34 \times 10^{10}\ M^{-1}\ s^{-1},\ 20\ °C), \qquad (3)$$

or escape into the bulk solution. As hydrogen peroxide is formed predominantly by the reaction[20]

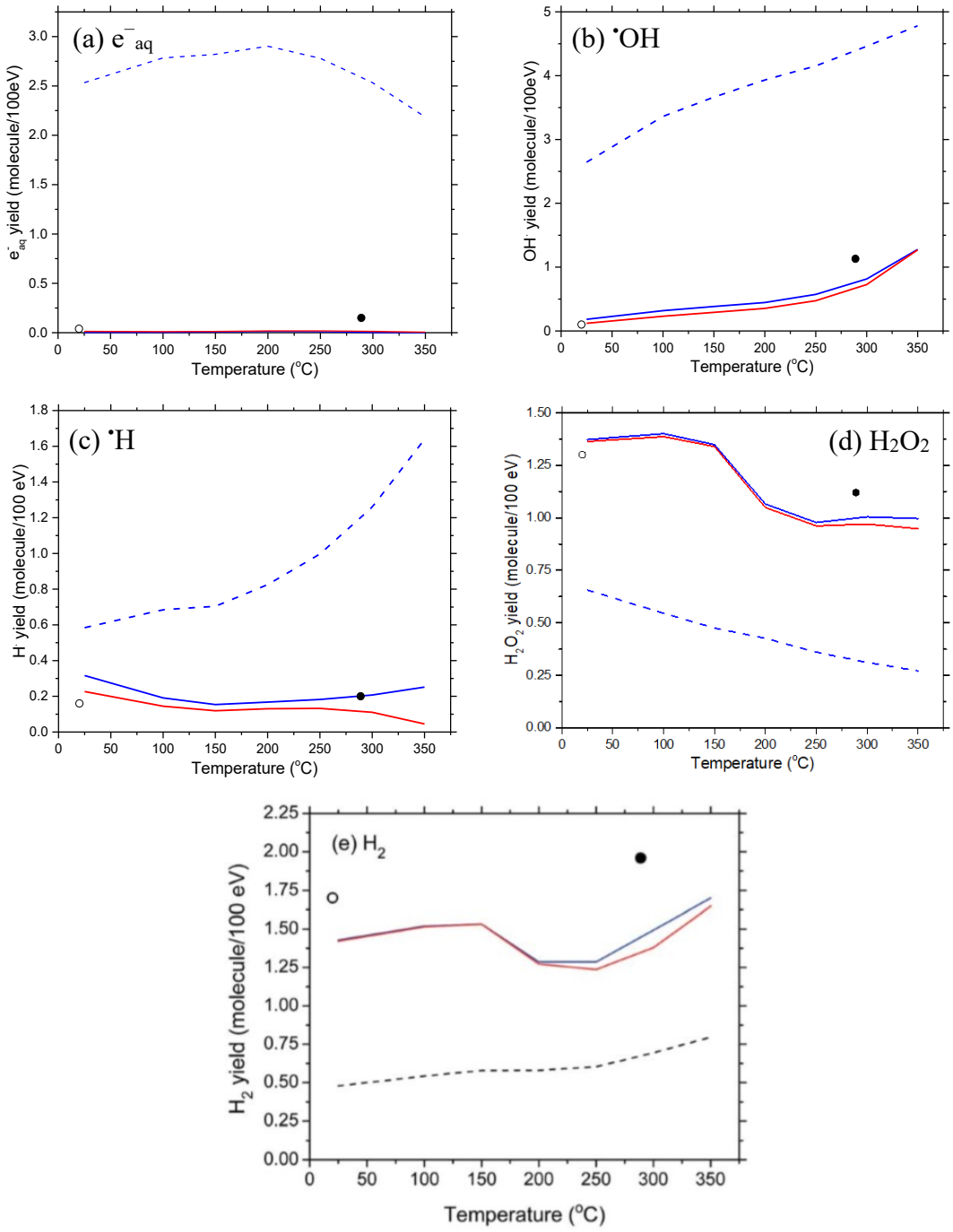

Fig. 3 *G*-values (in molecule per 100 eV) for the $^{10}B(n,\alpha)^{7}Li$ radiolysis of pure, deaerated liquid water as a function of temperature in the range of 25-350 °C: (a) $G(e^-_{aq})$; (b) $G(^{\bullet}OH)$; (c) $G(^{\bullet}H)$; (d) $G(H_2O_2)$; and (e) $G(H_2)$. Our simulated results, obtained at 10^{-7} and 10^{-6} s, are shown as solid, blue and red lines, respectively. Symbols are the water decomposition yields induced by the $^{10}B(n,\alpha)^{7}Li$ reaction estimated by Cohen (ref. 15) at 20 °C (based on the approximate relationship between LET and *G*-values given in Fig. 5.3 of Allen (ref. 43), using an average initial LET of 240 eV nm^{-1}) (–) and by Christensen (ref.

19) at 289 °C (,). The primary (or "escape") yields for the low-LET (~0.3 eV nm^{-1}) radiolysis of water (ref. 29) obtained using our previously calculated spur lifetimes between 25-350 °C (ref. 44) are also given (black dashed lines) for comparison purposes. Note that all yield curves shown in this figure were obtained under exactly the same conditions as in ref. 29 as far as the temperature dependences of the different parameters intervening in the early physicochemical stage (*e.g.*, the electron thermalization distance called r_{th} in ref. 29) and in the subsequent chemical stage [*e.g.*, the ($e^-_{aq} + e^-_{aq}$) reaction rate constant, represented by the non-Arrhenius black dashed line $k = k_a$ in Fig. 4(a)] of the radiolysis are concerned.

$$^{\bullet}OH + {}^{\bullet}OH \rightarrow H_2O_2 \quad (k_4 = 4.54 \times 10^9\ M^{-1}\ s^{-1},\ 20\ °C), \qquad (4)$$

the increased occurrence of reaction (3) above 150 °C also leads to a downward inflection in $G(H_2O_2)$, as shown in Fig. 3(d).

In connection with these predicted non-monotonic variations of $G(H_2)$ and $G(H_2O_2)$, we should briefly mention here the current controversy concerning the temperature dependence of k_2 (Fig. 4). In this work, we adopted the values of k_2, including the drop between 150 and 200 °C, recommended by Elliot and Bartels[20] as the "best values to use to model water radiolysis at temperatures up to 350 °C" [represented by the black dashed line, denoted k_a, in Fig. 4(a)]. However, this drop in k_2 has been measured only under alkaline conditions. Its applicability to neutral or slightly acidic (as the pH of water at 150-200 °C is about 5.7-6)[15] solution remains uncertain because it could be a function of the pH of the solution.[50]

Until recently, most computer modelers of the radiolysis of water at elevated temperatures have employed, in neutral solution, an Arrhenius extrapolation of the values of k_2 below 150 °C to 200-350 °C, as proposed previously by Elliot[50] and Stuart *et al.*,[51] and recently by Hatomoto *et al.*[52] This approach assumes that such an abrupt change in k_2 does not occur and that reaction (2) is diffusion controlled at temperatures greater than 150 °C. This assumption was originally justified by the good agreement between models and experiments.[45,46]

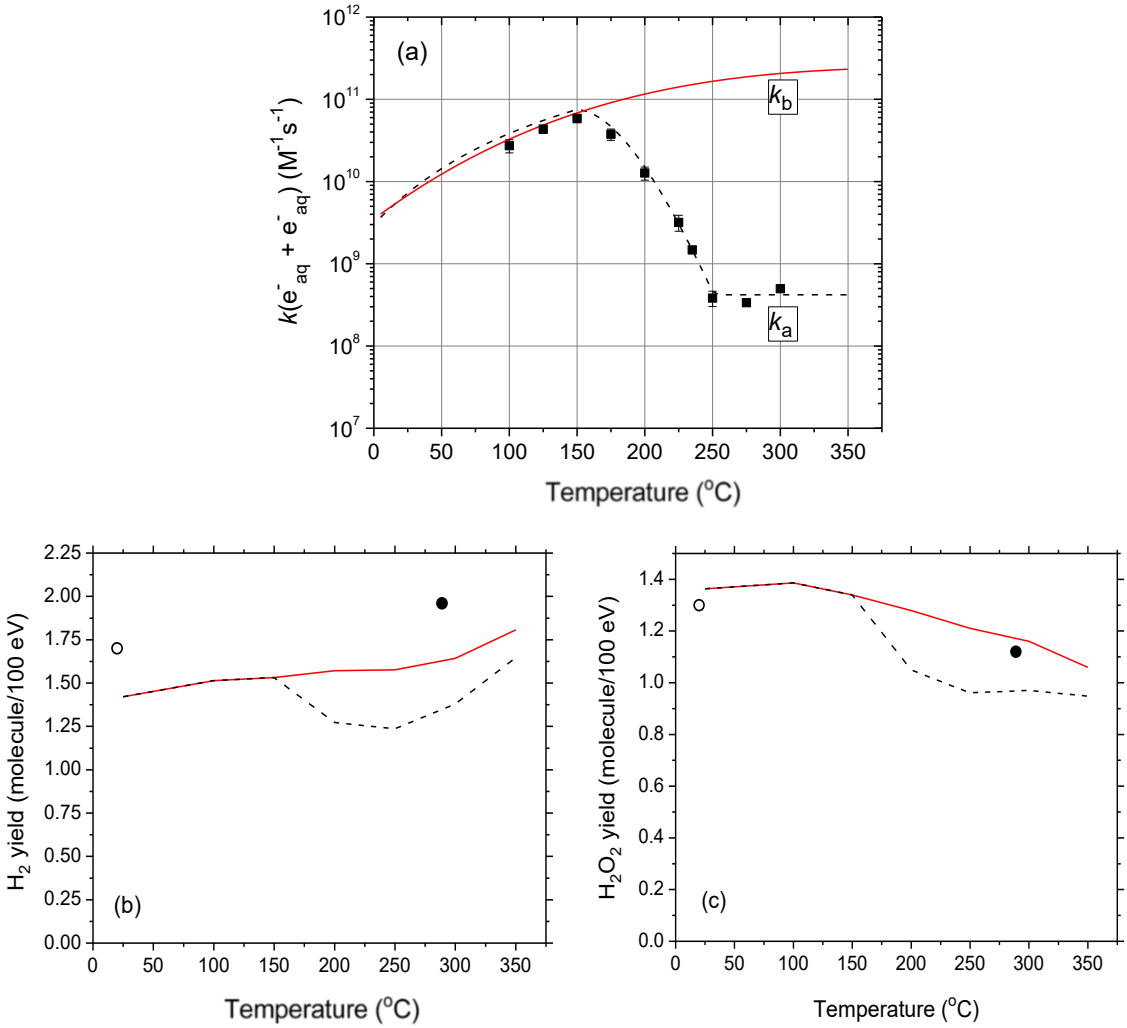

Fig. 4 (a) Rate constant for the self-reaction of two hydrated electrons as a function of temperature (ref. 49). The black dashed line (denoted k_a) shows the ($e^-_{aq} + e^-_{aq}$) reaction rate constant measured under alkaline conditions (ref. 20). The symbols (■) are experimental data. The red solid line (denoted k_b) shows the ($e^-_{aq} + e^-_{aq}$) reaction rate constant obtained by using an Arrhenius extrapolation procedure above ~150 °C (ref. 50-52). (b) and (c) The red solid lines show our Monte Carlo simulation results for $G(H_2)$ and $G(H_2O_2)$ (in molecule per 100 eV), at 10^{-6} s, as a function of temperature, when k_b was used. A comparison is made with the corresponding yields of H_2 and H_2O_2 obtained when k_a was used [represented here by the black dashed lines, which are the same as the red solid lines in Fig. 3(e) and (d)]. The symbols (–) (ref.15) and (,) (ref.19) are the same as in Fig. 3(e) and (d).

To show the sensitivity of $G(H_2)$ and $G(H_2O_2)$ to k_2, our simulations were carried out for the temperature dependence of k_2 obtained by using an Arrhenius extrapolation procedure above ~150 °C (ref. 49-52) [represented by the red solid line, denoted k_b, in Fig. 4(a)]. The red solid lines in Fig. 4(b) and (c) display our calculated H_2 and H_2O_2 yields at 10^{-6} s after the ionizing event over the temperature range of 25-350 °C. A comparison with

our results obtained using the temperature dependence of k_2 measured in alkaline water (k_a) [black dashed lines in Fig. 4(b) and (c)] clearly indicates that $G(H_2)$ and $G(H_2O_2)$ are strongly affected by the choice of k_2. In particular, the sharp downward inflections predicted for $G(H_2)$ and $G(H_2O_2)$ above ~150 °C no longer appear. Considering the importance of the self-reaction of e^-_{aq} in high-temperature water radiolysis, further measurements of its rate constant in near-neutral water are obviously highly desirable.

Turning now to the $^{10}B(n,\alpha)^7Li$ radiolysis of deaerated 0.4 M sulfuric acid aqueous solutions, we present in Fig. 5 the results of our Monte Carlo simulations showing the variations of the *G*-values for $H^\bullet$ (considering the conversion of e^-_{aq} to $H^\bullet$ in the tracks in acidic solution),[55] $^\bullet OH$, H_2O_2, and H_2 (at 10^{-6} s) as a function of temperature over the range of 25-350 °C. As can be seen, the simulations agree reasonably well with the experimental data of Barr and Schuler[23] at 25 °C, which are also shown in the figure for the sake of comparison. Compared with the primary (or "escape") yield data obtained for low-LET radiation (^{60}Co γ-rays or fast electrons) (shown as dashed lines in Fig. 5), it is seen that, as in neutral water, our computed *G*-values for the $^{10}B(n,\alpha)^7Li$ radiolysis of deaerated 0.4 M H_2SO_4 aqueous solutions show essentially similar temperature dependences over the 25-350 °C temperature range studied. The same general trend is observed, but with much lower values for yields of radical species and higher values for molecular yields, reflecting again the high-LET character of the $^{10}B(n,\alpha)^7Li$ recoil ions.

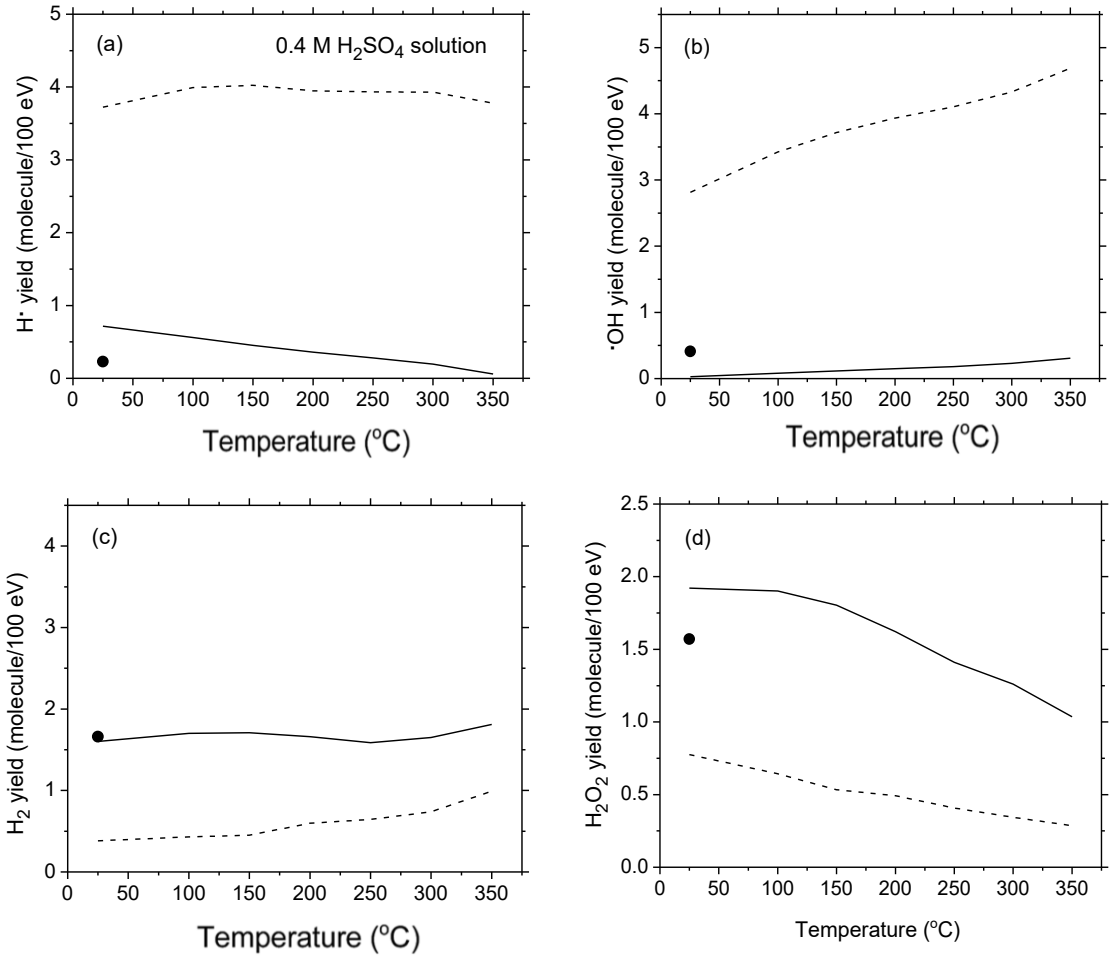

Fig. 5 *G*-values (in molecule per 100 eV) for the $^{10}B(n,\alpha)^7Li$ radiolysis of deaerated 0.4 M H_2SO_4 aqueous solutions (pH 0.46 at 25 °C) as a function of temperature in the range of 25-350 °C. Note that, at this high concentration of H_2SO_4, the H^+ ions very rapidly (<10^{-9} s) scavenge most, if not all, of the e^-_{aq} radicals in the tracks to form H• atoms (ref. 37). Note also that, in our simulations, the direct action of ionizing radiation on the sulfuric acid anions (mainly HSO_4^-) has been neglected. The solid curves represent the results of our Monte Carlo simulations for (a) *G*(H•), (b) *G*(•OH), (c) *G*(H_2), and (d) *G*(H_2O_2) at 10^{-6} s after the initial energy deposition. The yields of primary species induced by the $^{10}B(n,\alpha)^7Li$ reaction measured by Barr and Schuler (ref. 23) in acidic solutions at 25 °C are given by (,). The primary (or "escape") yields for the low-LET (~0.3 eV nm^{-1}) radiolysis of 0.4 M H_2SO_4 aqueous solutions (ref. 53) obtained from our previously calculated spur lifetimes between 25-350 °C (ref. 44) are also shown (dashed lines) for the sake of comparison. Finally, in all calculations, the reaction of the H• atom with water: $H^\bullet + H_2O \rightarrow H_2 + {}^\bullet OH$ was assumed to follow an Arrhenius temperature dependence over the 25-350 °C range studied, with a rate constant of 4.6×10^{-5} $M^{-1}s^{-1}$ at 25 °C and 10^4 M^{-1} s^{-1} at 300 °C, in agreement with recent muon spin spectroscopy experiments using muon as an analogue of a hydrogen atom (ref. 54).

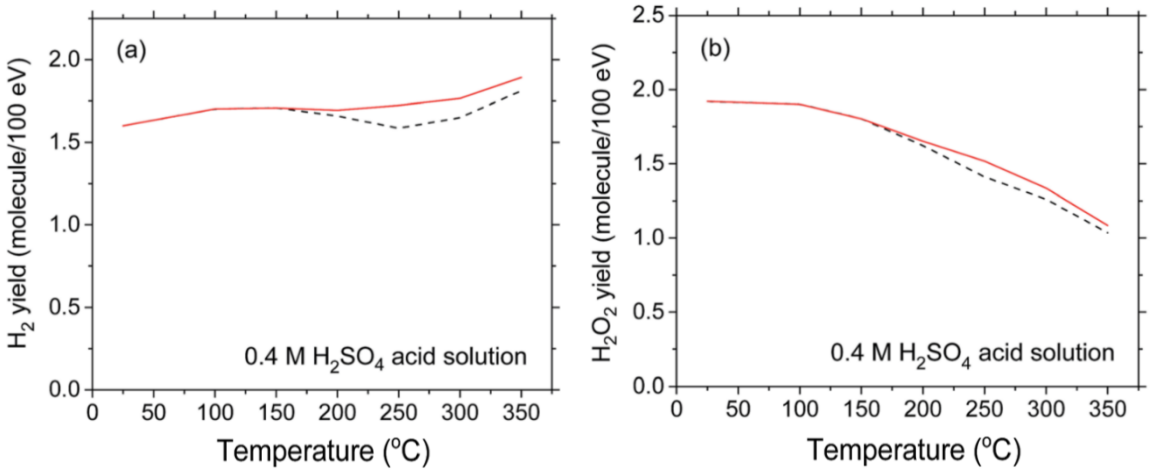

Fig. 6 Yields of H_2 (panel a) and H_2O_2 (panel b) (in molecule per 100 eV) formed during the $^{10}B(n,\alpha)^7Li$ radiolysis of deaerated 0.4 M H_2SO_4 aqueous solutions as a function of temperature over the range of 25-350 °C. The black dashed lines show our Monte Carlo simulation results for $G(H_2)$ and $G(H_2O_2)$ at 10^{-6} s when the $(e^-_{aq} + e^-_{aq})$ reaction rate constant $k_2 = k_a$ [see Fig. 4(a)] was used [note that these curves are the same as the lines in Fig. 5(c) and (d)]. A comparison is made with the corresponding yields of H_2 and H_2O_2 obtained when $k_2 = k_b$ [see Fig. 4(a)] was used (represented by the red solid lines).

For the sake of completeness, we show in Fig. 6 the sensitivity of $G(H_2)$ and $G(H_2O_2)$ to the temperature dependence for the $(e^-_{aq} + e^-_{aq})$ reaction rate constant k_2 chosen in the simulations. Compared to the results obtained in near-neutral water and shown in Fig. 4(b) and (c), the choice of k_2 [namely, k_a or k_b in Fig. 4(a)] in acidic solution is relatively unimportant. Indeed, as can be seen from Fig. 6(a) and (b), the H_2 and H_2O_2 yield (red solid) curves obtained using $k_2 = k_a$ differ only slightly from the corresponding (black dashed) curves calculated for $k_2 = k_b$ and the downward inflections predicted for $G(H_2)$ and $G(H_2O_2)$ above ~150 °C are practically no longer apparent. This is easily understandable since in 0.4 M H_2SO_4 solutions, hydrated electrons are very rapidly ($<10^{-9}$ s) transformed into $H^\bullet$ atoms in the tracks,[37] thereby making reaction (2) quickly inoperative in contributing to these yields whatever the temperature. Removal of this reaction thus prevents the possibility of observing any clear difference in the temperature dependence of $G(H_2)$ and $G(H_2O_2)$ above ~150 °C when either k_a or k_b is used for the $(e^-_{aq} + e^-_{aq})$ reaction rate constant.

4. Conclusion

In this work, Monte Carlo simulations were used to calculate the *G*-values for the primary species of the radiolysis of neutral liquid water and 0.4 M H_2SO_4 aqueous solutions by the recoil ions of the $^{10}B(n,\alpha)^7Li$ nuclear reaction at temperatures between 25 and 350 °C. Overall, the simulation results for neutral deaerated water agreed well with existing estimates at 20 and 289 °C. For 0.4 M H_2SO_4 solutions, reasonable agreement between experiment and simulation was also found at room temperature. Compared with the data obtained for low-LET radiation, our computed yields showed essentially similar temperature dependences over the range of temperatures studied, but with lower values for yields of free radicals and higher values for molecular yields, which reflect the high-LET character of the densely ionizing $^{10}B(n,\alpha)^7Li$ recoil ions. More experimental data are required for both neutral and acidic solutions to better describe the dependence of radiolytic yields on temperature and to test our modeling calculations more thoroughly. Moreover, measurements of the ($e^-_{aq} + e^-_{aq}$) reaction rate constant in near-neutral water would help us to determine whether the predicted non-monotonic inflections above ~150 °C in $G(H_2)$ and $G(H_2O_2)$ are confirmed.

Acknowledgements

The authors thank Professor Takayuki Terai, Professor Yusa Muroya, and Dr. Shin-ichi Yamashita for their support and advices. They are also grateful to Professor James F. Ziegler for his helpful correspondence with regard to the use of the SRIM simulation software. M. M. I. is the recipient of a scholarship from the “Centre de Recherche Médicale de l’Université de Sherbrooke”. P. L. thanks the Ministry of Education, Culture, Sports, Science, and Technology (MEXT) of Japan for financial support through a MEXT scholarship. The research of J.-P. J.-G. is supported by the Natural Sciences and Engineering Research Council of Canada (NSERC) Grant No. RGPIN-2015-06100.

Notes and references

1. *Neutron Capture Therapy. Principles and Applications*, ed. W. A. G. Sauerwein, A. Wittig, R. Moss and Y. Nakagawa, Springer, Berlin, 2012.
2. G. F. Knoll, *Radiation Detection and Measurement*, Wiley, New York, 3rd edn, 2000, p. 507.
3. D. E. Watt, *Quantities for Dosimetry of Ionizing Radiations in Liquid Water*, Taylor & Francis, London, 1996.
4. É. Sèche, R. Sabattier, J.-C. Bajard, G. Blondiaux, N. Breteau, M. Spotheim-Maurizot and M. Charlier, *Radiat. Res.*, 2002, 158, 292.
5. N. S. Hosmane, J. A. Maguire, Y. Zhu and M. Takagaki, *Boron and Gadolinium Neutron Capture Therapy for Cancer Treatment*, World Scientific, Singapore, 2012.
6. G. L. Locher, *Am. J. Roentgenol. Radium Ther.*, 1936, **36**, 1.
7. J. Chadwick, *Proc. R. Soc. London, Ser. A*, 1932, **136**, 692.
8. P. G. Kruger, *Proc. Natl. Acad. Sci. U. S. A.*, 1940, **26**, 181.
9. W. Sauerwein, *Strahlenther. Onkol.*, 1993, **169**, 1.
10. J. W. Hopewell, G. M. Morris, A. Schwint and J. A. Coderre, *Appl. Radiat. Isot.*, 2011, **69**, 1756.
11. R. F. Barth, M. G. H. Vicente, O. K. Harling, W. S. Kiger III, K. J. Riley, P. J. Binns, F. M. Wagner, M. Suzuki, T. Aihara, I. Kato and S. Kawabata, *Radiat. Oncol.*, 2012, **7**, 146.
12. R. L. Moss, *Appl. Radiat. Isot.*, 2014, **88**, 2.
13. J. Pucheault, M. Lefort and M. Haïssinsky, *J. Chim. Phys. Phys.-Chim. Biol.*, 1952, **49**, 286.
14. M. Koike, E. Tachikawa and T. Matsui, *J. Nucl. Sci. Technol.*, 1969, **6**, 163.
15. P. Cohen, *Water Coolant Technology of Power Reactors*, American Nuclear Society, La Grange Park, 1980.
16. J. Takagi, B. J. Mincher, M. Yamaguchi and Y. Katsumura, in *Charged Particle and Photon Interactions with Matter: Recent Advances, Applications, and Interfaces*, ed. Y. Hatano, Y. Katsumura and A. Mozumder, Taylor & Francis Group, Boca Raton, 2011, p. 959.

17. E. J. Hart, W. R. McDonell and S. Gordon, *Proceedings of the International Conference on the Peaceful Uses of Atomic Energy, Geneva, 8-20 Aug. 1955, P/839*, United Nations, New York, 1956, vol. 7, p. 593.
18. D. R. McCracken, K. T. Tsang and P. J. Laughton, *Aspects of the physics and chemistry of water radiolysis by fast neutrons and fast electrons in nuclear reactors, Report AECL-11895*, Atomic Energy of Canada Limited, Chalk River, Ontario, 1998.
19. H. Christensen, *Fundamental aspects of water coolant radiolysis, SKI Report 2006:16*, Swedish Nuclear Power Inspectorate, Stockholm, Sweden, April 2006.
20. A. J. Elliot and D. M. Bartels, *The reaction set, rate constants and g-values for the simulation of the radiolysis of light water over the range 20° to 350 °C based on information available in 2008*, Report AECL No. 153-127160-450-001, Atomic Energy of Canada Limited, Chalk River, Ontario, 2009.
21. R. L. Cowan, *Water Chemistry of Nuclear Reactor Systems 7, Bournemouth, UK, 13-17 Oct. 1996*, British Nuclear Energy Society, London, 1996, p. 196.
22. Y. Wada, A. Watanabe, M. Tachibana, K. Ishida, N. Uetake, S. Uchida, K. Akamine, M. Sambongi, S. Suzuki and K. Ishigure, *J. Nucl. Sci. Technol.*, 2001, **38**, 183.
23. N. F. Barr and R. H. Schuler, *Radiat. Res.*, 1957, **7**, 302; N. F. Barr and R. H. Schuler, *J. Phys. Chem.*, 1959, **63**, 808.
24. M. Lefort, *Annu. Rev. Phys. Chem.*, 1958, **9**, 123.
25. J. Pucheault and P. Sigli, *Int. J. Radiat. Phys. Chem.*, 1976, **8**, 613; see also P. Sigli, Ph.D. thesis, Université Paris VI, Paris, 1972.
26. P. Lertnaisat, Y. Katsumura, J. Meesungnoen, J.-P. Jay-Gerin, S. Mukai, R. Umehara, Y. Shimizu and M. Suzuki, *15th International Congress of Radiation Research, Kyoto*, Japan, 25-29 May 2015, Poster 2-PS6D-06.
27. J. Meesungnoen and J.-P. Jay-Gerin, *J. Phys. Chem. A*, 2005, **109**, 6406.
28. J. Meesungnoen and J.-P. Jay-Gerin, in *Charged Particle and Photon Interactions with Matter: Recent Advances, Applications, and Interfaces*, ed. Y. Hatano, Y. Katsumura and A. Mozumder, Taylor & Francis Group, Boca Raton, 2011, p. 355;

see also J. Meesungnoen, Ph.D. thesis, Université de Sherbrooke, Sherbrooke, Québec, Canada, 2007.

29. S. Sanguanmith, Y. Muroya, J. Meesungnoen, M. Lin, Y. Katsumura, L. Mirsaleh Kohan, D. A. Guzonas, C. R. Stuart and J.-P. Jay-Gerin, *Chem. Phys. Lett.*, 2011, **508**, 224.
30. J. Meesungnoen, S. Sanguanmith and J.-P. Jay-Gerin, *RSC Adv.*, 2015, **5**, 76813.
31. R. L. Platzman, in *Radiation Biology and Medicine. Selected Reviews in the Life Sciences*, ed. W. D. Claus, Addison-Wesley, Reading, 1958, p. 15.
32. M. Tachiya, *Radiat. Phys. Chem.*, 1983, **21**, 167.
33. S. M. Pimblott, M. J. Pilling and N. J. B. Green, *Radiat. Phys. Chem.*, 1991, **37**, 377.
34. Y. Frongillo, T. Goulet, M.-J. Fraser, V. Cobut, J. P. Patau and J.-P. Jay-Gerin, *Radiat. Phys. Chem.*, 1998, **51**, 245.
35. T. Goulet, M.-J. Fraser, Y. Frongillo and J.-P. Jay-Gerin, *Radiat. Phys. Chem.*, 1998, **51**, 85.
36. I. Plante, Ph.D. thesis, Université de Sherbrooke, Sherbrooke, Québec, Canada, 2009.
37. N. Autsavapromporn, J. Meesungnoen, I. Plante and J.-P. Jay-Gerin, *Can. J. Chem.*, 2007, **85**, 214.
38. T. Tippayamontri, S. Sanguanmith, J. Meesungnoen, G. R. Sunaryo and J.-P. Jay-Gerin, *Recent Res. Dev. Phys. Chem.*, 2009, **10**, 143.
39. J. F. Ziegler, J. P. Biersack and M. D. Ziegler, *SRIM – The Stopping and Range of Ions in Matter*, SRIM Co., Chester, MD, 2015; see also J. F. Ziegler, M. D. Ziegler and J. P. Biersack, *Nucl. Instrum. Methods Phys. Res., Sect. B*, 2010, **268**, 1818.
40. J. A. LaVerne, in *Charged Particle and Photon Interactions with Matter: Chemical, Physicochemical, and Biological Consequences with Applications*, ed. A. Mozumder and Y. Hatano, Marcel Dekker, New York, 2004, p. 403.
41. S. Gordon, K. H. Schmidt and J. R. Honekamp, *Radiat. Phys. Chem.*, 1983, **21**, 247.
42. J. Meesungnoen, J.-P. Jay-Gerin, A. Filali-Mouhim and S. Mankhetkorn, *Radiat. Res.*, 2002, **158**, 657.

43. A. O. Allen, *The Radiation Chemistry of Water and Aqueous Solutions*, D. Van Nostrand Co., Princeton, NJ, 1961.
44. S. Sanguanmith, J. Meesungnoen, Y. Muroya, M. Lin, Y. Katsumura and J.-P. Jay-Gerin, *Phys. Chem. Chem. Phys.*, 2012, **14**, 16731.
45. D. Swiatla-Wojcik and G. V. Buxton, *J. Phys. Chem.*, 1995, **99**, 11464.
46. M.-A. Hervé du Penhoat, T. Goulet, Y. Frongillo, M.-J. Fraser, Ph. Bernat and J.-P. Jay-Gerin, *J. Phys. Chem. A*, 2000, **104**, 11757.
47. S. L. Butarbutar, Y. Muroya, L. Mirsaleh Kohan, S. Sanguanmith, J. Meesungnoen and J.-P. Jay-Gerin, *At. Indones.*, 2013, **39**, 51.
48. S. L. Butarbutar, S. Sanguanmith, J. Meesungnoen, G. R. Sunaryo and J.-P. Jay-Gerin, *Radiat. Res.*, 2014, **181**, 659.
49. S. Sanguanmith, J. Meesungnoen, D. A. Guzonas, C. R. Stuart and J.-P. Jay-Gerin, *J. Nucl. Eng. Radiat. Sci.*, 2016, **2**, 021014.
50. A. J. Elliot, *Rate constants and g-values for the simulation of the radiolysis of light water over the range 0-300 °C, Report AECL-11073*, Atomic Energy of Canada Limited, Chalk River, Ontario, 1994.
51. C. R. Stuart, D. C. Ouellette and A. J. Elliot, *Pulse radiolysis studies of liquid heavy water at temperatures up to 250 °C, Report AECL-12107*, Atomic Energy of Canada Limited, Chalk River, Ontario, 2002.
52. D. Hatomoto, Y. Muroya, Y. Katsumura, S. Yamashita and T. Kozawa, in *Book of Abstracts, 5th Asia-Pacific Symposium on Radiation Chemistry, University of Tokyo*, Tokyo, Japan, 8-11 Sept. 2014, Paper No. P08, p. 140.
53. S. Sanguanmith, Y. Muroya, T. Tippayamontri, J. Meesungnoen, M. Lin, Y. Katsumura and J.-P. Jay-Gerin, *Phys. Chem. Chem. Phys.*, 2011, **13**, 10690.
54. C. D. Alcorn, J.-C. Brodovitch, P. W. Percival, M. Smith and K. Ghandi, *Chem. Phys.*, 2014, **435**, 29.
55. C. Ferradini and J.-P. Jay-Gerin, *Res. Chem. Intermed.*, 2000, **26**, 549.

5. ARTICLE no. 2

In situ generation of ultrafast transient "acid spikes" in the $^{10}B(n,\alpha)^{7}Li$ radiolysis of water.

Authors: **Muhammad Mainul Islam,** Vanaja Kanike, Jintana Meesungnoen, Phantira Lertnaisat, Yosuke Katsumura and Jean-Paul Jay-Gerin

Status: Published in *Chemical Physics Letters*, 2018, vol.: **693** (February 1st, 2018), pages: 210-215 (DOI: 10.1016/j.cplett.2017.12.037). Impact factor: 1.815.

Forward: The *in situ* formation of H_3O^+ by the $^{10}B(n,\alpha)^{7}Li$ radiolysis of water renders the trajectories of the two helium and lithium recoiling ions temporarily very acidic. Using both Monte Carlo track chemistry simulations and an axially homogeneous cylindrical track model, characteristic of high linear energy transfer radiation (LET), we find that the pH remains near 0 at times less than ~100 ps after which it gradually returns to neutrality at ~0.1 ms. In a cellular environment, which contains a large amount of water, these initial conditions of high acidity are about two orders of magnitude longer than in free water due to the much slower intracellular mobility of the free proton. The implications of this "acid spike" effect in boron neutron capture therapy (BNCT) and, more generally, in hadrontherapy, is discussed briefly.

Résumé : La formation *in situ* de H_3O^+ lors de la radiolyse de l'eau par les ions de recul (particules α et ions lithium) de la réaction nucléaire $^{10}B(n,\alpha)^{7}Li$ rend les régions autour des trajectoires natives du rayonnement temporairement très acides. En utilisant à la fois les simulations Monte Carlo et un modèle de trajectoire cylindrique caractéristique des rayonnements à haut transfert d'énergie linéaire (TEL), nous avons observé que le pH le long de ces trajectoires est proche de 0 jusqu'à ~100 ps puis revient graduellement à la neutralité à ~0,1 ms. En milieu cellulaire, qui contient une grande quantité d'eau, le pic d'acidité s'étend sur une plus longue période de temps (environ deux ordres de grandeur) à cause de la faible mobilité du proton dans ce milieu, ce qui soulève plusieurs questions en relation avec la boroneutrothérapie et, plus généralement, l'hadronthérapie.

In situ generation of ultrafast transient "acid spikes" in the $^{10}B(n,\alpha)^{7}Li$ radiolysis of water.

by

Muhammad Mainul Islam [a], Vanaja Kanike [a], Jintana Meesungnoen [a], Phantira Lertnaisat [b,†], Yosuke Katsumura [b,‡], Jean-Paul Jay-Gerin [a,*]

[a] *Département de Médecine Nucléaire et de Radiobiologie, Faculté de Médecine et des Sciences de la Santé, Université de Sherbrooke, 3001, 12e Avenue Nord, Sherbrooke (Québec) J1H 5N4, Canada*

[b] *Department of Nuclear Engineering and Management, School of Engineering, The University of Tokyo, Hongo 7-3-1, Bunkyo-ku, Tokyo 113-8656, Japan*

Abstract

Monte Carlo track chemistry simulations of the $^{10}B(n,\alpha)^{7}Li$ radiolysis of water show that the *in situ* formation of H_3O^+ by the two He and Li recoiling ions renders the native track regions temporarily very acidic. For these irradiating ions, the pH remains near 0 at times less than ~100 ps after which the system gradually returns to neutral pH at ~0.1 ms. These "acid spikes" have never been invoked in water or in a cellular environment exposed to densely ionizing radiations. The question of their implications in boron neutron capture therapy and, more generally, in hadrontherapy, is discussed briefly.

***Keywords*:** $^{10}B(n,\alpha)^{7}Li$ nuclear reaction, α-particles and Li recoil ions, liquid/cell water, radiolysis, H_3O^+ radiolytic yield, pH, acid spike, Monte Carlo track chemistry simulation, boron neutron capture therapy (BNCT), hadrontherapy.

†*Present address*: Mott MacDonald, 19th Floor Chamnan Phenjati Building, 65/159 Rama 9 Road, Huay Kwang, Bangkok 10310, Thailand.

‡*Present address*: Japan Radioisotope Association (JRIA), Honkomagome 2-28-45, Bunkyo-ku, Tokyo 113-8941, Japan.

*Corresponding author. *E-mail address:* jean-paul.jay-gerin@USherbrooke.ca

Chem. Phys. Lett. **693**, 210-215 (2018).

1. Introduction

All biological systems are damaged by ionizing radiation. While fundamental biological processes are numerous and complex, they are triggered in aqueous environments as living cells consist mainly of water (~70-85% by weight). As a result, a thorough knowledge of the radiation chemistry of water is critical to our understanding of the early stages in the chain of radiobiological events that follow the absorption of radiation. Indeed, reactive chemical species generated by water radiolysis may damage all biomolecules, including nuclear acids, proteins and membrane lipids. DNA and its associated water molecules of hydration are considered to be the most critical target in defining the radiobiological response. Lesions randomly induced in cellular DNA by ionizing radiation can be repaired or can result in cytotoxic and mutagenic effects and chromosomal instability, all of which can contribute to tumorigenesis [1-7].

The nuclear reaction produced when boron-10 (a stable isotope) is bombarded with thermal or epithermal neutrons, represented by $^{10}B(n,\alpha)^{7}Li$, is one of the most favorable ones for use in targeted chemo-radiotherapies for cancer treatment known as "boron neutron capture therapy" (abbreviated BNCT) [8,9]. BNCT utilizes boron-10 that is attached to a suitable tumor-seeking drug. It is an ideal treatment to kill cancer cells selectively without harming healthy cells nearby. This is because the capture cross-section for slow neutrons by ^{10}B (3835 barns, 1 barn = 10^{-28} m^2) is about three orders of magnitude greater than that of the nuclei of living tissues. The high linear energy transfer (LET) α-particles (^{4}He) and recoiling lithium-7 (^{7}Li) nuclei emitted during the neutron capture reaction (Fig. 1) have path lengths in the range of ~5-8 μm in water or biological tissue (approximately the diameter of a mammalian cell) and deposit most of their energy within the boron-containing cells. Thus, if sufficient amounts of ^{10}B can be preferentially delivered to a cancer cell, and bombarded with slow neutrons, cell damage would be confined to that particular

cell as a result of the $^{10}B(n,\alpha)^{7}Li$ capture reaction, with the concomitant sparing of adjacent healthy cells. This is the basis of BNCT as a clinical treatment modality.

It is customary to separate the complex succession of the events that follow the irradiation of water into five consecutive, temporal stages [11-13]. Briefly, the first or "physical" stage consists of the phenomena by which energy is transferred from the incident radiation to the water. The duration of this stage is around 10^{-16} s or less. This energy deposition gives rise, along and around the "native" radiation tracks, to a large number of ionized ($H_2O^{\bullet+}$) and excited (H_2O^*) water molecules distributed in a specific, highly non-homogeneous "track structure" which depends on the type and energy of the radiation used. On average, secondary electrons generated in the ionization events have kinetic energies of less than ~100 eV [14-18]. They therefore have sufficient energy to ionize or excite one or more other water molecules in close proximity, creating copious quantities of low-energy electrons with mean energy below 10 eV. The second or "physicochemical" stage consists of the re-establishment of thermal equilibrium in the bulk medium with reactions and reorganization of initial products to give new chemical species such as stable molecules and water free radicals. It lasts ~10^{-12} s. During this stage, secondary electrons slow down to subexcitation (e^-_{sub}, < 7.3 eV) and then thermal (e^-_{th}) energies, and, following thermalization, they become trapped (e^-_{tr}) and finally hydrated (e^-_{aq}) [16,19].

From ~10^{-16} to 10^{-12} s after the initial energy deposition, the radiolysis of water can simply be described by the following reactions [20]:

$$H_2O \rightarrow H_2O^{\bullet+} + e^- \quad (\text{ionization}) \qquad (1)$$

$$H_2O \rightarrow H_2O^* \quad (\text{excitation}) \qquad (2)$$

$$H_2O^{\bullet+} + H_2O \rightarrow H_3O^+ + {}^{\bullet}OH \qquad (3)$$

(proton transfer reaction, ~200 fs; H_3O^+ represents the hydrated proton)

- $e^- + H_2O^{\bullet+} \rightarrow H_2O^* \left(\text{electron-cation geminate recombination}\right)$ (4)
- $e^- \rightarrow e^-_{sub} \rightarrow e^-_{th} \rightarrow e^-_{tr} \rightarrow e^-_{aq}$ (~240 fs to 1 ps) (5)
- $e^- + H_2O \rightarrow \left(H_2O^{\bullet-*}\right) \rightarrow H^- + {}^{\bullet}OH$ (6)

(resonant "dissociative electron attachment", or DEA, process)
followed by the reaction of H^- with water

$H^- + H_2O \rightarrow H_2 + OH^-$ (7)

- $H_2O^* \rightarrow e^-_{aq} + H_2O^{\bullet+}$ (threshold at ~6.5 eV) (8)

$\rightarrow H^{\bullet} + {}^{\bullet}OH$ (9)

$\rightarrow H_2 + O(^1D)$ (oxygen atom in its singlet ^1D first excited state) followed by

$O(^1D) + H_2O \rightarrow H_2O_2$ (or possibly also 2 ${}^{\bullet}OH$) (10)

$\rightarrow H^{\bullet} + H^{\bullet} + {}^{\bullet}O^{\bullet}(^3P)$ (oxygen atom in its triplet ^3P ground state, rather inert to water but reacts with most additives) (11)

$\rightarrow H_2O$ (non-radiative decay back to ground-state water) (12)

By ~1 ps, the "initial" radiolysis products are e^-_{aq}, $H^{\bullet}$, ${}^{\bullet}OH$, H_3O^+, OH^-, H_2, H_2O_2, $O_2^{\bullet-}$ [or its protonated form $HO_2^{\bullet}$; $pK_a\left(HO_2^{\bullet}/O_2^{\bullet-}\right) = 4.8$ in water at 25 °C], $O(^1D)$, ${}^{\bullet}O^{\bullet}(^3P)$, *etc*. In the third stage of "nonhomogeneous chemistry", the different radiolytic species diffuse away from the site where they originally formed. The result is that a fraction of them reacts with one another within the tracks as they develop in time while the remainder escape into the bulk solution. At 25 °C, all tracks have essentially dissipated on the microsecond time scale. The species that have escaped from track reactions become homogeneously distributed throughout the bulk of the solution [21,22]. There follows a stage of "homogeneous chemistry" and finally, in a physiologic system, a "biological" stage (~10^{-3} s or longer, depending very much upon the medium) [7] in which the cells respond to the damage resulting from the products formed in the preceding stages.

The yields (or *G*-values) of all the radiolytic species and their initial geometric distributions along the tracks are strongly dependent on the radiation type and energy, a measure of which is given by the LET. For low-LET radiation, such as fast electrons or γ-rays from ^{60}Co (LET ~ 0.3 eV/nm), tracks are formed initially by well-separated clusters of reactive species, commonly known as "spurs" (spherical in shape), that develop independently in time [23-25]. In this case, the predominant effect of radiolysis is radical production. However, with increasing LET, the isolated spur structure changes to a situation in which the spurs eventually overlap and form (initially) a dense continuous column (cylindrical in shape) of species [16,26-29]. This leads to an increased amount of intra-track chemistry, favoring radical-radical reactions in the diffusing tracks. Under these conditions, the free-radical yields diminish as the LET increases, whereas the molecular yields increase.

Most interestingly, the *in situ* formation of H_3O^+ in reaction (3) during the primary radiolysis processes in water irradiated with low/high-LET radiation renders the "native" spur/track regions temporarily very acidic. Such a transient *acid* pH response to the ionizing radiation during and shortly after irradiation was recently quantified by our group [20], using both Monte Carlo track chemistry simulations and simple, LET-dependent, space-time track models. In this work, we extend our previous calculations [10,20] to determine the yields of H_3O^+ produced by the $^{10}B(n,\alpha)^7Li$ radiolysis of water as a function of time. As expected, an abrupt "acid spike" effect is observed at early times around the trajectories of the two recoiling ions. In a cellular environment, this acidic pH, even local and transitory, could have important biological consequences. However, to the best of our knowledge, it has never been mentioned so far in the context of the BNCT nor other forms of hadrontherapy (recall here that when the irradiating beams are made of protons or other ions, such as carbon, radiotherapy is called "hadrontherapy").

2. Monte Carlo track chemistry simulations

The stochastic modeling of the radiolysis of liquid water at ambient temperature by both 1.47 MeV α-particles and 0.84 MeV lithium nuclei emitted from the neutron-boron nuclear reaction was performed using our Monte Carlo track chemistry simulation code IONLYS-IRT [15,19,30-33]. This code first models, in a 3D geometrical environment, the initial, highly nonhomogeneous radiation track structure ("IONLYS" program), and then the ensuing diffusion and chemical reactions of the various radical and molecular products formed by radiolysis ("IRT" program). A detailed description of the current version of the code under high-LET irradiation conditions is given in [10]. Briefly, the IONLYS program is used to model the early physical and physicochemical stages of radiation action up to ~1 ps in track development. It actually models, event by event, all the basic physical interactions (energy deposition) and the subsequent conversion of the physical products created locally into the various initial radical and molecular products of the radiolysis [see reactions (1)-(12)]. The complex, highly nonhomogeneous spatial distribution of reactants at the end of the physicochemical stage, which is provided as an output of the IONLYS program, is then used directly as the starting point for the subsequent nonhomogeneous chemical stage (typically from ~1 ps to the μs time scale at 25 °C). This third stage, during which the different radiolytic species diffuse randomly at rates determined by their diffusion coefficients and react with one another until all track processes are complete, is covered by our IRT program. This program employs the "independent reaction times" (IRT) method [30,34], a computationally efficient stochastic simulation technique that is used to simulate reaction times without having to follow the trajectories of the diffusive species. Its ability to give accurate time-dependent chemical yields under different irradiation conditions has been well validated by comparison with full random flights (or "step-by-step") Monte Carlo simulations, which do follow the reactant trajectories in detail [35]. This IRT program can obviously also be used efficiently to describe the reactions that

occur in the bulk solution in the homogeneous chemical stage (*i.e.*, in the time domain beyond a few microseconds).

The SRIM software [36] was used to calculate the trajectories of 1.47-MeV α-particles and 0.84-MeV lithium nuclei emitted from the $^{10}B(n,\alpha)^{7}Li$ reaction (Fig. 2), as well as the energies and LET values of the two recoil ions as a function of penetration depth in water. The details of these calculations have been presented previously [10]. Three major findings may be summarized as follows:

1. Using Watt's compilation of quantities for radiation dosimetry in liquid water [37], the "dose-average" LET values for both He (1.47 MeV) and Li (0.84 MeV) recoils were determined to be ~196 and 216 eV/nm, respectively.
2. To avoid complexity arising from energy-dependent charge exchange processes, our Monte Carlo simulations were performed under the simplifying approximation that the energies of the two recoil ions remained constant when passing through the water medium. Using SRIM simulation results, these constant average energy values $\bar{E}_{He}$ and $\bar{E}_{Li}$ were found to be ~0.3 and 0.4 MeV, respectively.
3. The actual effective charges carried by the two helium and lithium ions having these average energies were adjusted to the values Z_{eff} = 1.6 and 1.7, respectively, so as to reproduce the expected LET values.

All our calculations were performed by simulating short (typically, ~1-5 μm) ion track segments, over which the energy and LET of the ion are well defined and remain nearly constant. Such model calculations thus gave "track segment" yields [29] at a well-defined LET. The number of individual ion "histories" (usually ~2-10) was chosen to ensure only small statistical fluctuations in the computed averages of chemical yields, while keeping acceptable computer time limits.

Finally, the yields of primary free radical or molecular products due to the radiolysis of water induced by the $^{10}B(n,\alpha)^{7}Li$ reaction were calculated by summing the *G*-values for each recoil ion (obtained from our Monte Carlo simulations) weighted by its fraction of the total energy absorbed according to [38,39]

$$G(X_i) = \frac{G(X_i)_{He} E_{He} + G(X_i)_{Li} E_{Li}}{E_T}, \quad (13)$$

where $G(X_i)_{He}$ and $G(X_i)_{Li}$ are the yields of species X_i associated with the recoil helium and lithium ions, respectively, and $E_T = E_{He} + E_{Li}$ is the sum of the initial energies of the ion products of the reaction (*i.e.*, 2.31 MeV).

Absorption of the accompanying low-LET 0.478 MeV γ-ray in the aqueous solution (see Fig. 1) is small in our area of interest (indeed, the range of an incident electron of this energy is ~1 mm in liquid water at 25 °C [40]; this is more than 100 times larger than the penetration ranges of the He and Li ions, which are only ~5-8 μm). In this study, we neglected its contribution to the overall chemical reaction.

Throughout this paper, *G*-values are quoted in units of molecules formed or consumed per 100 eV of radiation energy absorbed. For conversion into SI units, 1 molecule/100 eV = 0.10364 μmol/J.

3. Results and discussion

Figure 3 shows the time evolution of $G(H_3O^+)$ as obtained from our simulations of the $^{10}B(n,\alpha)^{7}Li$ radiolysis of pure, deaerated liquid water at 25 °C, over the interval of ~1 ps to 1 ms. For the sake of reference, the simulated time-dependent yields of e^-_{aq}, $^\bullet OH$, $H^\bullet$, and OH^- are also shown in the figure. Quite obviously, the hydroxide ion OH^-, which is formed largely by the intra-track reaction [30,41]

$$e^-_{aq} + {}^\bullet OH \rightarrow OH^-, \; k_{14} = 3.5 \times 10^{10} \; M^{-1} \; s^{-1} \quad (14)$$

contributes to an alkaline track and consequently counteracts the acid spike effect discussed in this work. However, as we can see from Fig. 3, $G(OH^-)$ remains much smaller than $G(H_3O^+)$ over the time range of interest. As a result, its effect only slightly modifies the quantitative features of the pH and can be ignored to a good approximation.

Figure 4 shows the time dependence of the cumulative yield variations $\Delta G(H_3O^+)$ for the different reactions that contribute to $G(H_3O^+)$, calculated from our Monte Carlo simulations in the time interval ~1 ps to 1 ms. As can be seen, the decrease of $G(H_3O^+)$ as a function of time is mainly due to H_3O^+ reacting with OH^- and, to a lesser extent, with the hydrated electron, according to:

$$H_3O^+ + OH^- \rightarrow 2H_2O,\ k_{15} = 1.18 \times 10^{11}\ M^{-1}\ s^{-1} \quad (15)$$

$$H_3O^+ + e_{aq}^- \rightarrow H^\bullet + H_2O,\ k_{16} = 2.13 \times 10^{10}\ M^{-1}\ s^{-1} \quad (16)$$

where k_{15} and k_{16} are the rate constants for the two individual reactions. Other reactions, such as

$$H_3O^+ + HO_2^- \rightarrow H_2O_2 + H_2O,\ k_{17} = 5 \times 10^{10}\ M^{-1}\ s^{-1} \quad (17)$$

and

$$H_3O^+ + O^{\bullet -} \rightarrow {}^\bullet OH + H_2O,\ k_{18} = 5 \times 10^{10}\ M^{-1}\ s^{-1}, \quad (18)$$

also contribute to the decay of $G(H_3O^+)$, but only relatively weakly.

Next, to calculate the pH values prevailing in the He and Li recoil track regions, we estimated the concentrations of H_3O^+ radiolytically generated *in situ* in these regions as a function of time using a cylindrical track model (characteristic of high-LET radiation) [20]. For both of these radiations, we assumed the ion's track as being an axially homogeneous cylinder, of length L = 1 μm and initial radius r_c equal to the radius of the physical track "core" [16,27]. For the sake of illustration, Fig. 5 shows two-dimensional representations of 1 μm track segments of, respectively, 0.3 MeV helium ion (Z_{eff} = 1.6) and 0.4 MeV lithium ion (Z_{eff} = 1.7) in liquid water at 25 °C. They were calculated (at ~10^{-13} s) with our IONLYS

simulation code. In this case, the track concentrations of radiolytically produced H_3O^+ can be derived from [19,20]

$$\left[\mathrm{H_3O^+}\right]_{\mathrm{radiolytic}}(t) = G\left(\mathrm{H_3O^+}\right)(t)\left[\frac{\mathrm{LET}}{\pi\, r(t)^2}\right], \tag{19}$$

where

$$r(t)^2 = r_c^2 + 4Dt \tag{20}$$

represents the change with time of r_c due to the (2D) diffusive expansion of the track. Here, t is time and D is the diffusion coefficient for the proton in pure water (D = 9.46 × 10^{-9} m^2 s^{-1} at 25 °C) [30,41]. r_c was estimated directly from our simulations. According to Fig. 5, we adopted r_c = 2 nm for both He and Li ions.

Finally, the total concentration of H_3O^+ is the sum of $[H_3O^+]_{radiolytic}$ given by Eqs. (19) and (20) and of the non-radiolytic, pre-irradiation concentration $[H_3O^+]_{autoprotolysis}$ (10^{-7} M in the present study) that arises through water's autoprotolysis:

$$\left[\mathrm{H_3O^+}\right]_{\mathrm{total}}(t) = \left[\mathrm{H_3O^+}\right]_{\mathrm{radiolytic}}(t) + \left[\mathrm{H_3O^+}\right]_{\mathrm{autoprotolysis}}. \tag{21}$$

The pH in the corresponding track regions is then simply given by the negative logarithm (to the base 10) of $[H_3O^+]_{total}$:

$$\mathrm{pH}(t) = -\log\left\{\left[\mathrm{H_3O^+}\right]_{\mathrm{total}}(t)\right\}, \tag{22}$$

The time evolution of the pH values calculated for the $^{10}B(n,\alpha)^7Li$ radiolysis of pure, deaerated liquid water at 25 °C using the $G(H_3O^+)$ values of Fig. 3 and the aforementioned cylindrical track geometry is shown in Fig. 6. As shown, there is an abrupt temporary acid pH effect at early times immediately after the initial energy release. For both He (LET ~ 196 eV/nm) and Li (LET ~ 216 eV/nm) ions, the

observed “acid-spike” effect is most intense for times shorter than ~100 ps. In this time range, the pH remains nearly constant, slightly below zero. Beyond ~100 ps, the pH increases gradually, ultimately reaching a value of 7 (pH of the body of the solution) at ~100 μs (*i.e.*, slightly longer than the beginning of homogeneous chemistry).

To the best of our knowledge, the production of an early acid spike around charged particle tracks has so far been ignored in water or in aqueous environments such as living cells subject to high-LET (densely ionizing) radiation. In this regard and considering that many cellular processes depend on pH [42,43], the present work raises the question of whether this acidic pH response, which extends over spatial dimensions of the order of tens of nanometers, has biological significance in the context of BNCT and of course, more generally, of hadrontherapy. In particular, does the generation of an acidic pH spike be potentially toxic to cells, for example, by triggering molecular mechanisms (*e.g.*, DNA breaks, defects in mitochondrial functions, modification of normal biochemical reactions, or yet triggering of different signaling cascades that respond to these stress conditions) that result in biological damage, “bystander” responses, or enhanced cell lethality [2,7,44]? Such a question becomes even more relevant when one considers that the diffusion of a proton in intracellular water is ~100-1000 times lower than in free water [45,46]. In this case, indeed, the decreased H^+ ion mobility in bulk cell water leads to a marked increase in the period of time during which the strong acidity (pH ~ 0) around the He and Li recoil ion trajectories is observed (Fig. 7).

4. Conclusion

In this work, we extended our previous calculations to determine the yields of H_3O^+ produced by the $^{10}B(n,\alpha)^7Li$ radiolysis of water as a function of time. The concentrations of H_3O^+ and the corresponding pH values for both the helium and lithium recoil ions considered were then obtained from our calculated $G(H_3O^+)$ values using an axially

homogeneous “cylindrical” track model, characteristic of high-LET radiation. An abrupt “acid spike” effect is observed at early times around the trajectories of the two He and Li recoiling ions. Most interestingly, in a cellular environment, these initial conditions of high acidity are about two orders of magnitude longer than in free water due to the much lower value of the intracellular mobility of the free proton. This acidic pH, even local and transitory, could have important consequences as it may trigger molecular mechanisms that result in biological damages and cell lethality. To the best of our knowledge, the production of such acid spikes has never been mentioned before in BNCT in addition of the overall field of hadrontherapy.

Acknowledgements

M.M.I. is the recipient of a scholarship from the “Centre de Recherche Médicale de l’Université de Sherbrooke”. P.L. thanks the Ministry of Education, Culture, Sports, Science, and Technology (MEXT) of Japan for financial support through a MEXT scholarship. The research of J.-P.J.-G. is funded by the Natural Sciences and Engineering Research Council of Canada (NSERC) Grant No. RGPIN-2015-06100.

References

[1] C. von Sonntag, Free-Radical-Induced DNA Damage and its Repair. A Chemical Perspective, Springer-Verlag, Berlin, 2006.

[2] E.J. Hall, A.J. Giaccia, Radiobiology for the Radiologist, sixth ed., Lippincott Williams & Wilkins, Philadelphia, 2006.

[3] D. Becker, A. Adhikary, M.D. Sevilla, in: Y. Hatano, Y. Katsumura, A. Mozumder (Eds.), Charged Particle and Photon Interactions with Matter: Recent Advances, Applications, and Interfaces, Taylor & Francis Group, Boca Raton, 2011, p. 503.

[4] J. Cadet, M. Berger, T. Douki, J.L. Ravanat, Rev. Physiol. Biochem. Pharmacol. 131 (1997) 1.

[5] P. O'Neill, in: C.D. Jonah, B.S.M. Rao (Eds.), Radiation Chemistry: Present Status and Future Trends, Elsevier, Amsterdam, 2001, p. 585.

[6] W.A. Bernhard, D.M. Close, in: A. Mozumder, Y. Hatano (Eds.), Charged Particle and Photon Interactions with Matter: Chemical, Physicochemical, and Biological Consequences with Applications, Marcel Dekker, New York, 2004, p. 431.

[7] E.I. Azzam, J.-P. Jay-Gerin, D. Pain, Cancer Lett. 327 (2012) 48.

[8] W.A.G. Sauerwein, A. Wittig, R. Moss, Y. Nakagawa (Eds.), Neutron Capture Therapy. Principles and Applications, Springer, Berlin, 2012.

[9] R.F. Barth, M.G.H. Vicente, O.K. Harling, W.S. Kiger III, K.J. Riley, P.J. Binns, F.M. Wagner, M. Suzuki, T. Aihara, I. Kato, S. Kawabata, Radiat. Oncol. 7 (2012) 146.

[10] M.M. Islam, P. Lertnaisat, J. Meesungnoen, S. Sanguanmith, J.-P. Jay-Gerin, Y. Katsumura, S. Mukai, R. Umehara, Y. Shimizu, M. Suzuki, RSC Adv. 7 (2017) 10782.

[11] R.L. Platzman, in: W.D. Claus (Ed.), Radiation Biology and Medicine. Selected Reviews in the Life Sciences, Addison-Wesley, Reading, 1958, p. 15.

[12] A. Kuppermann, J. Chem. Educ. 36 (1959) 279.

[13] A. Chatterjee, W.R. Holley, Adv. Radiat. Biol. 17 (1993) 181.

[14] J.A. LaVerne, S.M. Pimblott, Radiat. Res. 141 (1995) 208.

[15] V. Cobut, Y. Frongillo, J.P. Patau, T. Goulet, M.-J. Fraser, J.-P. Jay-Gerin, Radiat. Phys. Chem. 51 (1998) 229.

[16] A. Mozumder, Fundamentals of Radiation Chemistry, Academic Press, San Diego, 1999.

[17] B.C. Garrett et al. (46 authors), Chem. Rev. 105 (2005) 355.

[18] L. Mirsaleh Kohan, S. Sanguanmith, J. Meesungnoen, P. Causey, C.R. Stuart, J.-P. Jay-Gerin, RSC Adv. 3 (2013) 19282.

[19] J. Meesungnoen, J.-P. Jay-Gerin, in: Y. Hatano, Y. Katsumura, A. Mozumder (Eds.), Charged Particle and Photon Interactions with Matter: Recent Advances, Applications, and Interfaces, Taylor & Francis Group, Boca Raton, 2011, p. 355.

[20] V. Kanike, J. Meesungnoen, J.-P. Jay-Gerin, RSC Adv. 5 (2015) 43361.

[21] Y. Muroya, I. Plante, E.I. Azzam, J. Meesungnoen, Y. Katsumura, J.-P. Jay-Gerin, Radiat. Res. 165 (2006) 485.

[22] I. Plante, A. Filali-Mouhim, J.-P. Jay-Gerin, Radiat. Phys. Chem. 72 (2005) 173.

[23] G.V. Buxton, in: Farhataziz, M.A.J. Rodgers (Eds.), Radiation Chemistry: Principles and Applications, VCH Publishers, New York, 1987, p. 321.

[24] J.W.T. Spinks, R.J. Woods, An Introduction to Radiation Chemistry, third ed., Wiley, New York, 1990.

[25] C. Ferradini, J.-P. Jay-Gerin, Can. J. Chem. 77 (1999) 1542.

[26] C. Ferradini, J. Chim. Phys. 76 (1979) 636.

[27] J.L. Magee, A. Chatterjee, in: G.R. Freeman (Ed.), Kinetics of Nonhomogeneous Processes, Wiley, New York, 1987, p. 171.

[28] A. Appleby, Radiat. Phys. Chem. 34 (1989) 121.

[29] J.A. LaVerne, in: A. Mozumder, Y. Hatano (Eds.), Charged Particle and Photon Interactions with Matter: Chemical, Physicochemical, and Biological Consequences with Applications, Marcel Dekker, New York, 2004, p. 403.

[30] Y. Frongillo, T. Goulet, M.-J. Fraser, V. Cobut, J.P. Patau, J.-P. Jay-Gerin, Radiat. Phys. Chem. 51 (1998) 245.

[31] J. Meesungnoen, J.-P. Jay-Gerin, J. Phys. Chem. A 109 (2005) 6406.

[32] S. Sanguanmith, Y. Muroya, J. Meesungnoen, M. Lin, Y. Katsumura, L. Mirsaleh Kohan, D.A. Guzonas, C.R. Stuart, J.-P. Jay-Gerin, Chem. Phys. Lett. 508 (2011) 224.

[33] J. Meesungnoen, S. Sanguanmith, J.-P. Jay-Gerin, RSC Adv. 5 (2015) 76813.

[34] S.M. Pimblott, M.J. Pilling, N.J.B. Green, Radiat. Phys. Chem. 37 (1991) 377.

[35] I. Plante, Ph.D. Thesis, Université de Sherbrooke, Sherbrooke, Québec, Canada, 2009.

[36] J.F. Ziegler, J.P Bierdack, M.D. Ziegler, SRIM – The Stopping and Range of Ions in Matter, SRIM Co., Chester, MD, 2015.

[37] D.E. Watt, Quantities for Dosimetry of Ionizing Radiations in Liquid Water, Taylor & Francis, London, 1996.

[38] S. Gordon, K.H. Schmidt, J.R. Honekamp, Radiat. Phys. Chem. 21 (1983) 247.

[39] T. Tippayamontri, S, Sanguanmith, J. Meesungnoen, G.R. Sunaryo and J.-P. Jay-Gerin, Recent Res. Dev. Phys. Chem. 10 (2009) 143.

[40] J. Meesungnoen, J.-P. Jay-Gerin, A. Filali-Mouhim, S. Mankhetkorn, Radiat. Res. 158 (2002) 657.

[41] A.J. Elliot, D.M. Bartels, The reaction set, rate constants and *g*-values for the simulation of the radiolysis of light water over the range 20 to 350 °C based on information available in 2008, Report AECL-153-127160-450-001, Atomic Energy of Canada Ltd., Chalk River, Ontario, Canada, 2009.

[42] I.F. Tannock, D. Rotin, Cancer Res. 49 (1989) 4373.

[43] V. Kanike, M.Sc. Thesis, Université de Sherbrooke, Sherbrooke, Québec, Canada, 2016.

[44] B. Halliwell, J.M.C. Gutteridge, Free Radicals in Biology and Medicine, fifth ed., Oxford University Press, Oxford, 2015.

[45] W. Negendank, L. Edelmann, The State of Water in the Cell, Scanning Microscopy International, Chicago, 1988.

[46] P. Swietach, R.D. Vaughan-Jones, J. Physiol. 566 (2005) 793.

Figure captions

Figure 1: Schematic of the nuclear reaction resulting from the low-energy (< 0.5 eV) neutron capture by a ^{10}B atom. After absorption, an excited ^{11}B is formed that almost immediately (~10^{-12} s) undergoes a fission reaction producing, in 94% of the cases, two high-LET heavy ions, $^{4}He^{2+}$ (α-particle) and $^{7}Li^{3+}$, and a low-LET γ-ray (see [10]). Note that the ^{4}He and ^{7}Li recoil ions are emitted in opposite directions (*i.e.*, at a 180° angle), away from the site of the compound nucleus, and hence they form one straight track.

Figure 2: SRIM simulation of the penetration of 1000 recoil 1.47-MeV helium and 0.84-MeV lithium nuclei of the $^{10}B(n,\alpha)^{7}Li$ reaction into liquid water at 25 °C. A major contribution to the observed straggling comes from the changes in the charge state of the respective ions as they go into and through the water.

Figure 3: Time evolution of $G(H_3O^+)$ (in molecule/100 eV) for the radiolysis of pure, deaerated liquid water by the recoil of α-particles and lithium ions ("dose average" LET of ~196 and 216 eV/nm, respectively) from the $^{10}B(n,\alpha)^{7}Li$ nuclear reaction at 25 °C from ~1 ps to 1ms. The red solid line shows the hydrogen ion yield values obtained from our Monte Carlo simulations (see text). Our computed yields of e^-_{aq}, $^{\bullet}OH$, OH^- and $H^{\bullet}$ are shown as blue, grey, red, and green dashed lines, respectively.

Figure 4: Time dependence of the extents $\Delta G(H_3O^+)$ (in molecule per 100 eV) of the different reactions that are involved in the decay of H_3O^+, calculated from our Monte Carlo simulations of the $^{10}B(n,\alpha)^{7}Li$ radiolysis of pure, deaerated water at 25 °C, in the interval of ~1 ps to 1 ms.

Figure 5: Simulated track history (at ~10^{-13} s, projected into the *XY* plane of figure) of a 0.3 MeV helium ion (LET ~ 196 eV/nm) (*A*) and of a 0.4 MeV lithium ion

(LET ~ 216 eV/nm) (*B*) traversing through liquid water at 25 °C. The irradiating ion is generated at the origin and starts traveling along the *Y*-axis. Dots represent the energy deposited at points where an interaction occurred. The tracks can be described as two coaxial cylindrical volumes centered on the path of the ions. The inner cylindrical volume (*i.e.*, the region adjacent to the trajectory) is the track "core" with radius r_c. Surrounding the core is a much larger region called the "penumbra" where all of the energy is deposited by energetic secondary electrons (δ-rays) created in knock-on collisions by the ion.

Figure 6: Variation of pH with time calculated for pure, deaerated liquid water at 25 °C and in the interval of ~1 ps to 1 ms, for irradiating 0.3 MeV helium (Z_{eff} = 1.6, LET ~ 196 eV/nm) and 0.4 MeV lithium (Z_{eff} = 1.7, LET ~ 216 eV/nm) using the axially homogeneous cylindrical track model (characteristic of high-LET radiation) with r_c = 2 nm for both ions (see text). The pH values reported here are simply the average of the pH obtained for the two ions. For the sake of comparison, the dashed line shows the time evolution of pH in an isolated (spherical) "spur" (characteristic of low-LET radiation) [20] as calculated previously for 300 MeV incident protons (which mimic ^{60}Co γ/fast electron irradiation; LET ~ 0.3 eV/nm) using an initial spur radius of 11.7 nm (see Fig. 4 of [20]).

Figure 7 : Variation of pH with time calculated for deaerated bulk cellular water at 25 °C and in the interval of ~1 ps to 1 μs, under the same irradiation conditions as in Fig. 6, using the axially homogeneous cylindrical track model with r_c = 2 nm for both He and Li ions (solid line). Simulations were performed using an intracellular proton mobility 100 times lower than that in free liquid water (note that, in the calculations, the diffusion coefficients of all other species were also

lowered by a factor of 100 relative to their liquid water values). Comparison is made with the pH values calculated for irradiated free liquid water (as shown in Fig. 6) (dashed line).

FIG. 1

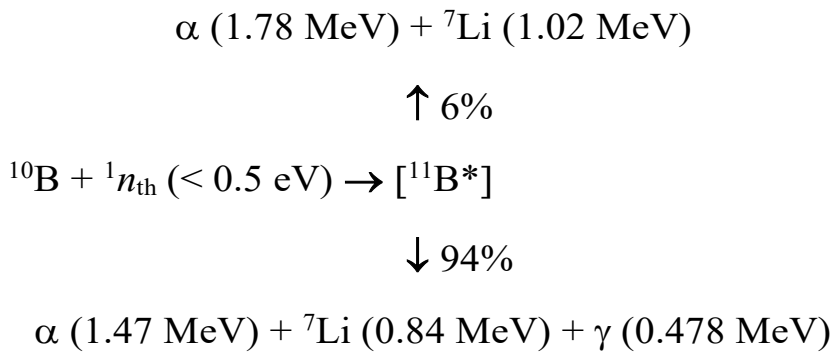
α (1.78 MeV) + ^{7}Li (1.02 MeV)
↑ 6%
^{10}B + $^{1}n_{th}$ (< 0.5 eV) → [^{11}B*]
↓ 94%
α (1.47 MeV) + ^{7}Li (0.84 MeV) + γ (0.478 MeV)

FIG. 2

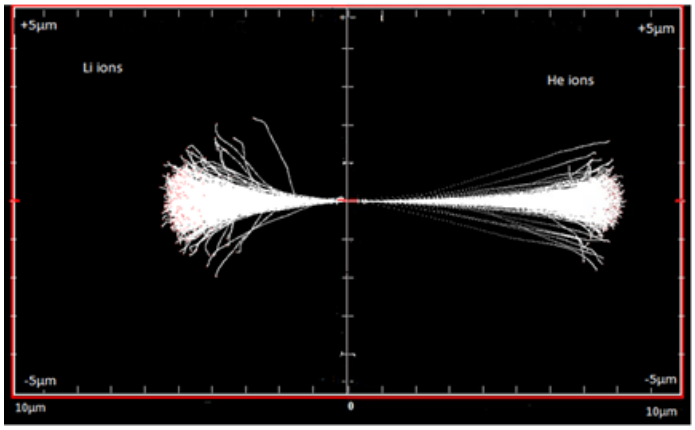

FIG. 3

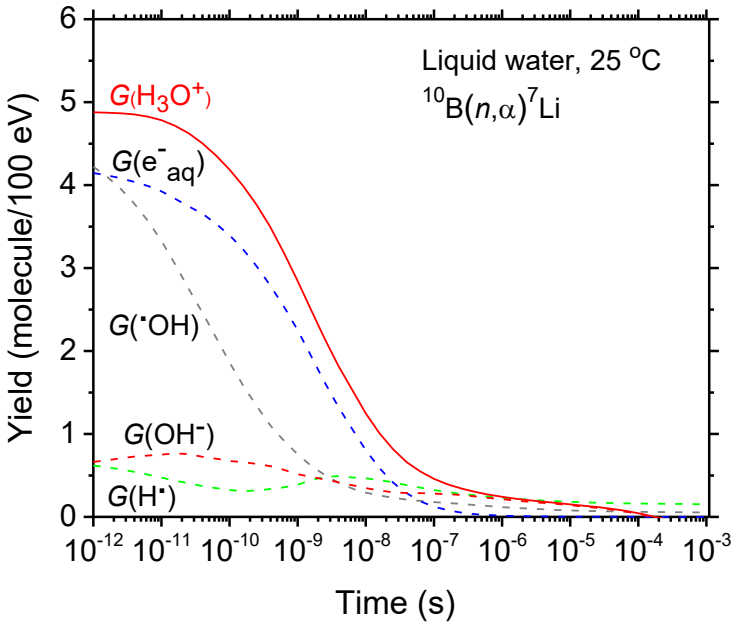
Liquid water, 25 °C
$^{10}B(n,\alpha)^{7}Li$
$G(H_3O^+)$
$G(e^-_{aq})$
$G(^{\bullet}OH)$
$G(OH^-)$
$G(H^{\bullet})$
Yield (molecule/100 eV)
Time (s)
0
1
2
3
4
5
6
10^{-12} 10^{-11} 10^{-10} 10^{-9} 10^{-8} 10^{-7} 10^{-6} 10^{-5} 10^{-4} 10^{-3}

FIG. 4

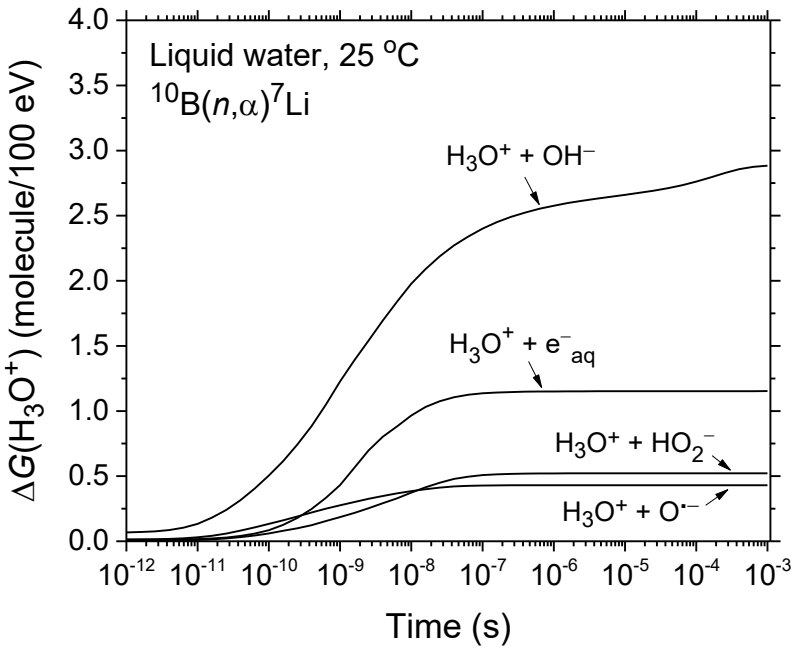
Liquid water, 25 °C
$^{10}B(n,\alpha)^{7}Li$
$H_3O^+ + OH^-$
$H_3O^+ + e^-_{aq}$
$H_3O^+ + HO_2^-$
$H_3O^+ + O^{\bullet -}$
$\Delta G(H_3O^+)$ (molecule/100 eV)
Time (s)
4.0
3.5
3.0
2.5
2.0
1.5
1.0
0.5
0.0
10^{-12} 10^{-11} 10^{-10} 10^{-9} 10^{-8} 10^{-7} 10^{-6} 10^{-5} 10^{-4} 10^{-3}

FIG. 5

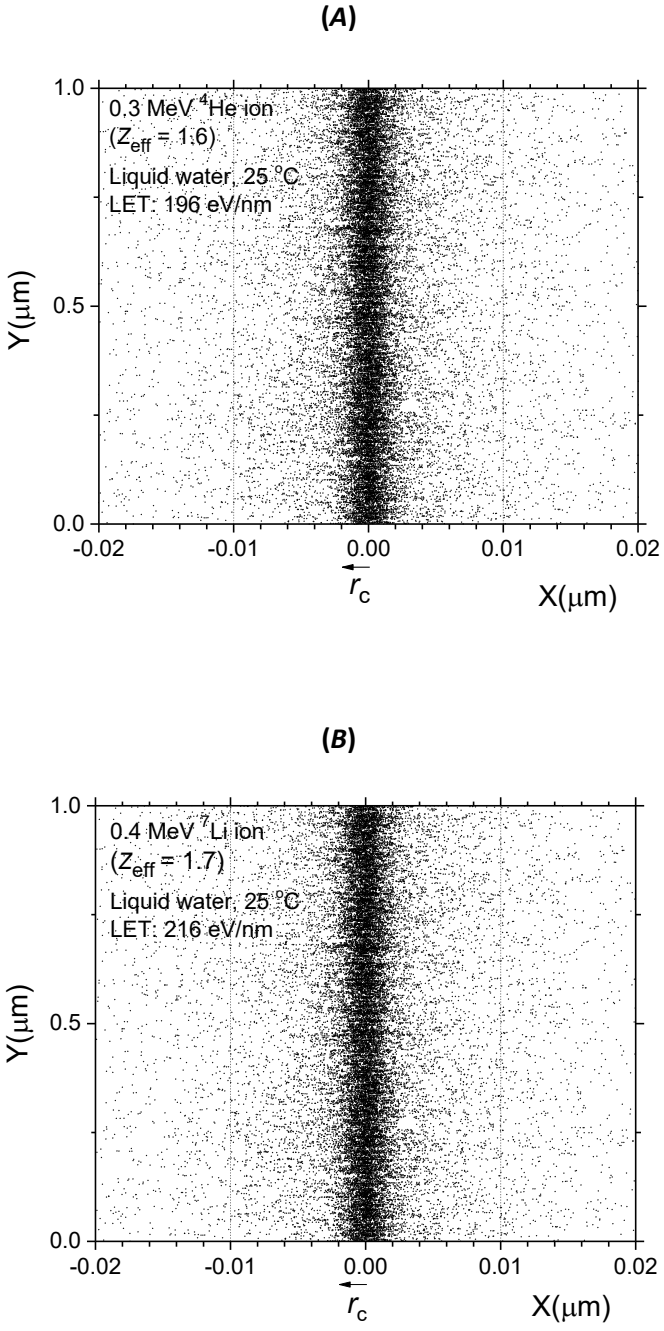
(A)
0.3 MeV 4He ion
(Zeff = 1.6)
Liquid water, 25 °C
LET: 196 eV/nm
Y(μm)
X(μm)
rc
(B)
0.4 MeV 7Li ion
(Zeff = 1.7)
Liquid water, 25 °C
LET: 216 eV/nm
Y(μm)
X(μm)
rc

FIG. 6

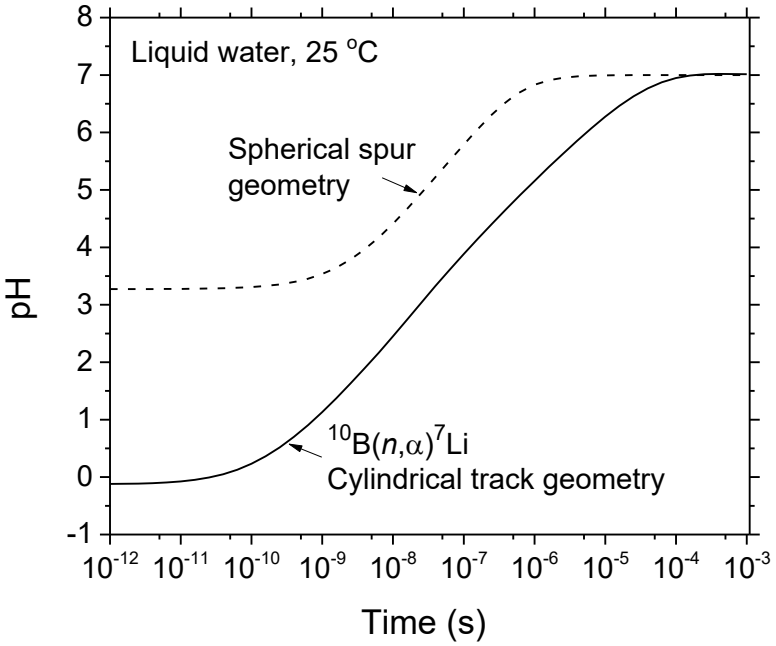
Liquid water, 25 °C
Spherical spur
geometry
$^{10}B(n,\alpha)^{7}Li$
Cylindrical track geometry
pH
Time (s)
8
7
6
5
4
3
2
1
0
-1
10^{-12} 10^{-11} 10^{-10} 10^{-9} 10^{-8} 10^{-7} 10^{-6} 10^{-5} 10^{-4} 10^{-3}

FIG. 7

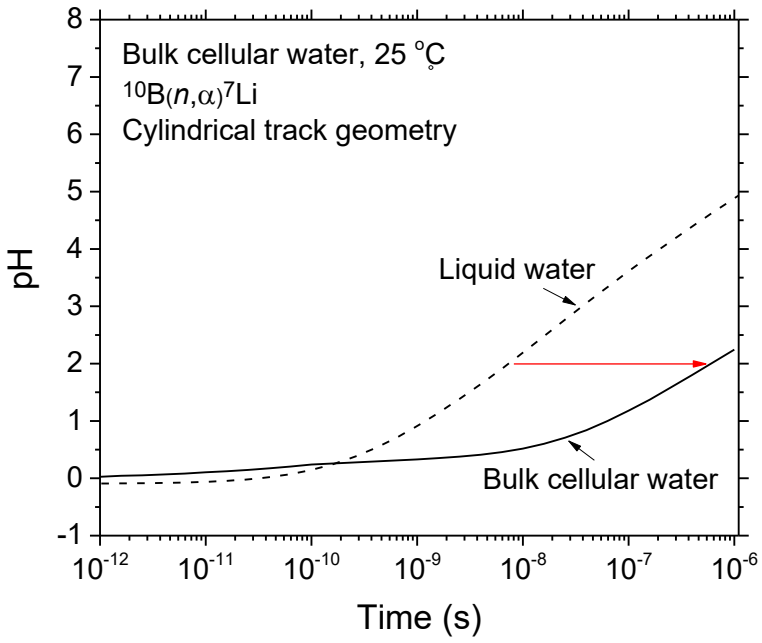
Bulk cellular water, 25 °C
$^{10}B(n,\alpha)^{7}Li$
Cylindrical track geometry
Liquid water
Bulk cellular water
pH
Time (s)
8
7
6
5
4
3
2
1
0
-1
10^{-12}
10^{-11}
10^{-10}
10^{-9}
10^{-8}
10^{-7}
10^{-6}

6. Discussion

Boron neutron capture reaction is very important both for glioblastoma, melanoma, recurrent head and neck cancers and, at high temperatures, in the nuclear industry. To predict the effects of the $^{10}B(n,\alpha)^{7}Li$ nuclear reaction in radiobiology/medicine and in the nuclear industry, it is most important to estimate the yields of the various primary products of the radiolysis of water by the two He and Li recoiling ions emitted from the neutron capture reaction, namely, e^-_{aq}, $H^\bullet$, $^\bullet OH$, and $HO_2^\bullet/O_2^{\bullet-}$ (free radical products) and H_2, H_2O_2, and O_2 (molecular products).

In our first article, we have calculated, and discussed, the yields of the free radicals and molecular species produced in the $^{10}B(n,\alpha)^{7}Li$ radiolysis of water as a function of temperature in the range from 25 to 350 °C. Computer simulations and chemical models of the radiation chemistry of the coolant water in reactors (*i.e.*, at high temperatures) are crucial because direct experimental observations are difficult under the extreme operating conditions involved. This theoretical modeling is used for the prediction of corrosion. In this respect, it contributes to maintain the proper chemical environment that will minimize the degradation/corrosion of structural materials, and in turn optimize the plant performance.

6.1 Yield of H_2 and importance of the bimolecular self-reaction of e^-_{aq}

Detailed quantitative understanding of the production of molecular hydrogen due to water radiolysis in a nuclear reactor is necessary in order to mitigate risk of corrosion. The radiolysis data obtained from ELLIOT and BARTELS (2009) have been used in our Monte Carlo track chemistry simulations. We observed a sharp downward inflection in the yield of H_2 above ~150 °C (see Article no. 1). The non-Arrhenius behavior of the rate constant of the bimolecular self-reaction of e^-_{aq} is responsible for such an abrupt inflection in the temperature dependence of $G(H_2)$ (SANGUANMITH et al., 2011). However, we observe that the yield of e^-_{aq} is very low at both 0.1 and 1 μs (Fig. 6.1*a*). To better understand the importance of this reaction, we analyzed the kinetics of the hydrated electron. As we can see from Fig. 6.1*b*, the initial (at $\sim 10^{-12}$ s) production yield of e^-_{aq} is about 4 molecules/100

eV. As a function of time, e^-_{aq} reacts with several species, the main reactions contributing to its decay being:

$$e^-_{aq} + {}^\bullet OH \rightarrow OH^-, \; k = 3.34 \times 10^{10}\ M^{-1}\ s^{-1} \qquad \text{(R1)}$$

$$e^-_{aq} + H^+ \rightarrow H^\bullet, \; k = 2.1 \times 10^{10}\ M^{-1}\ s^{-1} \qquad \text{(R2)}$$

$$e^-_{aq} + e^-_{aq}\ (+2H_2O) \rightarrow H_2 + 2OH^-, \; k = 7.3 \times 10^{9}\ M^{-1}\ s^{-1} \qquad \text{(R3)}$$

At room temperature, these reactions are comparatively slower, that is why we observe a slower decay of e^-_{aq} at 25 °C compared with its decay at 350 °C [see Appendix A of ELLIOT and BARTELS (2009) which gives the rate constants of these reactions as a function of temperature between 25 and 350 °C].

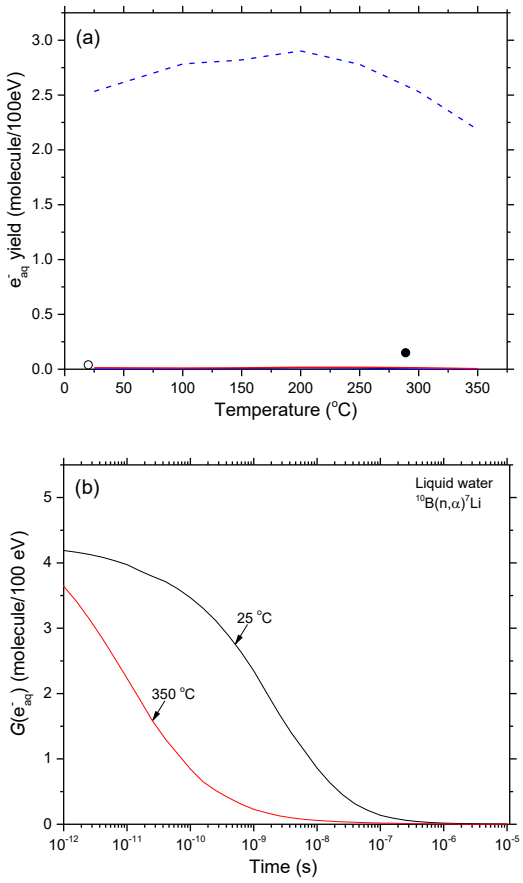

Fig. 6.1: (a) Yields of e^-_{aq} due to the $^{10}B(n,\alpha)^7Li$ radiolysis of pure, deaerated water at 10^{-6} and 10^{-7} s, shown as the red and blue solid lines, respectively. The dashed blue line shows the "escape" yield of e^-_{aq} for low-LET irradiation (γ-rays or fast electrons). (b) Comparison of the decay of e^-_{aq} at 25 °C (black line) and 350 °C (red line) as a function of time.

In pure water radiolysis, it is now well-known that the major part of the molecular hydrogen is produced on the sub-picosecond time scale (PASTINA et al., 1999) by the dissociation of the excited water molecules (H_2O^*) formed by the recombination of a subexcitation-energy electron with its parent cation $H_2O^{\bullet+}$ ("geminate recombination") and by the dissociative attachment of such a subexcitation electron to a water molecule ("dissociative electron attachment" or DEA) (COBUT et al., 1996; STERNICZUK and BARTELS, 2016). The rest of the formation of H_2 is produced on the picosecond-microsecond time scale in the three following combination reactions, with the first two dominating (COBUT et al., 1996; SPINKS and WOODS, 1990; FERRADINI and JAY-GERIN, 1999; ELLIOT and BARTELS, 2009; STERNICZUK and BARTELS, 2016):

$$e^-_{aq} + e^-_{aq} (+ 2H_2O) \rightarrow H_2 + 2OH^- \quad \text{(R3)}$$

$$e^-_{aq} + H^\bullet (+ H_2O) \rightarrow H_2 + OH^- \quad \text{(R4)}$$

$$H^\bullet + H^\bullet \rightarrow H_2 \quad \text{(R5)}$$

and (above ~200 °C) (SANGUANMITH et al., 2011)

$$H^\bullet + H_2O \rightarrow H_2 + {}^\bullet OH \quad \text{(R6)}$$

Reaction (R3) is assumed to be a two-step process with the formation of an intermediate dielectron ($e_2^{2-}{}_{aq}$) (CHRISTENSEN and SEHESTED, 1986; MARIN et al., 2007):

$$e^-_{aq} + e^-_{aq} \rightleftharpoons e_2^{2-}{}_{aq} \rightarrow H_2 + 2OH^- \quad \text{(R7)}$$

Considering the non-Arrhenius behavior of the rate constant for the self-reaction of the hydrated electron, similar downward discontinuity at ~150 °C in the yield of H_2 has also been found in the low-LET radiolysis of water (SANGUANMITH et al., 2011) as well as in the radiolysis of water by fast (2 MeV) neutrons (which produce high-LET recoil protons and oxygen ions) (BUTARBUTAR et al., 2013, 2014; BUTARBUTAR, 2014). Simulations further showed that the magnitude of this discontinuity increases as the LET increases. However, this simulated downward inflection in the H_2 yield is not observed experimentally, not only for low-LET, but also for high-LET radiation. To obtain

acceptable fits of the calculated yields to the experimental data above 150 °C, SANGUANMITH et al. (2011) were led, for low-LET irradiation, to adjust the temperature dependence of certain parameters involved in the early ($<10^{-12}$ s) physicochemical stage of the radiolysis, in particular the thermalization distance of subexcitation-energy electrons (r_{th}). Indeed, to compensate for the decrease of the rate constant for the self-reaction of e^-_{aq}, a sharp decrease of r_{th} above 100-150 °C (invoking a change in the structure of water at ~150 °C) had to be included in their simulations. Under these conditions, very good agreement was found between simulated and experimental yields, the sharp downward discontinuity predicted in $G(H_2)$ at 150 °C no longer appearing (SANGUANMITH et al., 2011).

Unfortunately, the modification of the temperature dependence of r_{th} made at low LET by SANGUANMITH et al. (2011) turns out to be insufficient at high LET, as the abrupt downward inflection in $G(H_2)$ at ~150 °C reappears, not only in the radiolysis of water by fast (2 MeV) neutrons (BUTARBUTAR et al., 2013, 2014) but also in the radiolysis of water by the $^{10}B(n,\alpha)^7Li$ recoiling ions (Article no. 1). These findings are contrary to experiment (ELLIOT et al., 1996; CHRISTENSEN, 2006).

BUTARBUTAR (2013) concluded that, under such high-LET conditions, it is rather difficult, if not impossible, to further modify the temperature dependence of r_{th} (as it was done at low LET). Moreover, it is hardly conceivable that r_{th} would be a function of the LET of the radiation. Therefore, based on previous and present studies, we tend to believe the argument that the drop in the ($e^-_{aq} + e^-_{aq}$) reaction rate constant observed at 150 °C in *alkaline* water (CHRISTENSEN and SEHESTED, 1986; STERNICZUK and BARTELS, 2016) is a function of the pH of the solution (ELLIOT, 1994; STUART et al., 2002). In strongly acidic medium such as 0.4 M H_2SO_4 acid solutions, the H^+ ions very rapidly ($<10^{-9}$ s) scavenge most, if not all, of the e^-_{aq} radicals in the tracks to form $H^\bullet$ atoms in the tracks (AUTSAVAPROMPORN et al., 2007), thereby making reaction (R3) quickly inoperative in contributing to $G(H_2)$ whatever the temperature. Removal of this reaction thus prevents the possibility of observing any clear evidence of a discontinuity in the temperature dependence of $G(H_2)$ above 150 °C. As further emphasized in Article no. 1, the applicability of the sudden drop in the ($e^-_{aq} + e^-_{aq}$) reaction rate constant observed at

150 °C in alkaline water to near-neutral water is questionable. Measurements of this rate constant in *neutral or slightly acidic* (as the pH of water at 150-200 °C is about 5.7-6) *solution* are highly desirable.

6.2 Yield of H_2O_2

Hydrogen peroxide is the other major molecular product of water radiolysis. Its production is due mainly to $^{\bullet}OH$ radical combination reactions (LAVERNE, 2004):

$$^{\bullet}OH + {}^{\bullet}OH \rightarrow H_2O_2, \quad k = 4.54 \times 10^9\ M^{-1}\ s^{-1} \text{ at } 20\ ^{\circ}C \qquad \text{(R8)}$$

H_2O_2 is unstable in water at elevated temperature and decomposes to molecular oxygen according to:

$$H_2O_2 \rightarrow \tfrac{1}{2}O_2 + H_2O. \qquad \text{(R9)}$$

A wide variety of studies have shown that hydrogen peroxide and its decomposition product O_2 are the major oxidants involved in corrosion and stress corrosion cracking processes associated with nuclear reactors and waste storage containers (COHEN, 1980; SATOH et al., 2004; GUZONAS et al., 2018).

H_2O_2 is fairly reactive with all the radical species produced in water radiolysis. In particular, hydrated electrons react very fast with $^{\bullet}OH$ radicals to form water:

$$e^-_{aq} + {}^{\bullet}OH \rightarrow OH^-, \quad k = 3.34 \times 10^{10}\ M^{-1}\ s^{-1} \text{ at } 20\ ^{\circ}C \qquad \text{(R1)}$$

Reaction (R1) is the main cause of the decay of e^-_{aq} and $^{\bullet}OH$. Its rate constant is about ten times higher than that of reaction (R9) of dimerization of the $^{\bullet}OH$ radicals. As a consequence, an increase in the number of hydrated electrons will lead to a decreased number of available hydroxyl radicals to produce H_2O_2. This is exactly what we observe between 150 and 200 °C when the abrupt drop in the rate constant for the self-reaction of e^-_{aq} is included in our simulations. In fact, as a result of this drop, there are more available e^-_{aq} to undergo reaction (R1), and therefore the yield of H_2O_2 is lowered. This explains the origin of the marked downward inflection observed in $G(H_2O_2)$ above ~150 °C (Article no. 1). We should note, however, that this result is in contrast to the estimated data reported by

CHRISTENSEN (2006) at 289 °C, which seem to indicate a rather *monotonic* variation of $G(H_2O_2)$ with temperature.

6.3 Yields of radicals

The boron neutron capture nuclear reaction in liquid water produces high-LET ^{4}He and ^{7}Li recoil ions (with "dose average" LETs at 25 °C of ~196 and 216 eV/nm, respectively). The radiolysis of water by these ions results in the formation of various free radicals, including e^-_{aq}, $^{\bullet}OH$, and $^{\bullet}H$, and the molecular products H_2 and H_2O_2. Figure 6.2 shows the time evolution of the yields of the radical species so formed as calculated from our Monte Carlo simulations from ~1 ps to 1 ms (Article no. 2). As can be seen, these yields are very small at the microsecond time scale (*i.e.*, after all the track reactions are complete). This is in contrast to the corresponding "escape" yield data obtained for low-LET ^{60}Co γ-ray or fast electron irradiation [~2.5, 2.6, and 0.6 molecule/100 eV, respectively) (Article no. 2). Such differences can readily be explained as reflecting the high-LET character of the densely ionizing $^{10}B(n,\alpha)^{7}Li$ recoil ions. Indeed, in the latter case, the intervention of radical-radical reactions is favored as the local concentrations of radicals along the "native" radiation tracks are high and many radical interactions occur before the products can escape into the bulk solution. In other words, this allows fewer radicals to escape combination and recombination reactions during the expansion of tracks and, concomitantly, leads to the formation of more molecular products (LAVERNE, 2004; MEESUNGNOEN and JAY-GERIN, 2011).

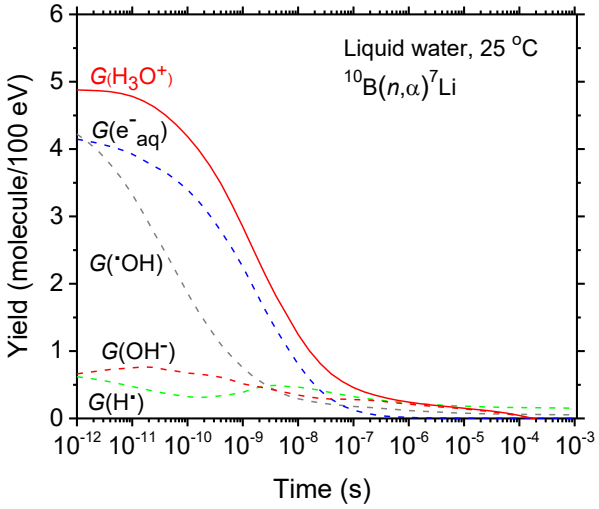

Figure 6.2 **Yields of the different chemical species (in molecule/100 eV) for the radiolysis of pure, deaerated liquid water by the recoil of α-particles and lithium ions from the $^{10}B(n,\alpha)^{7}Li$ nuclear reaction at 25 °C from ~1 ps to 1ms. Our computed yields of e^-_{aq}, •OH, and H• are shown as blue, grey, and green dashed lines, respectively.**

6.4 Local acidity inside of the regions encased by radiation tracks

The biological response of living cells to ionizing radiation is mostly due to "indirect effects" (at least for low-LET radiation), *i.e.*, via reactions of the cellular components (mainly DNA) with the chemical species produced by the radiolysis of the cellular water, especially with •OH radicals. This response is, most generally, potentially toxic to cells, for example, by producing a wide range of biochemical damage in DNA, including single- and double-strand breaks, base lesions, abasic sites, damaged sugars, tandem lesions, DNA-protein cross-links, and damage clusters (or multiply damaged sites). In particular, damage clusters are very devastating to cells as they cannot readily repair this type of damage (CADET et al., 1997; von SONNTAG, 2006; HALL and GIACCIA, 2006; LEHNERT, 2008; BECKER et al., 2011). Remarkably, these biochemical modifications may occur not only in the irradiated cells but also in the neighboring non-targeted "bystander" cells through intercellular communication mechanisms (AZZAM et al., 2003; MOTHERSILL and SEYMOUR, 2004; HEI et al., 2011).[1]

In this work, we observed a strong local and transitory "acid spike" effect around the trajectories of the two He and Li recoiling ions produced by the $^{10}B(n,\alpha)^{7}Li$ radiolysis of water (Article no. 2). Even if the radiobiological damage in irradiated cells is usually explained through the intervention of the water radiolysis products (mostly free radicals) mentioned above, one may wonder whether this increase in acidity – expressed in terms of hydronium ions H_3O^+ – along the radiation tracks would also not be a key factor in the biological action of ionizing radiation (BYAKOV and STEPANOV, 2006; KANIKE et al., 2015; ISLAM et al., 2018).

---

[1] *Bystander effect*: Ionizing radiation-induced bystander effects, commonly observed in cell populations exposed to low- and high-LET radiations, are initiated by damage to a cellular molecule, which then gives rise to a toxic signal exported to neighboring cells not directly hit by radiation. Cellular phenotype, radiation quality (or LET), and dose are likely modulators of molecular and biochemical signaling events involved.

Because many cellular processes critically depend on pH (*e.g.*, synthesis of macromolecules and cell proliferation, activity of enzymes, and transport of metabolites and drugs (TANNOCK and ROTIN, 1989; KANIKE, 2016), the occurrence of such an abrupt highly acidic response (pH ~ 0) in a biological system could likely have important consequences in triggering molecular mechanisms, both biochemical and physical, that would result in biological damage and enhanced cell lethality. The present study in fact strongly suggests this intra-track acid spike effect, given its high intensity, could interfere with and affect the biological processes in the cell, even if cells have a well-known *buffering* capacity (*i.e.*, cellular mechanisms that regulate pH when *small* amounts of acids – or bases – are added).

According to the Brønsted-Lowry definition, an acid is a proton donor. Strong acids (*e.g.*, H_2SO_4, HNO_3, HCl) readily dissociate when they go into solution in water, whereas weak acids (*e.g.*, CH_3COOH, HCOOH, $HO_2^{\bullet}$) only partly dissociate to provide a proton in aqueous solutions. Most organic acids are weak in nature. The partial dissociation of a weak acid in water can be described by the following equilibrium equation:

$$HA \overset{K_a}{\rightleftharpoons} H^+ + A^-, \qquad \text{(R10)}$$

where A^- is the conjugate base of the weak acid HA. K_a is the equilibrium constant (also known as the "acid dissociation constant"), given by

$$K_a = [H^+][A^-] / [HA] \qquad \text{(R11)}$$

at equilibrium. By analogy to the definition of pH, namely,

$$pH = -\log_{10}([H^+]) , \qquad \text{(R12)}$$

where $[H^+]$ is the concentration of protons, we often use pK_a as the negative logarithm (base 10) of K_a:

$$pK_a = -\log_{10}(K_a) . \qquad \text{(R13)}$$

Rearranging the K_a equilibrium expression (R11), we can get the Henderson-Hasselbalch equation (HARRIS, 2013):

$$pH = pK_a + \log_{10} \{[A^-] / [HA]\} \ . \qquad \text{(R15)}$$

The Henderson-Hasselbalch equation is the central equation for *buffers*. Biochemists are interested in buffers because the functioning of biological systems depends critically on pH. Cells contain different buffers to control the pH within the physiological limit and to regulate the biochemical reactions. For instance, bicarbonate ($H_2CO_3 \rightleftharpoons H^+ + HCO_3^-$, $pK_a = 6.04$), (mono-/di-basic) phosphate ($H_2PO_4^- \rightleftharpoons H^+ + HPO_4^{2-}$, $pK_a = 6.8$), and some proteins such as hemoglobin, provide physiologically relevant buffering capacity (ENGELKING, 2015; KRIEG et al., 2015).

Enzymes are highly selective biocatalysts, which catalyze very specific bio-reactions in living organisms. In general, enzymes are proteins in nature with special conformations, where reactants (or "substrates") bind to a specific region called the *active site*. Their role is to enhance reaction rates by decreasing the activation energy (or barrier) of the (uncatalyzed) bio-reaction without themselves being consumed in the process (FERSHT, 1985). Each enzyme shows its optimal activity under certain thermodynamically controlled conditions. Most importantly, the catalytic activity of an enzyme is pH sensitive as the intra- and intermolecular bonds that hold proteins in their structures are disrupted by changes in pH. It follows that most enzymes are active *only* within a narrow pH range, usually between ~5 and 9 (STRYER, 1995; PARK and ZIPP, 2000).

A change in cell pH can also lead to the formation of new radical products of biological and biomedical importance. For instance, in an aerobic cellular environment at physiological pH, molecular oxygen can be reduced by hydrated electrons and produce the superoxide radical anion ($O_2^{\bullet-}$). This $O_2^{\bullet-}$ radical is poorly reactive (*e.g.*, its rates of reaction with DNA, lipids, amino acids, and most other biomolecules are low) (HALLIWELL and GUTTERIDGE, 2015). However, $O_2^{\bullet-}$ is always in a pH-dependent equilibrium with its conjugated acid, the hydroperoxyl radical $HO_2^{\bullet}$:

$$HO_2^{\bullet} \rightleftharpoons H^+ + O_2^{\bullet-}, \qquad \text{(R15)}$$

the pK_a of the protonation/deprotonation equilibrium being approximately 4.8 in water at 25 °C (BIELSKI et al., 1985). Although at the pH of most body tissues the ratio of $[O_2^{\bullet-}]/[HO_2^{\bullet}]$ is large [100/1 at pH 6.8, 1000/1 at pH 7.8, according to the Henderson-Hasselbalch equation (R14)], $HO_2^{\bullet}$, but not $O_2^{\bullet-}$, can induce lipid peroxidation reactions in the inner membrane of mitochondria (KOWALD, 1999). The greater reactivity of $HO_2^{\bullet}$ and because it is uncharged (which allows it to cross membranes more easily than the charged $O_2^{\bullet-}$), suggest that it has the potential to cause damage and that it can also contribute to the propagation of signaling events from among cells (*e.g.*, intercellular communication, bystander effects) (DE GREY, 2002; AZZAM et al., 2012; HALLIWELL and GUTTERIDGE, 2015). It is to be expected, therefore, that the conversion of the harmless $O_2^{\bullet-}$ into the harmful $HO_2^{\bullet}$ in cells at low pH may consequently result in an increased growth of potentially toxic effects *in vivo*.

By contrast, if $O_2^{\bullet-}$ is in general poorly reactive, it does react quickly with nitric oxide ($^{\bullet}NO$), an uncharged, relatively stable free radical implicated in multiple, important physiological processes. $^{\bullet}NO$ reacts slowly, if at all, with most biological molecules (HALLIWELL and GUTTERIDGE, 2015). As a gas, it can cross membranes and diffuse readily between and within cells. A large part of the toxicity of $^{\bullet}NO$ *in vivo* is due to its combination with superoxide to give a powerful (non-radical) oxidant, *peroxynitrite* ($ONOO^-$) (PRYOR and SQUADRITO, 1995; KOPPENOL, 1998; JAY-GERIN and FERRADINI, 2000; HALLIWELL and GUTTERIDGE, 2015):

$$^{\bullet}NO + O_2^{\bullet-} \rightarrow ONOO^-, \quad k = 1.9 \times 10^{10}\ M^{-1}\ s^{-1}. \qquad \text{(R16)}$$

The pK_a of peroxynitrite is ~6.8 at 37 °C. It is protonated in acidic solution to form the neutral peroxynitrous acid ONOOH:

$$ONOO^- + H^+ \rightleftharpoons ONOOH. \qquad \text{(R17)}$$

For instance, at pH 6.2, about 75% of the peroxynitrite anions are protonated. Because the stability and reactivity of $ONOO^-$ and ONOOH are quite different, the biochemistry of peroxynitrite in biological systems is highly pH-dependent. Peroxynitrite in its protonated (acid) form is much more reactive than $ONOO^-$. Although some controversy still exists as

to the mode of action of peroxynitrous acid, it has been proposed that ONOOH spontaneously decomposes to produce nitrogen dioxide ($^{\bullet}NO_2$) and a highly reactive species with hydroxyl radical-like properties, each capable of oxidizing a large variety of biological molecules (CROW and BECKMAN, 1996; KOPPENOL et al., 2012; RADI, 2013).

In biological cells, acid pH may also have some other toxic effects, leading to DNA damage and causing carcinogenic activity. We should mention here, for instance, the loss of purines or pyrimidines by hydrolytic cleavage of the base-sugar (N-C glycosidic) bond in DNA, which is acid catalyzed and thus increases at low pH (SHEPPARD et al., 2000; von SONNTAG, 2006; GATES, 2009; KANIKE, 2016). In the reaction mechanism, the depurination is promoted by the protonation of the purine base, thus, weakening the N-C glycosidic bond and increasing the leaving ability of the base. Acid-catalyzed depyrimidination also proceeds in a similar mechanism as depurination. Abasic sites are common DNA lesions. However, if unrepaired efficiently, they can inhibit DNA replication and transcription and contribute to cytotoxicity or mutagenesis (DEMPLE and HARRISON, 1994).

From our present Monte Carlo simulation study of the $^{10}B(n,\alpha)^{7}Li$ radiolysis of pure liquid water at 25 °C (Article no. 2), we observed that the peak of acidity in the two He and Li recoiling ion track regions typically lasted ~1 ms after the initial energy release. In contrast, in the case of water in living cells, this acidity was found to persist over a much longer period of time (about two orders of magnitude) due to a much reduced mobility of the proton in cellular water (~100-1000 times lower than in free water) (NEGENDANK and EDELMANN, 1988; SWIETACH and VAUGHAN-JONES, 2005). Using an intracellular proton mobility 100 times lower than that in pure water, we observed at 1 μs the two recoil ion tracks are still very acidic (pH ~2.4) (ISLAM et al., 2018).

Most interestingly, a qualitative physical picture of the origin of this acidity in the "native" track regions after the passage of an ionizing particle was developed just after World War II by LEA (1946) and later by MORRISON (1950). It is certainly important (and instructive) to show here (see Fig. 6.3) the scheme originally presented by MORRISON (1950) in a Symposium on radiobiology in Oberlin College in June 1950,

which shows the lateral distribution of the various radiolytic species formed after a heavy α-particle has traversed water, about 10^{-6} s earlier. As we can see, there is a clear charge separation between the more concentrated positive-ion (mainly H_3O^+ and $^{\bullet}OH$) core of the track and the negative ions (mainly OH^- and $H^{\bullet}$) in the surrounding medium somewhat distant from the track. As correctly explained by the author, this "*charge separation is due to the faster motion of the secondary electrons which are captured some distance from the track*" (MORRISON, 1950).

Indeed, the numerous energetic ("dry") secondary electrons, produced in the early stages of the radiolysis of water, have, on the average, an initial kinetic energy of ~40-50 eV, depending on the authors (LAVERNE and PIMBLOTT, 1995; COBUT et al., 1998; AUTSAVAPROMPORN, 2006; MIRSALEH KOHAN et al., 2013). The range (or "penetration distance", or yet "thermalization distance") of such electrons in liquid water at 25 °C is ~11.7 nm as calculated previously by MEESUNGNOEN and JAY-GERIN (2005) using Monte Carlo simulations. In other words, they travel a long distance while slowing down, fairly far away from the site where they were originally produced. These electrons eventually get hydrated, typically ~1 ps after the initial energy deposition (BERNAS et al., 1996).

The long penetration range of the dry secondary electrons greatly limits the production of $H^{\bullet}$ radicals and OH^-, as the intra-track combination reactions of these electrons with H_3O^+ and $^{\bullet}OH$ – species that have comparatively a very low mobility – are not favored. As a result, the high initial H_3O^+ concentration in the track core is directly responsible for the "acid spike" effect observed at early time. As a function of time, it is easy to see that this local acidity will last until the diffusion of H_3O^+ and $^{\bullet}OH$ has brought these two species to the remote positions then occupied by the hydrated electrons.

It is most remarkable that our present simulations fully agree with the qualitative physical picture of Fig. 6.3 developed by LEA (1946) and MORRISON (1950) some 70 years ago (at a time when the hydrated electron had not yet been discovered).

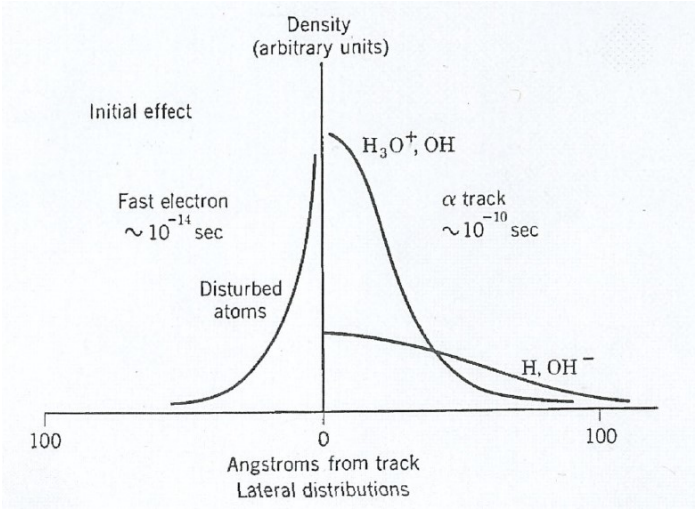

Fig. 6.3: Qualitative representation of the lateral distribution of the radiolytic products formed after a heavy α-particle has traversed water (right side of the figure). The separation of the positive (core of the track) and negative (at some distance from the track) charges is clearly visualized (LEA, 1946; MORRISON, 1950).

6. Conclusion

In this work, Monte Carlo track chemistry simulations were used to calculate the *G*-values for the primary species of the radiolysis of pure, neutral liquid water and 0.4 M H_2SO_4 aqueous solutions by the $^{10}B(n,\alpha)^7Li$ nuclear reaction recoil ions at temperatures between 25 and 350 °C. Overall, our simulation results agreed well with existing estimates at 20 and 289 °C. For deaerated 0.4 M H_2SO_4 solutions, reasonable agreement between experiment and simulation was also found at room temperature. Compared with the data obtained for low-LET radiation, our computed yields showed essentially similar temperature dependences over the range of temperatures studied, but with lower values for yields of free radicals and higher values for molecular yields, reflecting the high-LET character of the densely ionizing $^{10}B(n,\alpha)^7Li$ recoil ions.

Moreover, considering the rate constant of the bimolecular self-reaction of the hydrated electron measured in alkaline conditions, our simulated results predicted a non-monotonic downward inflection in the temperature dependence of $G(H_2)$ and $G(H_2O_2)$ above ~150 °C, which is not confirmed by the existing experimental data. More experimental data would be required for both neutral and acidic solutions to better describe the dependence of radiolytic yields on temperature and to test our modeling calculations more thoroughly. Measurements of the (e^-_{aq} + e^-_{aq}) reaction rate constant in near-neutral water would help us to determine whether the predicted non-monotonic inflections above ~150 °C in $G(H_2)$ and $G(H_2O_2)$ are confirmed.

Finally, we also extended our previous calculations to determine the yields of H_3O^+ produced by the $^{10}B(n,\alpha)^7Li$ radiolysis of water as a function of time. The concentrations of H_3O^+ and the corresponding pH values for both the high-LET helium and lithium recoil ions considered were then obtained from our calculated $G(H_3O^+)$ values using an axially homogeneous “cylindrical” track model. In pure deaerated liquid water at 25 °C, we observed an abrupt transient “acid spike” effect at early times around the trajectories of the two ^4He and ^7Li recoiling ions. Most interestingly, in a cellular environment, these initial conditions of very high acidity are about two orders of magnitude longer than in free water due to the much lower value of the intracellular diffusion coefficient of the free proton.

This acidic pH, even local and transitory, could have important consequences as it may trigger molecular mechanisms that result in biological damages and cell lethality. The transient acid pH effect that we have described in this study does not appear to have been considered in water or in a cellular environment subject to the action of densely ionizing radiation. In this regard, this work raises a number of provocative questions about the potential implications of this acid spike effect in boron neutron capture therapy (BNCT) and, more generally, in the overall field of hadrontherapy.

7. Acknowledgments

I would like to thank the Department of Nuclear Medicine and Radiobiology, Faculty of Medicine and Health Sciences, Université de Sherbrooke. I also thank the "Centre de Recherche Médicale de l'Université de Sherbrooke" (CRMUS), which awarded me a two-year scholarship. I am very honored and grateful to have been selected for this award.

I would like to thank Prof. Jean-Paul Jay-Gerin, my supervisor, for the opportunity he gave me to join his group, his advices, numerous discussions, encouragement and support. I am very grateful to him for opening the window of knowledge and wisdom through which I perceive the light of new horizon. I come to know that there is a tremendous coherence between life and scientific research. In both cases, we have to observe from different points of view, it might give us the opportunity to know the unknown, to see the unseen.

I appreciated the help and support of Dr. Jintana Meesungnoen, Sunuchakan Sanguanmith, Vanaja Kanike, and Md Mohsin Patwary. Also, I would like to thank my colleagues in our laboratory, Tait Du, and also all my colleagues in the department.

Special thanks go to Prof. Yosuke Katsumura for his helpful correspondence, discussions and necessary intellectual support to accomplish this research. I would like to thank Prof. James F. Ziegler for his kind help in order to use the SRIM software.

I am also very much grateful to Prof. Éric Rousseau and Prof. Johannes van Lier for their valuable suggestions and reviews. Their suggestions and guidelines helped to organize the thesis.

Finally, I would like to thank my parents who always supported me to pursue my dream. It would not have been possible to go forward for me without their support and guidelines. I would like to offer them my appreciation of the love and support they have given me through all my life.

8. References

ALLEN, A.O., 1948. Radiation chemistry of aqueous solutions. J. Phys. Colloid Chem. 52, 479- 490.

AMICHAI, O. and TREININ, A. 1969. Chemical reactivity of $O(^3P)$ atoms in aqueous solution. Chem. Phys. Lett. 3, 611-613.

ANBAR, M. and THOMAS, J.K., 1964. Pulse radiolysis studies of aqueous sodium chloride solutions. J. Phys. Chem. 68, 3829-3835.

ANDERSON, D.W., 1984, Absorption of Ionizing Radiation. University Park Press, Baltimore, MD.

AUTSAVAPROMPORN, N., 2006. The effects of pH and radiation quality (LET) on the radiolysis of liquid water and aqueous solutions: A study by using Monte Carlo simulations. M.Sc. thesis, Burapha University, Bangsaen, Thailand.

AUTSAVAPROMPORN, N., MEESUNGNOEN, J., PLANTE, I., and JAY-GERIN, J.-P., 2007. Monte Carlo simulation study of the effects of acidity and LET on the primary free-radical and molecular yields of water radiolysis. Application to the Fricke dosimeter. Can. J. Chem. 85, 214-229.

AZZAM, E.I., DE TOLEDO, S.M., and LITTLE, J.B., 2003. Oxidative metabolism, gap junctions and the ionizing radiation-induced bystander effect. Oncogene 22, 7050-7057.

AZZAM, E.I., JAY-GERIN, J.-P., and PAIN, D., 2012. Ionizing radiation-induced metabolic oxidative stress and prolonged cell injury. Cancer Lett. 327, 48-60.

BARTELS, D.M., 2009. Comment on the possible role of the reaction $H + H_2O \rightarrow H_2 + OH$ in the radiolysis of water at high temperatures. Radiat. Phys. Chem. 78, 191-194.

BARTH, R.F., 2003. A critical assessment of boron neutron capture therapy: An overview. J. Neurooncol. 62, 1-5.

BASS, A.D. and SANCHE, L., 2003, Dissociative electron attachment and charge transfer in condensed matter. Radiat. Phys. Chem. 68, 3-13.

BECKER, D., ADHIKARY, A., and SEVILLA, M.D., 2011. Physicochemical mechanisms of radiation-induced DNA damage. In: Charged Particle and Photon Interactions with Matter: Recent Advances, Applications, and Interfaces (Hatano, Y., Katsumura, Y., and Mozumder, A., Eds.), pp. 503-541. Taylor & Francis Group, Boca Raton, FL.

BERNAS, A., FERRADINI, C., and JAY-GERIN, J.-P., 1996. Électrons en excès dans les milieux polaires homogènes et hétérogènes. Can. J. Chem. 74, 1-23.

BETHE, H., 1930. Zur Theorie des Durchgangs schneller Korpuskularstrahlen durch Materie. Ann. Physik 397, 325-400.

BETHE, H.A. and ASHKIN, J., 1953. Passage of radiations through matter. In: Experimental Nuclear Physics (Segrè, E., Ed.), vol. 1, pp. 166-357. Wiley, New York.

BIEDENKAPP, D., HARTSHORN, L.G., and BAIR, E.J., 1970. The $O(^1D)$ + H_2O reaction. Chem. Phys. Lett. 5, 379-380.

BIELSKI, B.H.J., CABELLI, D.E., ARUDI, R.L., and ROSS, A.B., 1985. Reactivity of HO_2/O_2^- radicals in aqueous solution. J. Phys. Chem. Ref. Data 14, 1041-1100.

BIERSACK, J.P. and HAGGMARK, L.G., 1980. A Monte Carlo computer program for the transport of energetic ions in amorphous targets. Nucl. Instrum. Methods 174, 257-269.

BRAGG, W.H., 1907. On the ionization of various gases by the α particles of radium. Phil. Mag. 13, 333-357.

BRAGG, W.H., and KLEEMAN, R., 1905. On the α particles of radium, and their loss of range in passing through various atoms and molecules. Phil. Mag. 10, 318-340.

BRANDT, W. and KITAGAWA, M., 1982. Effective stopping-power charges of swift ions in condensed matter. Phys. Rev. B 25, 5631-5637.

BURNS, W.G. and MOORE, P.B., 1976. Water radiolysis and its effect upon in reactor zircaloy corrosion. Radiat. Eff. 30, 233-242.

BURTON, M., 1969. Radiation chemistry: A godfatherly look at its history and its relation to liquids. Chem. Eng. News 47, 86-96.

BUTARBUTAR, S.L., MUROYA, Y., MIRSALEH KOHAN, L., SANGUANMITH, S., MEESUNGNOEN, J., and JAY-GERIN, J.-P., 2013. On the temperature dependence of the rate constant of the bimolecular reaction of two hydrated electrons. Atom Indonesia 39, 51-56.

BUTARBUTAR, S.L., 2014. Monte Carlo simulation of the radiolysis of water by fast neutrons at elevated temperatures up to 350 °C, M.Sc. thesis, Université de Sherbrooke, Sherbrooke, Québec, Canada.

BUTARBUTAR, S.L., SANGUANMITH, S., MEESUNGNOEN, J., SUNARYO, G.R., and JAY-GERIN, J.-P., 2014. Calculation of the yields for the primary species formed from the radiolysis of liquid water by fast neutrons at temperatures between 25-350 °C. Radiat. Res. 181, 659-665.

BUXTON, G.V., 1987. Radiation chemistry of the liquid state: (1) Water and homogeneous aqueous solutions. In: Radiation Chemistry: Principles and Applications (Farhataziz and Rodgers, M.A.J., Eds.), pp. 321-349. VCH Publishers, New York.

BYAKOV, V.M. and STEPANOV, S.V., 2006. The mechanism for the primary biological effects of ionizing radiation. Phys. Usp. 49, 469-487.

CADET, J., BERGER, M., DOUKI, T., and RAVANAT, J.L., 1997. Oxidative damage to DNA: Formation, measurement, and biological significance. Rev. Physiol. Biochem. Pharmacol. 131, 1-87.

CHAPMAN, J.D., Biophysical models of mammalian cell inactivation. In: Radiation Biology in Cancer Research (Meyn, R.E. and Withers, H.R., Eds.), pp. 21-32. Raven Press, New York, 1980.

CHATTERJEE, A. and HOLLEY, W.R., 1993. Computer simulation of initial events in the biochemical mechanisms of DNA damage. Adv. Radiat. Biol. 17, 181-226.

CHATTERJEE, A. and SCHAEFER, H.J., 1976. Microdosimetric structure of heavy ion tracks in tissue. Radiat. Environ. Biophys. 13, 215-227.

CHRISTENSEN, H., 2006. Fundamental aspects of water coolant radiolysis. SKI Report 2006:16. Swedish Nuclear Power Inspectorate, Stockholm, Sweden.

CHRISTENSEN, H. and SEHESTED, K., 1986. The hydrated electron and its reactions at high temperatures. J. Phys. Chem. 90, 186-190.

CHRISTOPHOROU, L.G., McCORKLE, D.L., and CHRISTODOULIDES, A.A., 1984. Electron attachment processes. In: Electron-Molecule Interactions and their Applications (Christophorou, L.G., Ed.), vol. 1, pp. 477-617. Academic Press, Orlando, FL.

CLIFFORD, P., GREEN, N.J.B., OLDFIELD, M.J., PILLING, M.J., and PIMBLOTT, S.M., 1986. Stochastic models of multi-species kinetics in radiation-induced spurs. J. Chem. Soc. Faraday Trans. 1, 82, 2673-2689.

COBUT, V., 1993. Simulation Monte Carlo du transport d'électrons non relativistes dans l'eau liquide pure et de l'évolution du milieu irradié: rendements des espèces créées de 10^{-15} à 10^{-7} s. Ph.D. thesis, Université de Sherbrooke, Sherbrooke, Québec, Canada.

COBUT, V., FRONGILLO, Y., JAY-GERIN, J.-P., and PATAU, J.P., 1994. Calcul des rendements des produits de la radiolyse de l'eau en fonction du temps par une méthode Monte Carlo. J. Chim. Phys. 91, 1018-1024.

COBUT, V., JAY-GERIN, J.-P., FRONGILLO, Y., and PATAU, J.P., 1996. On the dissociative electron attachment as a potential source of molecular hydrogen in irradiated liquid water. Radiat. Phys. Chem. 47, 247-250.

COBUT, V., FRONGILLO, Y., PATAU, J.P., GOULET, T., FRASER, M.-J., and JAYGERIN, J.-P., 1998. Monte Carlo simulation of fast electron and proton tracks in liquid water. I. Physical and physicochemical aspects. Radiat. Phys. Chem. 51, 229-243.

COHEN, P., 1980. Water Coolant Technology of Power Reactors. American Nuclear Society, La Grange Park, Illinois.

CROW, J.P. and BECKMAN, J.S., 1996. The importance of superoxide in nitric oxide-dependent toxicity. Evidence for peroxynitrite-mediated injury. In: Biological Reactive Intermediates. V. Basic Mechanistic Research in Toxicology and Human Risk Assessment (Snyder, R., Kocsir, J.J., Sipes, I.G., Kalf, G.F., Jollow, D.J., Greim, H., Monks, T.J., and Witmer, C.M., Eds.), pp. 147-161. Springer Science, New York.

CURIE, P. and DEBIERNE, A., 1901. Sur la radio-activité induite et les gaz activés par le radium. C. R. Acad. Sci. Paris, 132, 768-770.

DEBIERNE, A., 1914. Recherches sur les gaz produits par les substances radioactives. Décomposition de l'eau. Ann. Physique 2, 97-127.

DE GREY, A.D.N.J., 2002. $HO_2^{\bullet}$: The forgotten radical. DNA Cell. Biol. 21, 251-257.

DEGROOT, M.H. and SCHERVISH, M.J., 2002. Probability and Statistics, 3rd edn. Addison-Wesley, Boston, MA.

DEMPLE, B. and HARRISON, L., 1994. Repair of oxidative damage to DNA: Enzymology and biology. Annu. Rev. Biochem. 63, 915-948.

DINGFELDER, M., INOKUTI, M., and PARETZKE, H.G., 2000. Inelastic-collision cross sections of liquid water for interactions of energetic protons. Radiat. Phys. Chem. 59, 255-275.

DINGFELDER, M. and FRIEDLAND, W., 2001. Basic data for track structure simulations: Electron interaction cross-sections in liquid water. In: Advanced Monte Carlo for Radiation Physics, Particle Transport Simulation and Applications (Kling, A., Barão, F.J.C., Nakagawa, M., Távora, L., and Vaz, P., Eds.), pp. 267-272. Springer-Verlag, Berlin.

DINGFELDER, M., RITCHIE, R.H., TURNER, J.E., FRIEDLAND, W., PARETZKE, H.G., and HAMM, R.N., 2008. Comparisons of calculations with PARTRAC and NOREC: Transport of electrons in liquid water. Radiat. Res. 169, 584-594.

DRAGANIĆ, I.G. and DRAGANIĆ, Z.D., 1971. The Radiation Chemistry of Water. Academic Press, New York.

EDWARDS, E.J., WILSON, P.P.H., ANDERSON, M.H., MEZYK, S.P., PIMBLOTT, S.M., and BARTELS, D.M., 2007. An apparatus for the study of high temperature water radiolysis in a nuclear reactor: Calibration of dose in a mixed neutron/gamma radiation field. Rev. Sci. Instrum. 78, 124101.

ELLIOT, A.J., 1994. Rate constants and *g*-values for the simulation of the radiolysis of light water over the range 0-300 °C. Report AECL-11073. Atomic Energy of Canada Limited, Chalk River, Ontario, Canada.

ELLIOT, A.J., OUELLETTE, D.C., and STUART, C.R., 1996. The temperature dependence of the rate constants and yields for the simulation of the radiolysis of heavy water. Report AECL-11658. Atomic Energy of Canada Limited, Chalk River, Ontario, Canada.

ELLIOT, A.J., CHENIER, M.P., OUELLETTE, D.C., and KOSLOWSKY, V.T., 1996. Temperature dependence of *g* values for aqueous solutions irradiated with 23 MeV $^{2}H^{+}$ and 157 MeV $^{7}Li^{3+}$ ion beams. J. Phys. Chem. 100, 9014-9020.

ELLIOT, A.J. and BARTELS, D.M., 2009. The reaction set, rate constants and g-values for the simulation of the radiolysis of light water over the range 20° to 350 °C based on information available in 2008. Report AECL No. 153-127160-450-001. Atomic Energy of Canada Limited, Chalk River, Ontario, Canada.

ENGELKING, L.R., 2015. Textbook of Veterinary Physiological Chemistry, 3rd edn., Chapt. 85. Elsevier, Amsterdam.

EVANS, R.D., 1955. The Atomic Nucleus. Krieger Publ. Co., Malabar, FL.

FARAGGI, M. and DÉSALOS, J., 1969. Effect of positively charged ions on the "molecular" hydrogen yield in the radiolysis of aqueous solutions. Int. J. Radiat. Phys. Chem. 1, 335-344.

FERRADINI, C., 1979. Actions chimiques des radiations ionisantes. J. Chim. Phys. 76, 636-644.

FERRADINI, C., 1990. Aspect hétérogène des phénomènes radiolytiques. In: Actions Biologique et Chimique des Radiations, Vol. 1, pp. 52-63. Éditions Ciaco, Bruxelles.

FERRADINI, C. and BENSASSON, R.V., 1989. Glimpses of ninety years of radiation chemistry in France. In: Early Developments in Radiation Chemistry, Kroh, J. (Ed.), pp. 99-140. Royal Society of Chemistry, Thomas Graham House, Cambridge.

FERRADINI, C. and JAY-GERIN, J.-P., 1999. La radiolyse de l'eau et des solutions aqueuses : historique et actualité. Can. J. Chem. 77, 1542-1575.

FERRADINI, C. and JAY-GERIN, J.-P., 2000. The effect of pH on water radiolysis: A still open question. A minireview. Res. Chem. Intermed. 26, 549-565.

FERSHT, A.R., 1985. Enzyme Structure and Mechanism, 2nd edn. W.H. Freeman, New York.

FREEMAN, G.R., 1987. Ionization and charge separation in irradiated materials. In: Kinetics of Nonhomogeneous Processes (Freeman, G.R., Ed.), pp. 19-87. Wiley, New York.

FRICKE, H. and HART, E.J., 1966. Chemical dosimetry. In: Radiation Dosimetry (Attix, F.H. and Roesch, W.C., Eds.), 3rd edn., vol. II, pp. 167-239. Academic Press, New York.

FRONGILLO, Y., FRASER, M.-J., COBUT, V., GOULET, T., JAY-GERIN, J.-P., and PATAU, J.P., 1996. Évolution des espèces produites par le ralentissement de protons rapides dans l'eau liquide : simulation fondée sur l'approximation des temps de réaction indépendants. J. Chim. Phys. 93, 93-102.

FRONGILLO, Y., GOULET, T., FRASER, M.-J., COBUT, V., PATAU, J.P., and JAY-GERIN, J.-P., 1998. Monte Carlo simulation of fast electron and proton tracks in liquid water. II. Nonhomogeneous chemistry. Radiat. Phys. Chem. 51, 245-254.

FORMAN, H.J, FUKUTO, J.M, and TORRES, M., 2004. Redox signaling: Thiol chemistry defines which reactive oxygen and nitrogen species can act as second messengers. Am. J. Physiol. Cell Physiol. 287, C246-C256.

GATES, K.S., 2009. An overview of chemical processes that damage cellular DNA: Spontaneous hydrolysis, alkylation, and reactions with radicals. Chem. Res. Toxicol. 22, 1747-1760.

GEORGAKILAS, A.G., 2011. From chemistry of DNA damage to repair and biological significance. Comprehending the future. Mutat. Res. 711, 1-2.

GOODHEAD, D.T., 1994. Initial events in the cellular effects of ionizing radiations: Clustered damage in DNA. Int. J. Radiat. Biol. 65, 7-17.

GOULET, T. and JAY-GERIN, J.-P., 1989. Thermalization of subexcitation electrons in solid water. Radiat. Res. 118, 46-62.

GOULET, T. and JAY-GERIN, J.-P., 1992. On the reactions of hydrated electrons with $^{\bullet}OH$ and H_3O^+. Analysis of photoionization experiments. J. Chem. Phys. 96, 5076-5087.

GOULET, T., PATAU, J.P., and JAY-GERIN, J.-P., 1990. Influence of the parent cation on the thermalization of subexcitation electrons in solid water. J. Phys. Chem. 94, 7312-7316.

GOULET, T., JAY-GERIN, J.-P., FRONGILLO, Y., COBUT, V., and FRASER, M.-J., 1996. Rôle des distances de thermalisation des électrons dans la radiolyse de l'eau liquide. J. Chim. Phys. 93, 111-116.

GOULET, T., FRASER, M.-J., FRONGILLO, Y., and JAY-GERIN, J.-P., 1998. On the validity of the independent reaction times approximation for the description of the nonhomogeneous kinetics of liquid water radiolysis. Radiat. Phys. Chem. 51, 85-91.

GUZONAS, D., NOVOTNY, R., PENTTILÄ, S., TOIVONEN, A., and ZHENG, W., 2018. Materials and Water Chemistry for Supercritical Water-cooled Reactors. Woodhead Publishing/Elsevier, Cambridge, MA.

HALL, E.J. and GIACCIA, A.J., 2006. Radiobiology for the radiologist, 6th edn. Lippincott Williams & Wilkins, Philadelphia.

HALLIWELL, B. and GUTTERIDGE, J.M.C., 2015. Free Radicals in Biology and Medicine, 5th edn. Oxford University Press, Oxford, UK.

HARRIS, D.C., 2013. Exploring Chemical Analysis, 5th edn. W.H. Freeman, New York.

HARRIS, R.E. and PIMBLOTT, S.M., 2002. On ^{3}H α-particle and ^{60}Co γ irradiation of aqueous systems. Radiat. Res. 158, 493-504.

HEI, T.K., ZHOU, H., CHAI, Y., PONNAIYA, B., and IVANOV, V.N., 2011. Radiation induced non-targeted response: Mechanism and potential clinical implications. Curr. Mol. Pharmacol. 4, 96-105.

HELLER, J.M., Jr., HAMM, R.N., BIRKHOFF, R.D., and PAINTER, L.R., 1974. Collective oscillation in liquid water. J. Chem. Phys. 60, 3483-3486.

HERVÉ DU PENHOAT, M.-A., GOULET, T., FRONGILLO, Y., FRASER, M.-J., BERNAT, Ph., and JAY-GERIN, J.-P., 2000. Radiolysis of liquid water at temperatures up to 300 °C: A Monte Carlo simulation study. J. Phys. Chem. A 104, 11757-11770.

HOSMANE, N. S., MAGUIRE, J. A., ZHU, Y., and TAKAGAKI, M., Boron and Gadolinium Neutron Capture Therapy for Cancer Treatment, World Scientific, Singapore, 2012.

HUMMEL, A., 1995. Radiation Chemistry: The Chemical Effects of Ionizing Radiation and their Applications. IRI-TUD, Delft, The Netherlands.

ICRU REPORT 16, 1970. Linear Energy transfer. International Commission on Radiation Units and Measurements, Washington, D.C.

ICRU REPORT 17, 1970. Radiation dosimetry: X rays generated at potentials of 5 to 150 kV. International Commission on Radiation Units and Measurements, Washington, D.C.

ICRU REPORT 31, 1979, Average energy required to produce an ion pair. International Commission on Radiation Units and Measurements, Washington, DC.

ICRU REPORT 55, 1996. Secondary electron spectra from charged particle interactions. International Commission on Radiation Units and Mesurements, Bethesa, MD.

IAEA-TECDOC-799, 1995. Atomic and molecular data for radiotherapy and radiation research, International Atomic Energy Agency, Vienna, Austria.

ISLAM, M.M., LERTNAISAT, P., MEESUNGNOEN, J., SANGUANMITH, S., JAY-GERIN, J.-P., KATSUMURA, Y., MUKAI, S., UMEHARA, R., SHIMIZU, Y.,

and SUZUKI, M., 2017. Monte Carlo track chemistry simulations of the radiolysis of water induced by the recoil ions of the $^{10}B(n,\alpha)^{7}Li$ nuclear reaction. 1. Calculation of the yields of primary species up to 350 °C. RSC Adv. 7, 10782-10790.

ISLAM, M.M., KANIKE, V., MEESUNGNOEN, J., LERTNAISAT, P., KATSUMURA, Y., and JAY-GERIN, J.-P., 2018. *In situ* generation of ultrafast transient "acid spikes" in the $^{10}B(n,\alpha)^{7}Li$ radiolysis of water. Chem. Phys. Lett., 693, 210-215.

INOKUTI, M., 1971. Inelastic collisions of fast charged particles with atoms and molecules: The Bethe theory revisited. Rev. Mod. Phys. 43, 297-347.

JAY-GERIN, J.-P. and FERRADINI, C., 2000. Are there protective enzymatic pathways to regulate high local nitric oxide ($^{\bullet}NO$) concentrations in cells under stress conditions? Biochimie 82, 161-166.

JAY-GERIN, J.-P., LIN, M., KATSUMURA, Y., HE, H., MUROYA, Y., and MEESUNGNOEN, J., 2008. Effect of water density on the absorption maximum of hydrated electrons in sub- and supercritical water up to 400 °C. J. Chem. Phys. 129, 114511.

JONAH, C.D., 1995. A short history of the radiation chemistry of water. Radiat. Res. 144, 141-147.

KANIKE, V., 2016. "Acid-spike" effect in spurs/tracks of the low/high linear energy transfer radiolysis of water: Potential implications for radiobiology and nuclear industry. M.Sc. thesis, Université de Sherbrooke, Sherbrooke,

KANIKE, V., MEESUNGNOEN, J., and JAY-GERIN, J.-P., 2015a. Transient acid pH effect in tracks in the radiolysis of water: Does this effect contribute to biological damage caused by ionizing radiation? Austin J. Nucl. Med. Radiother. 2, 1011-1016.

KANIKE, V., MEESUNGNOEN, J., and JAY-GERIN, J.-P., 2015b. Acid spike effect in spurs/tracks of the low/high linear energy transfer radiolysis of water: Potential implications for radiobiology. RSC Adv. 5, 43361-43370.

KANIKE, V., MEESUNGNOEN, J., SANGUANMITH, S., GUZONAS, D.A., STUART, C.R., and JAY-GERIN, J.-P., 2017. Generation of ultrafast transient acid spikes in high-temperature water irradiated with low linear energy transfer radiation. CNL Nucl. Rev. 6, 31-40.

KAPLAN, I.G. and MITEREV, A.M., 1987. Interaction of charged particles with molecular medium and track effects in radiation chemistry. Adv. Chem. Phys. 68, 255-386.

KATSUMURA, Y., SUNARYO, G., HIROISHI, D., and ISHIGURE, K., 1998. Fast neutron radiolysis of water at elevated temperatures relevant to water chemistry. Prog. Nucl. Energy 32, 113-121.

KIMMEL, G.A., ORLANDO, T.M., VÉZINA, C., and SANCHE, L., 1994. Low-energy electron-stimulated production of molecular hydrogen from amorphous water ice. J. Chem. Phys. 101, 3282-3286.

KNUTH, D.E., 1998. The Art of Computer Programming, 3rd ed., vol. 2. Addison-Wesley, Reading, MA.

KOPPENOL, W.H., 1998. The basic chemistry of nitrogen monoxide and peroxynitrite. Free Radic. Biol. Med. 25, 385-391.

KOPPENOL, W.H., BOUNDS, P.L., NAUSER, T., KISSNER, R., and RUEGGER, H., 2012. Peroxynitrous acid: Controversy and consensus surrounding an enigmatic oxidant. Dalton Trans. 41, 13779-13787.

KOWALD, A., 1999. The mitochondrial theory of aging: Do damaged mitochondria accumulate by delayed degradation? Exp. Gerontol. 34, 605-612.

KRAFT, G. and KRÄMER, M., 1993. Linear energy transfer and track structure, Adv. Radiat. Biol. 17, 1-52.

KREIPL, M.S., FRIEDLAND, W., and PARETZKE, H.G., 2009. Time- and space-resolved Monte Carlo study of water radiolysis for photon, electron and ion irradiation. Radiat. Environ. Biophys. 48, 11-20.

KRIEG, B.J., TAGHAVI, S.M., AMIDON, G.L., and AMIDON, G.E., 2015. *In vivo* predictive dissolution: Comparing the effect of bicarbonate and phosphate buffer on the dissolution of weak acids and weak bases. J. Pharm. Sci. 104, 2894-2904.

KROH, J. (Ed.), 1989. Early Developments in Radiation Chemistry. The Royal Society of Chemistry, Cambridge, UK.

KRYSYON, T.B., GEORGIEV, A.B., PISSIS, P., and GEORGAKILAS, A.G., 2011. Role of oxidative stress and DNA damage in human carcinogenesis, Mutat. Res. 711, 193–201.

KUPPERMANN, A., 1959. Theoretical foundations of radiation chemistry. J. Chem. Educ. 36, 279-285.

LAVERNE, J.A., 2000. Track effects of heavy ions in liquid water. Radiat. Res. 153, 487-496.

LAVERNE, J.A., 2004. Radiation chemical effects of heavy ions. In: Charged Particle and Photon Interactions with Matter: Chemical, Physicochemical, and Biological Consequences with Applications (Mozumder, A. and Hatano, Y., Eds.), pp. 403-429. Marcel Dekker, New York.

LAVERNE, J.A. and MOZUMDER, A., 1993. Concerning plasmon excitation in liquid water. Radiat. Res. 133, 282-288.

LAVERNE, J.A. and PIMBLOTT, S.M., 1993. Diffusion-kinetic modeling of the electron radiolysis of water at elevated temperatures. J. Phys. Chem. 97, 3291-3297.

LAVERNE, J.A. and PIMBLOTT, S.M., 1995. Electron energy-loss distributions in solid, dry DNA. Radiat. Res. 141, 208-215.

LAVERNE, J.A. and SCHULER, R.H., 1987. Track effects in radiation chemistry: Production of $HO_2^{\bullet}$ in the radiolysis of water by high-LET ^{58}Ni ions. J. Phys. Chem. 91, 6560-6563.

LEHNERT, S. 2008. Biomolecular Action of Ionizing Radiation. Taylor & Francis, New York.

LIND, S.C., 1912. On the nature of the chemical action produced by a particles and the probable role played by ion. J. Phys. Chem. **16,** 564.

LIND, S.C., 1921. The Chemical Effects of Alpha Particles and Electrons. Chemical Catalog Co., New York.

LOCHER, G.L., 1936. Biological effects and therapeutic possibilities of neutrons. Am. J. Roentgenol. Radium Ther. 36, 1-13.

MAGEE, J.L., 1953. Radiation chemistry. Annu. Rev. Nucl. Sci. 3, 171-192.

MAGEE, J.L. and CHATTERJEE, A., 1980. Radiation chemistry of heavy-particle tracks. 1. General considerations. J. Phys. Chem. 84, 3529-3536.

MAGEE, J.L. and CHATTERJEE, A., 1987. Track reactions of radiation chemistry. In: Kinetics of Nonhomogeneous Processes (Freeman, G.R., Ed.), pp. 171-214. Wiley, New York.

MALAKHOVA, L., BEZLEPKIN, V.G., ANTIPOVA, V., USHAKOVA, T., FOMENKO, L., SIROTA, N., and GAZIEV, A.I., 2005. The increase in mitochondrial DNA

copy number in the tissues of gamma-irradiated mice. Cell Mol. Biol. Lett. 10, 721-732.

MARIN, T.W., TAKAHASHI, K., JONAH, C.D., CHEMERISOV, S.D., and BARTELS, D.M., 2007. Recombination of the hydrated electron at high temperature and pressure in hydrogenated alkaline water. J. Phys. Chem. A 111, 11540-11551.

MATSUYAMA, A. and NAMIKI, M., 1965. Agr. Biol. Chem. 29, 593-594.

McCRACKEN, D.R., TSANG, K.T., and LAUGHTON, P.J., 1998. Aspects of the physics and chemistry of water radiolysis by fast neutrons and fast electrons in nuclear reactors. AECL-11895 Report. Atomic Energy of Canada Limited, Chalk River, Ontario, Canada.

McDANIEL, E.W., MITCHELL, J.B.A., and RUDD, M.E., 1993. Atomic Collisions: Heavy Particle Projectiles. Wiley, New York.

MEDIN, J., 1997. Studies of clinical proton dosimetry using Monte Carlo simulation and experimental techniques Ph.D. thesis, Stockholm University.

MEESUNGNOEN, J., BENRAHMOUNE, M., FILALI-MOUHIM, A., MANKHETKORN, S., and JAY-GERIN, J.-P., 2001. Monte Carlo calculation of the primary radical and molecular yields of liquid water radiolysis in the linear energy transfer range 0.3-6.5 keV/μm: Application to ^{137}Cs gamma rays. Radiat. Res. 155, 269-278.

MEESUNGNOEN, J., JAY-GERIN, J.-P., FILALI-MOUHIM, A., and MANKHETKORN, S., 2002a. On the temperature dependence of the primary yield and the product $G\varepsilon_{max}$ of hydrated electrons in the low-LET radiolysis of liquid water. Can. J. Chem. 80, 767-773.

MEESUNGNOEN, J., JAY-GERIN, J.-P., FILALI-MOUHIM, A., and MANKHETKORN, S., 2002b. Low-energy electron penetration range in liquid water. Radiat. Res. 158, 657-660.

MEESUNGNOEN, J., FILALI-MOUHIM, A., SNITWONGSE NA AYUDHYA, N., MANKHETKORN, S., and JAY-GERIN, J.-P., 2003. Multiple ionization effects on the yields of $HO_2^{\bullet}/O_2^{\bullet-}$ and H_2O_2 produced in the radiolysis of liquid water with high-LET $^{12}C^{6+}$ ions: A Monte Carlo simulation study. Chem. Phys. Lett. 377, 419-425.

MEESUNGNOEN, J. and JAY-GERIN, J.-P., 2005a. High-LET radiolysis of liquid water with $^{1}H^{+}$, $^{4}He^{2+}$, $^{12}C^{6+}$, and $^{20}Ne^{9+}$ ions: Effects of multiple ionization. J. Phys. Chem. A 109, 6406-6419.

MEESUNGNOEN, J. and JAY-GERIN, J.-P., 2005b. Effect of multiple ionization on the yield of H_2O_2 produced in the radiolysis of aqueous 0.4 M H_2SO_4 solutions by high LET $^{12}C^{6+}$ and $^{20}Ne^{9+}$ ions. Radiat. Res. 164, 688-694.

MEESUNGNOEN, J. and JAY-GERIN, J.-P., 2011. Radiation chemistry of liquid water with heavy ions: Monte Carlo simulation studies. In: Charged Particle and Photon Interactions with Matter. Recent Advances, Applications, and Interfaces (Hatano, Y., Katsumura, Y., and Mozumder, A., Eds.), pp. 355-400. Taylor and Francis Group, Boca Raton, FL.

MEESUNGNOEN, J., GUZONAS, D., and JAY-GERIN, J.-P., 2010. Radiolysis of supercritical water at 400 °C and liquid-like densities near 0.5 g/cm^3. A Monte Carlo calculation. Can. J. Chem. 88, 646-653.

MEESUNGNOEN, J., SANGUANMITH, S., and JAY-GERIN, J.-P., 2013. Density dependence of the yield of hydrated electrons in the low-LET radiolysis of supercritical water at 400 °C: Influence of the geminate recombination of subexcitation-energy electrons prior to thermalization. Phys. Chem. Chem. Phys. 15, 16450-16455.

MEESUNGNOEN, J., SANGUANMITH, S., and JAY-GERIN, J.-P., 2015. Yields of H_2 and hydrated electrons in low-LET radiolysis of water determined by Monte Carlo track chemistry simulations using phenol/N_2O aqueous solutions up to 350 °C. RSC Adv. 5, 76813-76824.

MICHAUD, M., CLOUTIER, P., and SANCHE, L., 1991. Low-energy electron-energy-loss spectroscopy of amorphous ice: Electronic excitations. Phys. Rev. A. 44, 5624-5627.

MICHAUD, M., WEN, A., and SANCHE, L., 2003. Cross sections for low-energy (1-100 eV) electron elastic and inelastic scattering in amorphous ice. Radiat. Res. 159, 3-22.

MIKKELSEN, R.B. and WARDMAN, P., 2003. Biological chemistry of reactive oxygen and nitrogen and radiation-induced signal transduction mechanisms. Oncogene 22, 5734-5754.

MIRSALEH KOHAN, L., SANGUANMITH, S., MEESUNGNOEN, J., CAUSEY, P., STUART, C.R., and JAY-GERIN, J.-P., 2013. Self-radiolysis of tritiated water. 1. A comparison of the effects of ^{60}Co γ-rays and tritium α-particles on water and aqueous solutions at room temperature. RSC Adv. 3, 19282-19299.

MONK, P.M.S., 2004. Physical Chemistry: Understanding our Chemical World. Wiley, Chichester, UK.

MOTHERSILL, C. and SEYMOUR, C.B., 2004. Radiation-induced bystander effects – Implications for cancer. Nature Rev. Cancer 4, 158-164.

MOZUMDER, A. and MAGEE, J.L., 1966a. Model of tracks of ionizing radiations for radical reaction mechanisms. Radiat. Res. 28, 203-214.

MOZUMDER, A. and MAGEE, J.L., 1966b. Theory of radiation chemistry. VII. Structure and reactions in low LET tracks. J. Chem. Phys. 45, 3332-3341.

MOZUMDER, A., CHATTERJEE, A., and MAGEE, J.L., 1968. Theory of radiation chemistry. IX. Model and structure of heavy particle tracks in water. Adv. Chem. Series 81, 27-48.

MOZUMDER, A. and MAGEE, J.L., 1975. The early events of radiation chemistry. Int. J. Radiat. Phys. Chem. 7, 83-93.

MOZUMDER, A., 1999. Fundamentals of Radiation Chemistry. Academic Press, San Diego, CA.

MUROYA, Y., MEESUNGNOEN, J., JAY-GERIN, J.-P., FILALI-MOUHIM, A., GOULET, T., KATSUMURA, Y., and MANKHETKORN, S., 2002. Radiolysis of liquid water: An attempt to reconcile Monte Carlo calculations with new experimental hydrated electron yield data at early times. Can. J. Chem. 80, 13671374.

MUROYA, Y., PLANTE, I., AZZAM, E.I., MEESUNGNOEN, J., KATSUMURA, Y., and JAY-GERIN, J.-P., 2006. High-LET ion radiolysis of water: Visualization of the formation and evolution of ion tracks and relevance to the radiation-induced bystander effect. Radiat. Res. 165, 485-491.

MUROYA, Y., LIN, M., DE WAELE, V., HATANO, Y., KATSUMURA, Y., and MOSTAFAVI, M., 2010. First observation of picosecond kinetics of hydrated electrons in supercritical water. J. Phys. Chem. Lett. 1, 331-335.

MUROYA, Y., SANGUANMITH, S., MEESUNGNOEN, J., LIN, M., YAN, Y., KATSUMURA, Y., and JAY-GERIN, J.-P., 2012. Time-dependent yield of the hydrated electron in subcritical and supercritical water studied by ultrafast pulse radiolysis and Monte Carlo simulation. Phys. Chem. Chem. Phys. 14, 14325-14333.

MUSTAREE, S., MEESUNGNOEN, J., BUTARBUTAR, S.L., CAUSEY, P., STUART, C.R., and JAY-GERIN, J.-P., 2014. Self-radiolysis of tritiated water. 3. The •OH scavenging effect of bromide ions on the yield of H2O2 in the radiolysis of water by 60Co γ-rays and tritium α-particles at room temperature. RSC Adv. 4, 43572-43581.

NATHAN, C., 2003. Specificity of a third kind: Reactive oxygen and nitrogen intermediates in cell signaling. J. Clin. Invest. 111, 769-778.

NEGENDANK, W., and EDELMANN, L., 1988. The State of Water in the Cell. Scanning Microscopy International, Chicago.

NIKJOO, H., O'NEILL, P., GOODHEAD, D.T., and TERRISSOL, M., 1997. Computational modelling of low-energy electron-induced DNA damage by early physical and chemical events. Int. J. Radiat. Biol. 71, 467-483.

OGURA, H. and HAMILL, W.H., 1973. Positive hole migration in pulse-irradiated water and heavy water. J. Phys. Chem. 77, 2952-2954.

PARETZKE, H.G., 1987. Radiation track structure theory. In: Kinetics of Nonhomogeneous Processes (Freeman, G.R., Ed.), pp. 89-170. Wiley, New York.

PARK, C.-W. and ZIPP, E., 2000. The effect of temperature and pH on enzyme kinetics. A webpage for introduction to biochemical engineering. Available from http://www.rpi.edu/dept/chem-eng/Biotech-Environ/Projects00/temph/enzyme.html

PASTINA, B., ISABEY, J., and HICKEL, B., 1999. The influence of water chemistry on the radiolysis of the primary coolant water in pressurized water reactors. J. Nucl. Mater. 264, 309-318.

PASTINA, B., LAVERNE, J.A., and PIMBLOTT, S.M., 1999. Dependence of molecular hydrogen formation in water on scavengers of the precursor to the hydrated electron. J. Phys. Chem. A. 103, 5841-5846.

PETKAU A., 1987. Role of superoxide dismutase in modification of radiation injury, Br. J. Cancer (Suppl. 8) (1987) 87–95.

PIMBLOTT, S.M., LAVERNE, J.A., MOZUMDER, A., and GREEN, N.J.B., 1990. Structure of electron tracks in water. 1. Distribution of energy deposition events. J. Phys. Chem. 94, 488-495.

PIMBLOTT, S.M. and MOZUMDER, A., 1991. Structure of electron tracks in water. 2. Distribution of primary ionizations and excitations in water radiolysis. J. Phys. Chem. 95, 7291-7300.

PIMBLOTT, S.M. and MOZUMDER, A., 2004. Modeling of physicochemical and chemical processes in the interactions of fast charged particles with matter. In: Charged Particle and Photon Interactions with Matter: Chemical, Physicochemical, and Biological Consequences with Applications (Mozumder, A. and Hatano, Y., Eds.), pp. 75-103. Marcel Dekker, New York.

PIMBLOTT, S.M., PILLING, M.J., and GREEN, N.J.B., 1991. Stochastic models of spur kinetics in water. Radiat. Phys. Chem. 37, 377-388.

PIMBLOTT, S.M. and GREEN, N.J.B., 1995. Recent advances in the kinetics of radiolytic processes. Res. Chem. Kinet. 3, 117-174.

PLANTE, I., FILALI-MOUHIM, A., and JAY-GERIN, J.-P., 2005. SimulRad: A Java interface for a Monte Carlo simulation code to visualize in 3D the early stages of water radiolysis. Radiat. Phys. Chem. 72, 173-180.

PLANTE, I., 2009. Développement de codes de simulation Monte-Carlo de la radiolyse de l'eau et de solutions aqueuses par des électrons, ions lourds, photons et neutrons. Applications à divers sujets d'intérêt expérimental. Ph.D. thesis, Université de Sherbrooke, Sherbrooke, Québec, Canada.

PLATZMAN, R.L., 1955. Subexcitation electrons. Radiat. Res. 2, 1-7.

PLATZMAN, R.L., 1958. The physical and chemical basis of mechanisms in radiation biology. In: Radiation Biology and Medicine. Selected Reviews in the Life Sciences (Claus, W.D., Ed.), pp. 15-72. Addison-Wesley, Reading, MA.

PLATZMAN, R.L., 1962a. Superexcited states of molecules. Radiat. Res. 17, 419-425.

PLATZMAN, R.L., 1962b. Dissociative attachment of subexcitation electrons in liquid water, and the origin of radiolytic "molecular" hydrogen. In: Abstracts of Papers, Second International Congress of Radiation Research, Harrogate, England, August 511, 1962, p. 128.

PRISE, K.M., and O'SULLIVAN, J.M, 2009. Radiation-induced bystander signalling in cancer therapy, Nat. Rev. Cancer 9, 351-360.

PRYOR, W.A. and SQUADRITO, G.L., 1995. The chemistry of peroxynitrite: A product from the reaction of nitric oxide with superoxide. Am. J. Physiol. 268 (Lung Cell. Mol. Physiol. 12), L699-L722.

PUCHEAULT, J., 1961. Actions des rayons alpha sur les solutions aqueuses. In: Actions Chimiques et Biologiques des Radiations (Haïssinsky, M., Ed.), Vol. 5, pp. 31-84. Masson, Paris.

RADI, R., 2013. Peroxynitrite, a stealthy biological oxidant. J. Biol. Chem. 288, 26464-26472.

RAMSAY, W. and SODDY, F., 1903. Experiments in radioactivity, and the production of helium from radium. Proc. Roy. Soc. London 72**,** 204-207.

ROWNTREE, P., PARENTEAU, L., and SANCHE, L., 1991. Electron stimulated desorption via dissociative attachment in amorphous H_2O. J. Chem. Phys. 94, 8570-8576.

SANGUANMITH, S., MUROYA, Y., MEESUNGNOEN, J., LIN, M., KATSUMURA, Y., MIRSALEH KOHAN, L., GUZONAS, D.A., STUART, C.R., and JAY-GERIN, J.-P., 2011a. Low-linear energy transfer radiolysis of liquid water at elevated temperatures up to 350 °C: Monte Carlo simulations. Chem. Phys. Lett. 508, 224-230.

SANGUANMITH, S., MUROYA, Y., TIPPAYAMONTRI, T., MEESUNGNOEN, J., LIN, M., KATSUMURA, Y., and JAY-GERIN, J.-P., 2011b. Temperature dependence of the Fricke dosimeter and spur expansion time in the low-LET hightemperature radiolysis of water up to 350 °C: A Monte Carlo simulation study. Phys. Chem. Chem. Phys. 13, 10690-10698.

SANGUANMITH, S., MEESUNGNOEN, J., MUROYA, Y., LIN, M., KATSUMURA, Y., and JAY-GERIN, J.-P., 2012. On the spur lifetime and its temperature dependence in the low linear energy transfer radiolysis of water. Phys. Chem. Chem. Phys. 14, 16731-16736.

SATOH, T., UCHIDA, S., SUGAMA, J.-I., YAMASHIRO, N., HIROSE, T., MORISHIMA, Y., SATOH, Y., and IINUMA, K., 2004. Effects of hydrogen peroxide on corrosion of stainless steel (I). J. Nucl. Sci. Tech. 41, 610-618.

SAUER, M.C., Jr., SCHMIDT, K.H., HART, E.J., NALEWAY, C.A., and JONAH, C.D., 1977. LET dependence of transient yields in the pulse radiolysis of aqueous systems with deuterons and α particles. Radiat. Res. 70, 91-106.

SAUERWEIN, W.A.G., 2012. Principles and roots of neutron capture therapy. In: Neutron Capture Therapy (Sauerwein, W.A.G., Wittig, A., Moss, R., and Nakagawa, Y., Eds.), pp. 1-16. Springer, Heidelberg.

SCHULER, R.H. and ALLEN, A.O., 1957. Radiation chemistry studies with cyclotron beams of variable energy: Yields in aerated ferrous sulfate solution. J. Am. Chem. Soc. 79, 1565-1572.

SHEPPARD, T.L., ORDOUKHANIAN, P., and JOYCE, G.F., 2000. A DNA enzyme with N-glycosylase activity. Proc. Natl. Acad. Sci. USA 97, 7802-7807.

SMITH, D.R. and STEVENS, W.H., 1963. Radiation-induced hydrolysis of acetal: Evidence for the reaction of H_3O^+ ions in spurs in the radiolysis of water. Nature 200, 66-67.

SPINKS, J.W.T. and WOODS, R.J., 1990. An Introduction to Radiation Chemistry, 3rd edn. Wiley, New York.

STERNICZUK, M. and BARTELS, D.M., 2016. Source of molecular hydrogen in high-temperature water radiolysis. J. Phys. Chem. A 120, 200-209.

STRYER, L., 1995. Biochemistry, 4t edn. W.H. Freeman, New York.

STUART, C.R., OUELLETTE, D.C., and ELLIOT, A.J., 2002. Pulse radiolysis studies of liquid heavy water at temperatures up to 250 C. Report AECL-12107, Atomic Energy of Canada Limited, Chalk River, Ontario, Canada.

SWIATLA-WOJCIK, D. and BUXTON, G.V., 1995. Modeling of radiation spur processes in water at temperatures up to 300 °C. J. Phys. Chem. 99, 11464-11471.

SWIETACH, P. and VAUGHAN-JONES, R.D., 2005. Relationship between intracellular pH and proton mobility in rat and guinea-pig ventricular myocytes. J. Physiol. 566, 793-806.

TAUBE, H., 1957. Photochemical reactions of ozone in solution. Trans. Faraday Soc. 53, 656-665.

TIPPAYAMONTRI, T., SANGUANMITH, S., MEESUNGNOEN, J., SUNARYO, G.R., and JAY-GERIN, J.-P., 2009. Fast neutron radiolysis of the ferrous sulfate (Fricke) dosimeter: Monte Carlo simulations. Recent Res. Dev. Physical Chem. 10, 143-211.

TOBUREN, L.H., 2004. Ionization and secondary electron production by fast charged particles. In: Charged Particle and Photon Interactions with Matter: Chemical, Physicochemical, and Biological Consequences with Applications (Mozumder, A. and Hatano, Y., Eds.), pp. 31-74. Marcel Dekker, New York.

TURNER, J.E., MAGEE, J.L., HAMM, R.N., CHATTERJEE, A., WRIGHT, H.A., and RITCHIE, R.H., 1981. Early events in irradiated water. In: Seventh Symposium on Microdosimetry, Oxford, UK, Sept. 8-12, 1980 (Booz, J., Ebert, H.G., and Hartfiel, H.D., Eds.), pp. 507-520. Harwood Academic Publ., London.

TURNER, J.E., MAGEE, J.L., WRIGHT, H.A., CHATTERJEE, A., HAMM, R.N., and RITCHIE, R.H., 1983. Physical and chemical development of electron tracks in liquid water. Radiat. Res. 96, 437-449.

TURNER, J.E., HAMM, R.N., WRIGHT, H.A., RITCHIE, R.H., MAGEE, J.L., CHATTERJEE, A., and BOLCH, W.E., 1988a. Studies to link the basic radiation physics and chemistry of liquid water. Radiat. Phys. Chem. 32, 503-510.

TURNER, J.E., HAMM, R.N., SOULEYRETTE, M.L., MARTZ, D.E., RHEA, T.A., and SCHMIDT, D.W., 1988b. Calculations for β dosimetry using Monte Carlo code (OREC) for electron transport in water. Health Phys. 55, 741-750.

UEHARA, S. and NIKJOO, H., 2006. Monte Carlo simulation of water radiolysis for low-energy charged particles. J. Radiat. Res. 47, 69-81.

VEAL, E.A., DAY, A.M., MORGAN, B.A., 2007. Hydrogen peroxide sensing and cell signaling. Molec. Cell 26, 1-14.

von SONNTAG, C., 2006. Free-Radical-Induced DNA Damage and its Repair. A Chemical Perspective. Springer-Verlag, Berlin.

WARD, J.F., 1994. The complexity of DNA damage: Relevance to biological consequences. Int. J. Radiat. Biol. 66, 427-432.

WARD, J.F., 1985. Biochemistry of DNA lesions. Radiat. Res. (Suppl. 8), S103-S111.

WADA, Y., WATANABE, A., TACHIBANA, M., ISHIDA, K., UETAKE, N., UCHIDA, S., AKAMINE, K., SAMBONGI, M., SUZUKI, S., and ISHIGURE, K., 2001. Effects of hydrogen peroxide on intergranular stress corrosion cracking of stainless steel in high temperature water. IV. Effects of oxide film on electrochemical corrosion potential. J. Nucl. Sci. Technol. 38, 183-192.

WATT, D.E., 1996. Quantities for Dosimetry of Ionizing Radiations in Liquid Water. Taylor & Francis, London.

WERNER, E. and WERB, Z., 2002. Integrins engage mitochondrial function for signal transduction by a mechanism dependent on Rho GTPases. J. Cell Biol. 158, 357-368.

WIKE-HOOLEY, J.L., HAVEMAN, J., and REINHOLD, H.S., 1984. The relevance of tumour pH to the treatment of malignant disease. Radiother. Oncol. 2, 343-366.

WILSON, C.D., DUKES, C.A., and BARAGIOLA, R.A., 2001. Search for the plasmon in condensed water. Phys. Rev. B 63, 121101.

ZAIDER, M. and BRENNER, D.J., 1984. On the stochastic treatment of fast chemical reactions. Radiat. Res. 100, 245-256.

ZIEGLER, J.F., BIERSACK, J.P., and LITTMARK, U., 1985. The Stopping and Range of Ions in Matter. Pergamon Press, New York.

ZIEGLER, J.F., BIERSACK, J.P., and ZIEGLER M.D., 2008. SRIM – The Stopping and Range of Ions in Matter. Ion Implantation Press. http://www.lulu.com/content/1524197.

ZIEGLER, J.F., ZIEGLER, M.D., and BIERSACK, J.P., 2010. SRIM – The stopping and range of ions in matter (2010). Nucl. Instrum. Methods Phys. Res. B 268, 1818-1823.

ZIEGLER, J.F., BIERSACK, J.P., and ZIEGLER, M.D., 2015. SRIM – The Stopping and Range of Ions in Matter. SRIM Co., Chester, MD.

ZIMBRICK, J.D., 2002. Radiation chemistry and the Radiation Research Society: A history from the beginning. Radiat. Res. 158, 127-140.

9. Appendices

1. *8th International Symposium on Supercritical Water-Cooled Reactors*

Chengdu, China
March 13-15, 2017

Monte Carlo calculation of water radiolysis induced by the recoil ions of the $^{10}B(n,\alpha)^{7}Li$ nuclear reaction: Yields of chemical species up to 350 °C

M.M. Islam[1], P. Lertnaisat[2], J. Meesungnoen[1], Y. Katsumura[2]*, S. Mukai[3], R. Umehara[4], Y. Shimizu[4], M. Suzuki[3], and J.-P. Jay-Gerin[1]*,

1. Université de Sherbrooke, Sherbrooke, Quebec, Canada;
2. University of Tokyo, Tokyo, Japan;
3. Nuclear Development Corporation, Tokai-mura, Ibaraki, Japan;
4. Mitsubishi Heavy Industries, Kobe, Japan)

*Corresponding authors: Prof. Yosuke Katsumura, E-mail: katsu@n.t.u-tokyo.ac.jp; Prof. Jean-Paul Jay-Gerin, E-mail: jean-paul.jay-gerin@USherbrooke.ca

Abstract: The radiolysis of water is closely linked to the corrosion of structural materials in water-cooled nuclear reactors. Boric acid, enriched in ^{10}B, is generally added as a neutron poison in the primary coolant water to control the neutron flux and the reactivity in the core. However, recoil nuclei (1.47 MeV α-particles and 0.84 MeV $^{7}Li^{3+}$ ions) resulting from the reaction $^{10}B(n,\alpha)^{7}Li$ act as sources of high linear energy transfer (LET) radiation, thereby complicating the radiolytic process. Unfortunately, little attention has been paid to water decomposition induced by this reaction, even at room temperature. In this work, Monte Carlo track chemistry simulations [1-4] were carried out to predict the yields (*G*-values) of all primary radical and molecular products formed from the radiolysis of pure, neutral water by the $^{10}B(n,\alpha)^{7}Li$ recoil ions as a function of temperature from 25 to 350 °C. The yields were calculated at 1 and 0.1 μs after the ionization event by summing the *G*-values for each recoil ion weighted by its fraction of the total energy absorbed. In the calculations, the actual effective charges carried by the two helium and lithium ions (due to charge exchange effects) were taken into account and the (small) contribution of the 0.478 MeV γ ray, also released from the $^{10}B(n,\alpha)^{7}Li$ reaction, was neglected. Compared with data obtained for low-LET radiation (^{60}Co γ rays or fast electrons), our computed yields for the $^{10}B(n,\alpha)^{7}Li$ radiolysis of water showed essentially similar temperature dependences over the range of temperatures studied, but with lower values for yields of free radicals and higher values for molecular yields. This general trend is a reflection of the high-LET character of the $^{10}B(n,\alpha)^{7}Li$ recoil ions.

Experimental data are needed to better describe the dependence of radiolytic yields on temperature and to test our modeling calculations more thoroughly.

Key words: Radiolysis; Boron; Heavy ion; Primary yields; Computer simulation

Notes and References

[1] LERTNAISAT P. Simulation study of high temperature water radiolysis relevant to PWRs. Doctoral thesis, University of Tokyo, Tokyo, Japan, 2015.

[2] MEESUNGNOEN J, SANGUANMITH S, JAY-GERIN J-P. Yields of H_2 and hydrated electrons in low-LET radiolysis of water determined by Monte Carlo track chemistry simulations using phenol/N_2O aqueous solutions up to 350 °C. RSC Advances, 2015, 5(94):76813-76824.

[3] MEESUNGNOEN J, JAY-GERIN J-P. High-LET radiolysis of liquid water with $^{1}H^{+}$, $^{4}He^{2+}$, $^{12}C^{6+}$, and $^{20}Ne^{9+}$ ions: Effects of multiple ionization. Journal of Physical Chemistry A, 2005, 109(29): 6406-6419.

[4] Note that our simulation model was validated at 25 °C by comparing the calculated yields of Fe^{3+} ions produced in the $^{4}He^{2+}$ radiolysis of acidic (0.4 *M* H_2SO_4) ferrous sulfate solution (the Fricke dosimeter) to the experimental values of $G(Fe^{3+})$ as a function of LET over the range of 1-200 keV/μm. Excellent agreement was obtained.

2. ***Molecular and Clinical Radiobiology Workshop***
McGill University Health Center, Montreal, QC, Canada
May 15-16, 2017

Monte Carlo track chemistry simulations of the radiolysis of water induced by the recoil ions of the $^{10}B(n,\alpha)^{7}Li$ nuclear reaction. *In situ* generation of an ultrafast transient "acid spike" effect in tracks: Potential implications for boron neutron capture therapy

M.M. Islam,[a] V. Kanike,[a] J. Meesungnoen,[a] P. Lertnaisat,[b] Y. Katsumura[b] and J.-P. Jay-Gerin[a]

[a]Département de médecine nucléaire et radiobiologie, Faculté de médecine et des sciences de la santé, Université de Sherbrooke, Sherbrooke (Québec) J1H 5N4, Canada; [b]Department of Nuclear Engineering and Management, School of Engineering, University of Tokyo, Tokyo 113-8686, Japan. Email of the presenting author (M.M. Islam): muhammad.mainul.islam@USherbrooke.ca

Purpose/Objectives

Since water is the major (~70-85% by weight) constituent of living cells and tissues, a thorough knowledge of the radiolysis of water is therefore critical to our understanding of the early stages in the complicated chain of radiobiological events that occurs during or shortly after the radiation exposure. Indeed, in a cellular environment, reactive chemical species generated by water radiolysis may damage all biomolecules, including nuclear acids, proteins and membrane lipids. The nuclear reaction produced when boron-10 is bombarded with slow neutrons, represented by $^{10}B(n,\alpha)^{7}Li$, is one of the most favorable ones known for use in biochemically targeted radiotherapies for cancer treatment known as "boron neutron capture therapy" (BNCT). This reaction produces high linear energy transfer (LET) α-particles (^{4}He) and ^{7}Li recoil ions in the opposite direction with path ranges of ~5-8 μm in water or biological tissue (approximately the diameter of one cell). In this work, we carried out the simulation of the radiolysis of water induced by these two ions with a particular focus on the *in situ* formation of H_3O^+ in the "native" radiation tracks.

Materials/Methods

Simple space-time model calculations using Monte Carlo track chemistry simulations were performed to quantitatively determine the yields (*G*-values) of the primary species [e^-_{aq}, $H^\bullet$, $^\bullet OH$, H_3O^+, OH^-, H_2, H_2O_2, $O_2^{\bullet-}$ (or its protonated form $HO_2^\bullet$, depending on the pH), $^\bullet O^\bullet(^3P)$, *etc*.] produced in the radiolysis of water by the recoil ions of the $^{10}B(n,\alpha)^7Li$ nuclear reaction. At ambient temperature, the calculations were carried out for 1.47 MeV α-particles and 0.84 MeV lithium nuclei with dose-average LET values of ~196 and ~225 eV/nm, respectively. The overall yields were calculated by summing the *G*-values for each recoil ion weighted by its fraction of the total energy absorbed. In the calculations, the actual effective charges carried by the two helium and lithium ions were taken into account.

Results

Track H_3O^+ concentrations and the corresponding pH values were obtained as a function of time (in the interval of ~1 ps to 1 ms). A striking feature of our simulated results is that, for both α-particles and lithium nuclei, an abrupt transient acid pH effect, which we call an "acid spike", was observed immediately after the initial energy deposition. This effect was found to be greatest for times shorter that ~100 ps. In this time range, the pH in the track regions remained nearly constant at ~0.5. At longer times, the pH increased gradually, ultimately reaching a value of 7 (neutral pH) at ~0.1 ms.

Conclusions

The transient acid pH effect that we have described does not appear to have been considered in water or in a cellular environment subject to the action of densely ionizing radiation. In this regard, this work raises a number of questions about the potential implications of this acid spike effect in BNCT, and more generally in high-LET radiobiology.

3. ***60th Annual Meeting of the Japanese Society of Radiation Chemistry***
Tsukuba, Japan
26-28 September 2017

P-02

$^{10}B(n,\alpha)^{7}Li$ 反応による水分解と acid spike 効果

ムハマド マイナル イスラム[1]、ヴァナヤ カニケ[1]、ジンタナ メーグンスノエン[1]、
パンティラ ラートナイサット[2]、○勝村庸介[3]、ジェイジェラン ジャンポール[3]

シャーブルック大・医[1]、東大・工[2]、日本アイソトープ協会[3]

熱中性子とボロンの $^{10}B(n,\alpha)^{7}Li$ 反応による水分解 G 値をモンテカルロ計算により算出した。高 LET 性を反映し、ラジカル収量 G 値は小さく、分子生成物 G 値は大きい。トラック近傍に生成する H_3O^+ の濃度の時間変化から pH は 0 程度となり、低 LET 放射線照射の pH 3 に比し、著しく高いことが判った。

はじめに

熱中性子と ^{10}B は 3838 barn の断面積を持つ $^{10}B(n,\alpha)^{7}Li$ 反応を生じる。この反応に基づく BNCT (boron neutron capture therapy) はがん治療のひとつで、生成した高 LET 粒子の殺傷効果を活用する。図 1 にこの反応を示す。この反応は PWR において H_3BO_3 を冷却水に添加することにより炉の余剰反応度の調整にも用いられている。しかし、この反応による水分解についての実験報告はない。本研究では、モンテカルロ計算により室温から 300 °C までの水の放射線分解 G 値の計算を行うとともに、トラック近傍に生成する H_3O^+ の濃度の時間的変化、acid spike 効果を評価し、低 LET 放射線の場合と比較した。

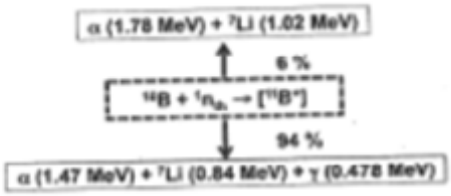

Fig. 1 Schematic of the nuclear reaction

モンテカルロ計算

モンテカルロ計算は以下のような手順で LET、エネルギー、Z*を評価した。
(1) Watt の水中の線量データより、He (1.47 MeV) と Li (0.84 Mev) の線量平均 LET を–196, –216 keV/μm と評価した。
(2) SRIM コードから平均エネルギーを He と Li イオンのエネルギーを–0.3, –0.4 MeV と評価し、荷電交換の過程を簡単化してモンテカルロ計算をした。
(3) LET を再現するために Z^*_{He}, Z^*_{Li} を 1.6, 1.7 とみなした。

この条件下で得られた水分解 G 値は He と Li イオンのエネルギーの重みをかけた平均値で算出した。

Radiolysis of water by $^{10}B(n,\alpha)^{7}Li$ reaction and acid spike effect

M. M. Islam[1], V. Kanike[1], J. Meesungnoen[1], P. Lertnaisat[2], Y. Katsumura[3], and J.-P. Jay-Gerin[1]
1: Univ. of Sherbrooke, 2: Univ. of Tokyo, 3: Japan Radioisotope Association

G-values for the $^{10}B(n,\alpha)^{7}Li$ radiolysis of water at room temperature up to 300 °C were calculated by Monte Carlo Track Chemistry simulation. The change of H_3O^+ as a function of time in the track was evaluated and compared with that by low LET radiolysis. Much lower pH value was obtained for $^{10}B(n,\alpha)^{7}Li$ radiolysis.

水分解 G 値の温度依存性

図 2 に室温でのラジカルと H_3O^+の時間依存性を示す。ラジカル G 値は急激に減少し、このうち OH 収量は 100 ps で半減していることがわかる．水和電子収量の減少はそれほどではない。いずれも、100 ns での G 値は 0.1 以下に到達する。一方の分子生成物 G 値は $G(H_2)$=~1.4, $G(H_2O_2)$= −1.26 と評価される。トラック内での反応が低 LET 放射線の場合と大きく異なる [1]。

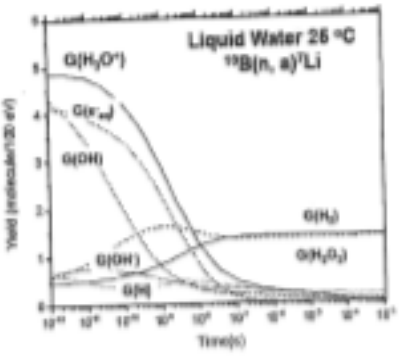

Fig. 2 Time dependent changes of G-values of radical products and H_3O^+.

トラック構造と acid spike

図 3 は 0.3 MeV の He イオンの飛跡近傍に 10^{-13} sec に形成されたトラック構造を示したものである。ドットはエネルギー付与が生じた地点を示す。簡単化するために飛跡では一定の LET として計算してある。これにより、r_C~10 nm 以下のコアの領域と 100 nm を超えて拡がるペナンブラの領域を見ることができる。Li イオンについても同様の結果が得られる。

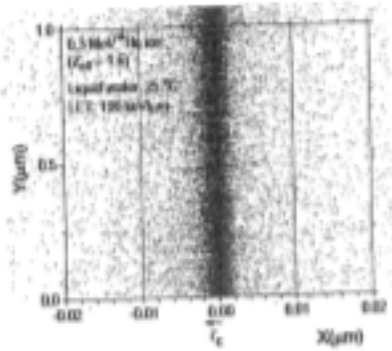

Fig. 3 Schematic track structure induced by 0.3 MeV He ion with Z* = 1.6, and LET = 196 eV/nm.

図 4 はイオンの飛跡に沿って、r_C = 2 nm の円筒状領域での pH の時間挙動を計算したものである。照射直後は pH = 0、100 ps 経過後も pH<1 を維持する [2]。低 LET の場合は、初期の酸性度はスパー半径 r_0 = 10 nm の領域では、pH = 3 程度であり、酸性度は 100 倍程度低いと評価される [3]。この酸性度の細胞への影響評価は興味深い。この点は今後の課題である。

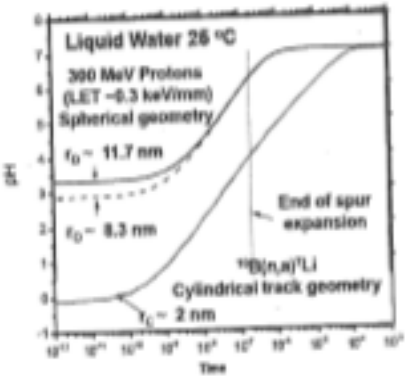

Fig. 4 Time dependent changes of pH in the axially homogeneous cylindrical space with r_C = 2 nm.

結論

$^{10}B(n,\alpha)^{7}Li$ 反応による水分解 G 値をモンテカルロ計算により算出し、ラジカル収量 G 値は小さく、分子生成物 G 値は大きいことを示した。トラック近傍に生成する H_3O^+の濃度の時間変化から pH は 0 程度となる。Acid spike 効果は低 LET 放射線照射に比し、著しく高い。

References:

[1] M. M. Islam, *et al.*, *RSC Advances*, **7**, 10782-10790 (2017). [2] M. M. Islam, *et al.*, in preparation.

[3] V. Kanike, *et al.*, *RSC Advances*, **5**, 43361-43370 (2015).

4. ***46ème Journée scientifique annuelle de la Faculté de médecine et des sciences de la santé de l'Université de Sherbrooke, Québec, Canada***

May 25, 2017

Poster Presentation on the Boron Neutron Capture Therapy (BNCT)